

CHARACTERIZATION AND APPLICATION OF HIGHLY SPECIFIC 2'-F RNA  
APTAMERS TARGETING A POTENTIALLY NOVEL PANCREATIC DUCTAL  
ADENOCARCINOMA (PDAC) BIOMARKER(S)

Sarah Eileen Claypool

A dissertation submitted to the faculty at the University of North Carolina at Chapel Hill in partial fulfillment of the requirements for the degree of Doctor of Philosophy in the Department of Pharmaceutical Science in the Eshelman School of Pharmacy (Chemical Biology and Medicinal Chemistry).

Chapel Hill  
2015

Approved by:

Rihe Liu

Mike Jarstfer

Alex Tropsha

Tim Wiltshire

Sam Lai

Zibo Li

© 2015  
Sarah Eileen Claypool  
ALL RIGHTS RESERVED

## ABSTRACT

Sarah Eileen Claypool; Characterization and Application of Highly Specific 2'-F RNA Aptamers Targeting a Potentially Novel Pancreatic Ductal Adenocarcinoma (PDAC) Biomarker(s)  
(Under the direction of Rihe Liu)

Pancreatic ductal adenocarcinoma (PDAC) has an extremely dismal 5-year survival rate of only 6%. Highly specific targeting ligands that can aid in early stage diagnosis and improved treatment are urgently needed. To address the challenge, cell-SELEX was used to develop a panel of partially modified, 2'-F RNA aptamers that highly selectively recognize pancreatic ductal adenocarcinoma cells. One of the best aptamers, termed 1502, was optimized to be the shortest target-binding motif that retains the target-binding specificity and affinity, and further chemically synthesized with various 3' and 5' functional groups for characterization and application. Using hyperthermia treatment mediated by gold nanoparticles targeted with this optimized aptamer, it was found that the aptamer recognizes all the eleven pancreatic cancer cell lines we have tested, but not normal pancreas, nor numerous non-pancreatic cancer cells. Additionally, a hybrid lipid-PLGA nanoparticle was developed that can carry small molecule organic dyes or drugs for a therapeutic delivery application. With a 5'-modified variation of aptamer 1502, this nanoparticle was functionalized to target PDAC cells, and subsequently internalized to deliver a cytotoxic drug, resulting in selective cell-killing. We believe that this aptamer can be translated to *in vivo* delivery models and can be used to identify a putative novel biomarker of pancreatic ductal adenocarcinoma.

## **ACKNOWLEDGEMENTS**

The last five years of my graduate student life have been a roller coaster of successes and failures, milestones and setbacks, and extensive development of my personal, professional, and scientific self. This dissertation thesis summarizes the scientific accomplishments of my research, but doesn't encompass the accomplishments that I've been able to achieve outside of the lab. Neither the lab-based nor personal and professional accomplishments could have been achieved without the support of numerous people. While this section is not long enough to include all those who have positively affected my time in graduate school, I will try my best to highlight the overwhelming love and support that I have received.

First I want to acknowledge my advisor, Dr. Rihe Liu. Rihe allowed me the opportunity to rotate and eventually join his lab without much prior experience in molecular biology. His lab is an interest driven environment, and with that came the support to explore new and ongoing stages of my project. Rihe has helped me learn how to think critically and understand the conceptual basis for everything that I performed on the bench. These skills have made me a better scientist, and will prove extremely useful in my future career.

I'd also like to thank the rest of my committee, Drs. Mike Jartsfer, Alex Tropsha, Tim Wiltshire, Sam Lai, and Zibo Li. Each and every committee member was chosen with care, and I am very thankful for my selection. They have been a great support system for me over the last five years. Mike Jarstfer, my committee chair, has provided endless personal and professional guidance throughout my time at UNC. As he is for many students, he was one of my biggest advocates. Scientifically, Mike provided great insight into the field and always inquired with

challenging and constructive questions. I have greatly appreciated everything that he has done to lead my committee. I would also like to acknowledge Alex, Tim, Sam, and Zibo for their expertise and support. Each of them has contributed to my thesis in a significant manner.

I would like to acknowledge the Rihe Liu lab as well, both past and present. Dr. Hui (William) Chen was a postdoc in Rihe's lab when I joined and had led my thesis project for two years. In that time, William was able to perform the PDAC-specific selection and initial characterization of the selected RNA aptamers. While transitioning out of his postdoc in the lab, William offered me the opportunity to continue the great work that he had started. Without this opportunity, I would not be able to present the dissertation research that I have worked on for the last five years. In addition to William's contributions, Ke (Tracey) Mu aided in the selection studies and became a good friend throughout our time in the Liu lab. Previous postdocs, Drs. Jianwei Zou and Dongwook Kim were tremendously generous with their time by sharing their knowledge and expertise. Beyond his assistance in the lab, Dongwook became a great friend and continues to offer his insight and advice to this day. Finally, I would like to acknowledge other students in the lab, Yingqui Zhou, Lu Zhang, and Adam Friedman. Yingqui and Lu provided a lot of support throughout the years and that support went a long way during the graduate program. I wish them the best in finishing their studies.

Adam Friedman, now Dr. Adam Friedman, came into the program and joined Rihe's lab at the same time as I. Adam has been more than a co-worker and fellow graduate student to me. He has been one of my closest friends, someone that I can go to in times of happiness and frustration. As we both progressed through the program, Adam and I could relate and find solace in the fact that we were both going through a similar process. He would nicely listen to my rambling stories about nothing, and I would do the same for him. His family and mine quickly

became friends and I see that continuing for years to come. After sitting next to each other for the last 5 years, I already miss our daily conversations. I wish him the best in his career and know that he'll be successful in any endeavor he takes on.

I would like to thank the UNC Eshelman School of Pharmacy, Division of Chemical Biology and Medicinal Chemistry, for accepting me into the program. I couldn't be happier with my decision to come to UNC-Chapel Hill. There are a few administrators and faculty within the School of Pharmacy that I would like to acknowledge. First, Aaron Todd, for keeping his door open to myself and all other students. Aaron was a great supporter of the Graduate Student Organization, and I really appreciated everything that he has done for the program. I'd like to thank Drs. Bob Shrewsbury, Roy Hawke, Dihren Thakker, and Adam Persky for helping me through some of the tougher times of graduate school. Getting your doctorate is certainly a journey of ups and downs, and this faculty assisted me through this journey. Finally, I would like to acknowledge Dean Bob Blouin. Dean Blouin gave me the opportunity to develop my leadership skills by including me on various committees and initiatives. His Student Leadership Advisory Board allowed for me to represent the graduate students in a manner that was truly impactful and valued.

Throughout the program, I expressed a continuous interest in translating my research and moving my career goals towards clinical studies. Dr. Lynn Dressler, currently at Mission Health, was a great supporter of my goals. Through countless conversations, Lynn had helped me explore clinical career paths and advise me on the best "next steps" after graduate school. She spent time introducing me to her colleagues for career opportunities, and for that I am very grateful. One of those introductions was with Dr. Paul Watkins at The Hamner Institutes. Through that introduction, I was able to meet with Dr. Merrie Mosedale to learn more about the

Institutes. I would like to acknowledge both Drs. Watkins and Mosedale for offering me a postdoctoral fellowship at The Hamner. This opportunity allows me to pursue my clinical career goals and transition very easily out of my graduate program.

I would also like to greatly acknowledge the friends that I have made here in Chapel Hill over the last five years. To Julie, Josh, Kate, Catherine, Abhi, Mrudula, Jenni, Jared, James, Ericka, Dylan, Johannes, Kathleen, Theresa, and all of those in the Pharmaceutical Sciences program, thank you for being there for me and supporting me in more ways than you know. I couldn't have asked for better friends.

I would like to give special recognition of one friend in particular, Dr. Susan Wolfkamp. I first met Susan during our recruitment weekend for CBMC. Little did I know that we would both be starting the doctorate program together in the fall. Susan took an alternative track by going into the PharmD program after our first year; however our friendship only became stronger. She has been there for my professional and personally, and I hope that I have done the same. We have been in each other's weddings and have shared more with each other than most. I couldn't have asked for a better, more supportive friend, who would do anything to help me or anyone she cares about. Thank you Susan for always being there.

I want to also acknowledge my family. Thank you to my parents, Jim and Karen Claypool, and my brother and sister, James and Christina Claypool. My parents have always supported my scientific endeavors. Sometimes that meant staying up with me all night to rebuild a science project that the dog ate after I went to bed. Other times it meant allowing me to go out in a hurricane to run "scientific experiments." No matter what the crazy idea was, my parents have always done whatever they could to help me accomplish my goals and encourage me to pursue my dreams. It is because of them that I am so passionate about what I do. They taught me

that. I love and appreciate them very much, and although I am 5 ½ hours away, I know that they would do anything for me, and I for them. James and Christina have also been a great support system over the years. Growing up with me wasn't easy I am sure, but they did it well, and have become two of my greatest friends. They have continuously been there for me when I have needed someone to talk to or reminisce with. I was thrilled to have them be a part of my wedding recently and look forward to having them with me on my graduation day in December. I am very proud of both James and Christina, and am so very happy to have them both in my life.

In addition to my family that I was born into, I have been fortunate to have a family brought to me through my recent marriage. I would like to acknowledge Janet and Sam Thacker for taking me into their family early on with open arms. I truly feel like a daughter to you both and I cannot be happier to have you as in-laws. Also, I would like to acknowledge my sister-in-law and brother-in-law, Kelly and Chris Abrecht and their children, Connor, Caitlin, and the little one on the way. You have become such special people in my life and I am very grateful for all of you.

Finally, I would like to acknowledge my husband, Steve Thacker. Steve and I have been together since the beginning of this PhD program, as we started dating only 2 months before my move to Chapel Hill. In August 2015, just 3 weeks before my defense, we were married after 5+ years of dating. Steve has literally been there with me through the entire program, from start to finish, and he has truly been my most treasured supporter. Although we had 4 years of long distance, both of us going through graduate school, we were able to support each other through the stresses that graduate school and long distance brings. Steve helped me through countless tests, presentations, and late nights and weekends in the lab. He was there for me during all aspects of the program, lifting me up when I was down, and celebrating with me in times of



success. I couldn't have imagined anyone that I would rather have had by my side. I owe my success in this program to him. Steve, I love you very much, and I could not have done this without you.

## TABLE OF CONTENTS

ABSTRACT.....	iii
ACKNOWLEDGEMENTS.....	iv
TABLE OF CONTENTS.....	x
CHAPTER I.....	1
INTRODUCTION .....	1
1.1    Background on Pancreatic Ductal Adenocarcinoma.....	1
1.2    Unmet Need with PDAC.....	3
1.3    Cell-SELEX Preliminary Data.....	4
1.4    Selecting Aptamer 1502.....	11
1.5    Hypothesis, Aims, and Future Directions .....	14
1.5.a.    Hypothesis.....	14
1.5.b.    Specific Aims.....	15
1.5.c.    Ongoing Collaborations and Future Directions .....	17
1.6    Impact and Innovation.....	18
CHAPTER II.....	20
CHEMICAL SYNTHESIS AND CHARACTERIZATION OF APTAMER 1502.....	20
2.1 Introduction .....	20
2.2 Results and Discussion.....	22
2.3 Concluding Remarks .....	47
2.4    Materials and Methods .....	48
CHAPTER III .....	61
TARGETED HYPERTHERMIA APPLICATION OF 1502 FUNCTIONALIZED GOLD NANOPARTICLES DEMONSTRATES THE SPECIFICITY OF 1502 TO PANCREATIC DUCTAL ADENOCARCINOMA.....	61
3.1 Introduction .....	61
3.2    Results and Discussion.....	63

3.3. Concluding Remarks .....	84
3.3 Materials and Methods .....	86
CHAPTER IV .....	93
APPLICATION OF APTAMER 1502 FUNCTIONALIZED HYBRID LIPID-PLGA NANOPARTICLES FOR SELECTIVE CELL KILLING .....	93
4.1 Introduction .....	93
4.2 Results and Discussion.....	96
4.3. Concluding Remarks .....	117
4.4 Materials and Methods .....	119
CHAPTER V .....	125
COLLABORATIONS AND FUTURE DIRECTIONS .....	125
5.1 Introduction .....	125
5.2 Biomarker identification .....	126
5.3 <i>In vivo</i> delivery of 1502 and 1502 functionalized lipid-PLGA nanoparticle.....	137
REFERENCES .....	144

## **CHAPTER I**

### **INTRODUCTION**

#### **1.1 Background on Pancreatic Ductal Adenocarcinoma**

The pancreas is a gastrointestinal organ located behind the stomach and next to the spleen. This organ contains both endocrine and exocrine glands, both serving vital purposes in one's body. The endocrine glands, which make up a smaller percentage of the cells in the pancreas (~5%), play an important role in making critical hormones, such as insulin and glucagon. These cells, when clustered together, are called the "islet of Langerhans", and they release hormones into the blood, aiding in the regulation of sugar, among other things.

The exocrine glands synthesize pancreatic fluids that contain enzymes that help with food digestion in the intestines. These enzymes are released into small ducts that form together to become larger ducts, that empty into the pancreatic duct. This duct works with the bile duct to release the synthesized pancreatic fluids into the duodenum at the ampulla of Vater. These glands and ducts consist of the majority of the pancreatic cells, representing about 95%. Dysregulation or irregular growths within the exocrine glands of the pancreas would be devastating to the proper function of the majority of the pancreas and affect other organs within the gastrointestinal system.

As with any other organ system, growths and irregularities can unfortunately occur within the pancreas. Some of these issues can be associated with infection, such as pancreatitis, or growths that are benign. Patients are starting to receive more prevalent screening through CT

scans, which has helped to identify newly discovered benign pancreatic lesions. These include serous cystic neoplasms (SCNs), mucinous cystic neoplasms (MCNs), and intraductal papillary mucinous neoplasms (IPMNs). While SCNs are usually benign tumors, MCNs and IPMNs have the potential to become cancerous over time if not treated.

Additionally, there are rare cancerous tumors that can occur within or around the pancreas. One of these types is solid pseudopapillary neoplasms (SPNs), a slow-growing tumor that usually occurs in young women. Surgery is the best treatment for SPNs, and fortunately, the outlook is favorable. Another rarer cancer related to the pancreas is ampullary cancer, which starts in the ampulla of Vater, where the bile duct and pancreatic duct come together and empty into the small intestine. With ampullary cancer, the tumors typically develop to form a blockage in the bile duct. This causes bile build up, resulting in jaundice and dark colored urine. These noticeable symptoms allow for ampullary cancer to be detected at an early stage, giving patients a fairly promising prognosis.

The exocrine cells and endocrine cells of the pancreas can both form tumors. It is critical to distinguish between these different pancreatic cancer types when determining the diagnostic tests, symptoms, risk factors, treatment, and prognosis. The endocrine tumors are much less common than the exocrine, representing only 4% of pancreatic cancer diagnoses. Cancers that can form within the exocrine cells include adenosquamous carcinomas, squamous cell carcinomas, signet ring cell carcinomas, undifferentiated carcinomas, and undifferentiated carcinomas with giant cells. As a group, the endocrine cancers are sometimes known as pancreatic neuroendocrine tumors (NETs). Pancreatic NETs can be benign or malignant. Unfortunately, sometimes the diagnosis only becomes clear when the tumor spreads outside of the pancreas.

Exocrine tumors are by far the most common type of pancreatic cancer. Most patients that are diagnosed with pancreatic cancer has an exocrine type of cancer. Pancreatic ductal adenocarcinoma specifically is an adenocarcinoma that begins in the exocrine glands. About 95% of cancers that are exocrine are adenocarcinomas. These cancers usually begin in the ducts of the pancreas, however they can also develop from the cells that make the pancreatic enzymes, in which case they are considered acinar cell carcinomas. Pancreatic ductal adenocarcinoma (PDAC) is one of the worst human cancers, with diagnosis leading to an extremely poor chance of survival. In fact, only 7.2% of people with PDAC survive past five years of diagnosis. This dismal outlook is in part due to two major concerns regarding pancreatic cancer: a lack of effective therapies as well as poor early diagnostic tools<sup>1</sup>.

## **1.2 Unmet Need with PDAC**

Specifically, early diagnosis for PDAC has shown to be difficult for many reasons. One reason is that the symptoms of pancreatic cancer, such as loss of appetite, weight loss, and pain in the abdomen often go unnoticed until the cancer is beyond its early stages<sup>2</sup>. In addition, the diagnostic tools in place have limitations in their efficiency in detecting malignant tumors as opposed to benign tumors. For example, 20% of patients undergoing CT scans showed pancreatic cystic neoplasms and require biannual to annual imaging. Since 60-80% of these neoplasms are benign lesions, it is a growing diagnostic dilemma as to how to assess the risk of malignancy and the attendant need for an operation<sup>3</sup>. It has been seen with many cancers that targeted therapeutic and diagnostic agents can be beneficial in recognizing biomarkers that are overexpressed in only cancerous cells, reducing off-targeting side effects to normal cells while allowing for a tumor selective method for both treatment and early diagnoses.

Unfortunately, when it comes to pancreatic cancer, this approach has proven very difficult due to very few pancreatic cancer-specific biomarkers being proven and identified. Not to mention the effect that this has on discovering ligand-based biopharmaceuticals that can be used in targeted diagnosis and therapy<sup>4,5</sup>. Therefore, there is an urgent need for isolating and identifying novel biomarkers specific for PDAC, to enable the development of targeted therapies and diagnostic tools.

### **1.3 Cell-SELEX Preliminary Data**

To address this need, Dr. Hui Chen, a previous post-doc in the Liu lab, used the powerful directed molecular evolution technology to selectively isolate targeting ligands that sensitively and specifically bind to PDAC cells, and not normal cells, from a pool of nuclease-resistant RNA sequences with high diversity. All preliminary data in this chapter is attributed to Dr. Chen's efforts. Ideally, using living pancreatic cancer cells to target the ligand development is the best method for determining the physiological interactions of the ligand and the cell-surface biomarker. As a negative control, normal pancreas epithelial cells and other non-pancreatic cells can be used. This approach has a big advantage on using bioactive PDAC cell surface biomarkers without need for target identification, expression and purification, a process that is very challenging and time-consuming, particularly for membrane-bound biomarkers that are often extensively glycosylated. The method of selection that we chose to use is known as cell-SELEX, a technology that has shown to be very successful in our previous studies.

Thus far, only *in vivo* phage display and cell-SELEX methods allow the use of living cancer cells as targets for the development of targeting ligands<sup>6,7</sup>. *In vivo* phage display typically results in target-binding shorting peptides. Due to their unstructured nature, the short homing

peptides are less likely to bind a target with high affinity. In addition, most short peptides are quickly degraded by various proteases in plasma when applied under physiological conditions, even if they are PEGylated to minimize systemic clearance. One solution to the dilemma is to use nuclease-resistant nucleic acid molecules as targeting ligands. Aptamers are high affinity single stranded nucleic acid ligands (wild type RNA, DNA, or modified RNA), each specific for a given target molecule with high affinity and specificity. The term ‘aptamer’ was coined by the Szostak lab at Massachusetts General Hospital, where my thesis advisor, Dr. Liu, was well trained for the *in vitro* selection of functional macromolecular molecules<sup>8</sup>. The Liu lab at UNC Chapel Hill has published a number of papers on the selection of functional macromolecules from combinatorial libraries with unusually high diversity using sophisticated directed *in vitro* selection technologies<sup>9-13</sup>.

Nucleic acid-based aptamers possess several unique features that make them suitable for *in vivo* translational applications, including high target-binding specificity and affinity, little immunogenicity, low toxicity, and long shelf life. Aptamers can be developed through an amplification-based iterative round of selection approach called SELEX. Most of the aptamers reported so far were selected using purified targets. If successfully performed, the selected aptamers typically exhibit remarkable affinity and specificity to their targets, with dissociation constants ranging from medium picomolar ( $50 \times 10^{-12}$  M) to low nanomolar ( $10 \times 10^{-9}$  M), which are stronger than that typical for interactions between Fab fragments and their target antigens<sup>14</sup>. However, aptamers based on unmodified nucleic acids have very short half-lives (several seconds to minutes for unmodified RNAs and less than 1 hour for DNAs) under physiological conditions due to quick degradation by nucleases that are abundant in the plasma, and therefore cannot be used in translational research. The stability of a nucleic acid in plasma is largely



determined by its backbone composition. It was found that substitution of ribonucleotides with 2'-fluoro or 2'-O-Me nucleotides can greatly increase the plasma stability of an aptamer<sup>15-17</sup>. Significantly, 2'-fluoro CTP and 2'-fluoro UTP can be incorporated into RNA molecules during *in vitro* transcription by using appropriate T7 RNA polymerase mutants<sup>18-21</sup>. The Liu lab has developed and purified a series of T7 RNA polymerase mutants that allow for efficient incorporation of different combinations of 2'-fluoro or 2'-OMe NTPs into RNAs. The resulting 2'-modified RNA aptamers are resistant to nucleases and highly stable in plasma, with *in vitro* half-lives in the 10 to 15 hour range. The plasma stability of an aptamer can be further enhanced during post-selection optimization by capping the 5' and 3' termini and incorporating non-nucleotide linkers<sup>22</sup>.

When the putative cell surface biomarkers have unknown properties, interactions with other biomolecules, or roles in mediating downstream signaling pathways, as in pancreatic cancer, cell-SELEX is an ideal technology platform for the development of cancer-specific targeting ligands against such a putative biomarker. The conventional SELEX relies on using purified target molecule that has been well characterized. Since our knowledge on the targetable cell surface biomarkers for PDAC is extremely limited, we applied a method known as cell-SELEX, which allows the use of living cancer cells as targets. Compared to conventional SELEX, cell-SELEX has several major advantages<sup>7,23,24</sup>. First, the potential targetable PDAC biomarkers are present on the cell surface as their native conformation, and therefore bypasses the otherwise indispensable prerequisite of knowing, expressing, and purifying the bioactive target proteins. Second, different biomarkers are present on the cell surface, making it possible to simultaneously identify multiple aptamers, each specifically recognizing a unique targetable biomarker. In this project, we aim at addressing the critical needs in targeting PDAC by

developing 2'-fluoro aptamers that highly specifically recognize and tightly bind to PDAC cells but not the closely-related normal pancreas cells. For the target PDAC cells, we initially used AsPC-1 cells. Figure 1.1 represents a schematic of our approach, using cell-SELEX to select for 2'-fluoro RNA aptamers specific to PDAC cells. To avoid enrichment of aptamers that recognize cell surface molecules that are present on both pancreatic cancer cells and normal pancreas cells, we used well characterized hTERT-HPNE and hTERT-HPDE normal pancreas cells for the counter selection.

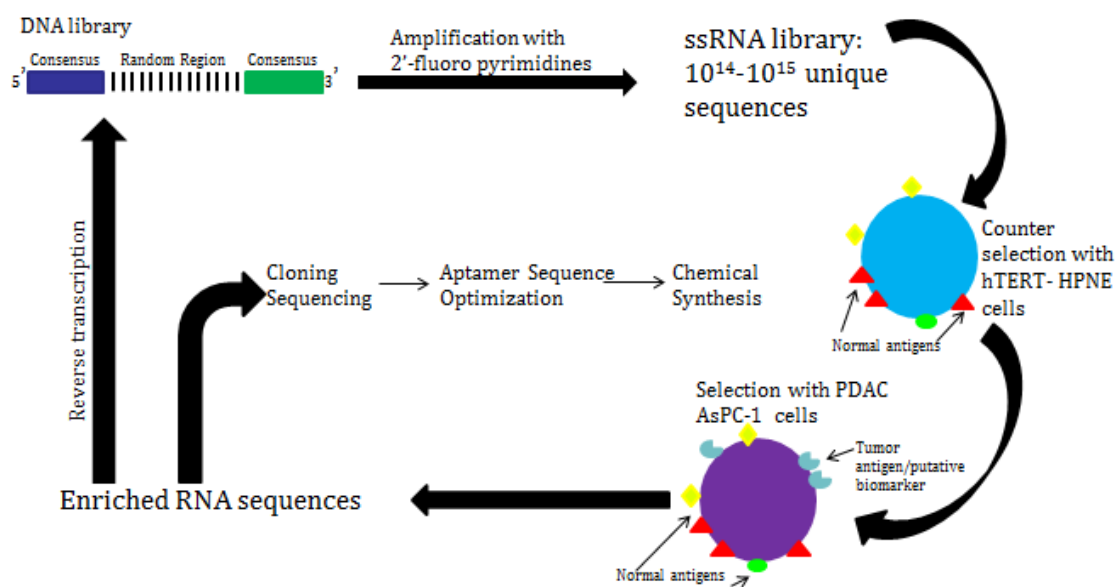


**Figure 1.1** Schematic of cell-SELEX.

To perform cell-SELEX, Dr. Chen started with a synthetic DNA library that consists of an equal molar mixture of two DNA templates, each containing 30 or 40 totally randomized nucleotides, respectively, flanked with consensus regions at both ends. The corresponding single-stranded 2'-fluoro RNAs were generated by *in vitro* transcription using Y639F T7 RNA

polymerase mutant. Dr. Chen performed 15 rounds of cell-SELEX using the 2'-fluoro RNA library at 4°C to facilitate the enrichment of surface receptor-bound aptamers. The selection stringency was gradually increased along with the selection progress by applying more extensive washing, using less number of PDAC cells, and shortening the incubation time. Negative selection using normal pancreas cells was introduced in the 6th round and repeated every 2 rounds thereafter. The selection progress was monitored by comparing the cell-binding properties using selected RNAs that were fluorescently labeled. As shown in Figure 1.2, a steady increase in fluorescence intensity from AsPC-1 cells was observed with increased number of selection cycles, and the increase of fluorescence was significant for the pool from the 15<sup>th</sup> round of selection. No significant change in fluorescence intensity from the negative normal pancreas cells was found, nor when tested using non-pancreatic cancer cells such as Jurkat (acute T cell leukemia), LNCaP (prostate carcinoma), MCF-7 (breast adenocarcinoma), HeLa (cervical adenocarcinoma), H292 (mucoepidermoid pulmonary carcinoma), and A431 (epidermoid carcinoma) cells, clearly indicating that 2'-fluoro aptamers that bind and recognize PDAC cells with the desired high selectivity were significantly enriched.

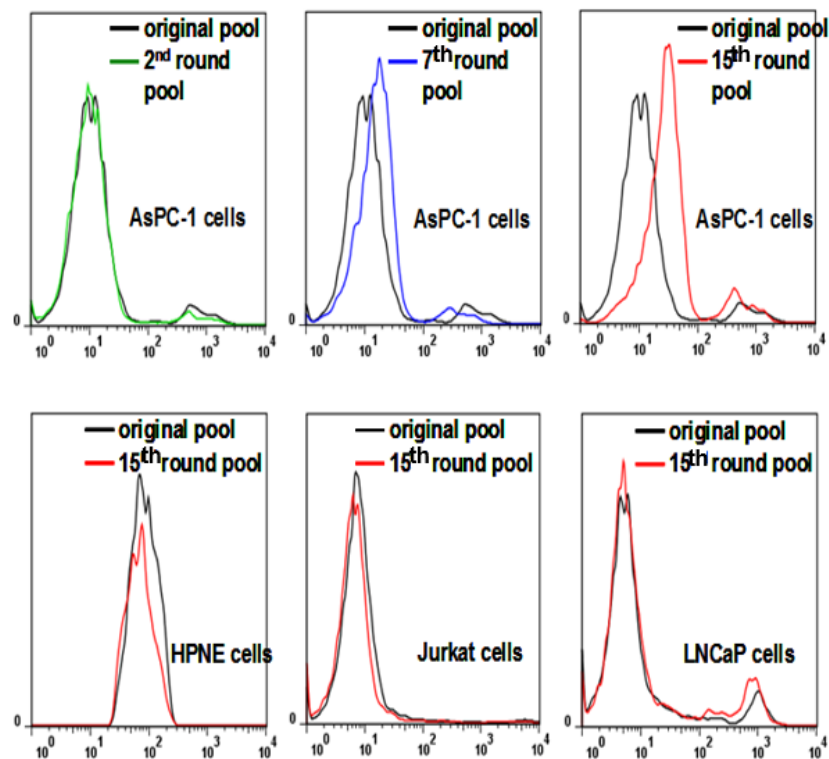


**Figure 1.2** Flow cytometry comparing the original selection pool to the 2<sup>nd</sup>, 7<sup>th</sup>, and 15<sup>th</sup> rounds of selection against AsPC-1 as well as the 15<sup>th</sup> round against HPNE (normal pancreas), Jurkat (acute T cell leukemia), and LNCaP (prostate adenocarcinoma) cells.

Our plan to thoroughly characterize the selected aptamers involved the utilization of a combination of different approaches. Dr. Chen already characterized some of the aptamers selected up until round 15 of the cell-SELEX selection. The initial characterization of these aptamers, as seen in this preliminary data, was a model for our plan for characterization and optimization of other aptamers from this selection.

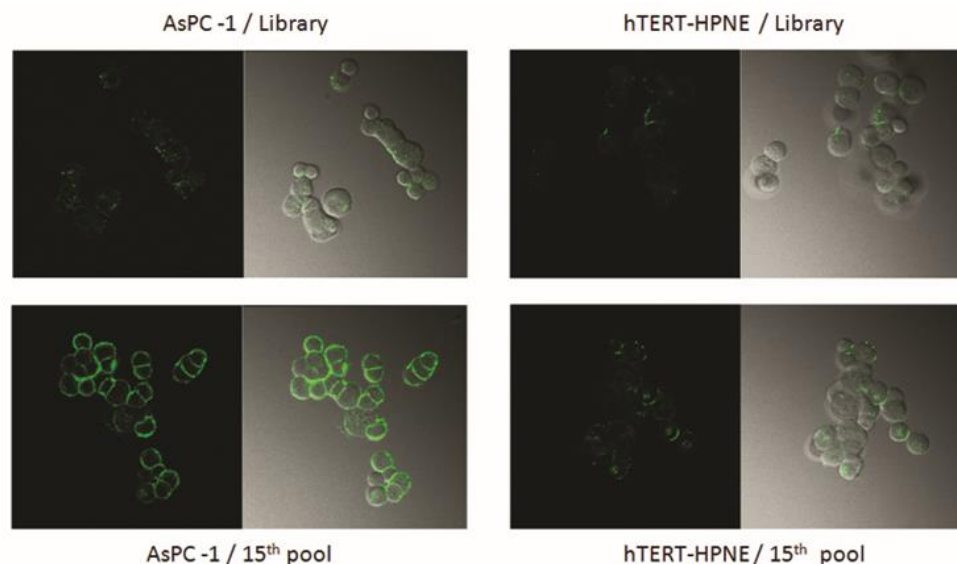


**Figure 1.3** Cell-surface binding to AsPC-1 cells after 15 rounds of selection can be seen, with no cell-surface binding of HPNE cells. The library, when incubated with AsPC-1 or HPNE cells, does not have a cell-surface binding.

The cell-binding specificity of the selected aptamers was first examined using confocal microscopy. As illustrated in Figure 1.3, the aptamer pool isolated from round 15 bound PDAC cells very well, whereas the unselected original library showed minimal binding. The cell-binding is specific to PDAC cells but not to normal pancreas cells or non-pancreatic cancer cells. When the incubation was performed at 4°C, a vast majority of the fluorescently labeled aptamers were bound on the surface of PDAC cells, suggesting they target PDAC cell surface receptors, while at 37°C, a number of the aptamers were present within the cells (Figure 1.4), presumably due to receptor-mediated endocytosis.

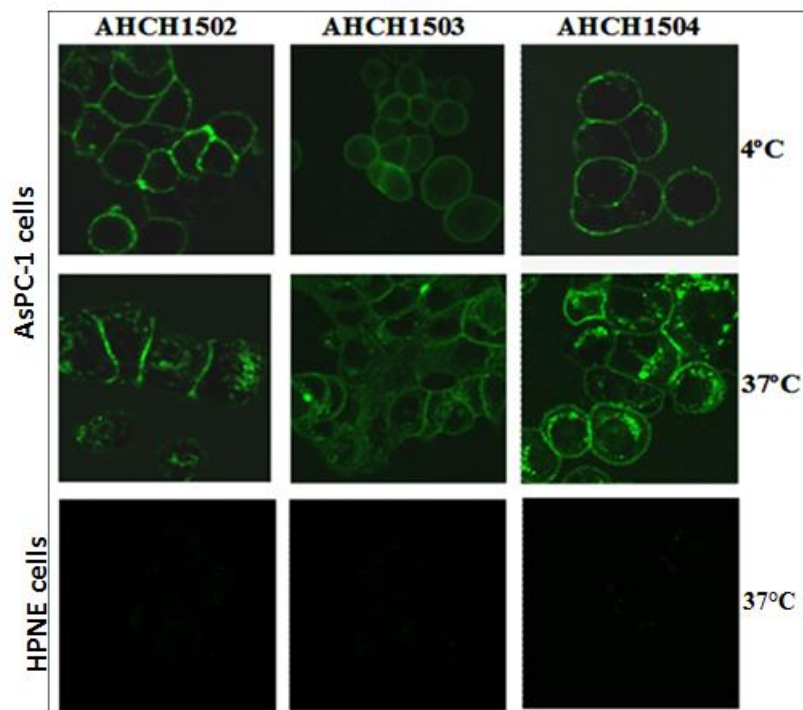


**Figure 1.4** At 4°C, aptamers 1502, 1503, 1504 bound to the cell's surface, however internalization of 15<sup>th</sup> round selected aptamers 1502, 1503, and 1504 at 37°C can be seen. HPNE (control) cells, however, treated with aptamers at 37°C, has no observed binding.

#### 1.4 Selecting Aptamer 1502

The full length 2'-F RNA aptamers contain 83 nucleotides, including a consensus sequence at each terminus for amplification and a central randomized region with 40 nucleotides. The current oligo synthesis technology does not allow for the chemical synthesis of a RNA aptamer with this length. Not all nucleotides in an aptamer are essential for binding to its target, and non-binding regions could potentially destabilize the aptamer and functional structure. This enabled Dr. Chen to map the shortest region that retains the target-binding affinity and specificity, a tactic that was both possible and necessary. To identify which regions on the selected aptamers are essential for target cell recognition and to facilitate the chemical synthesis of the PDAC-specific aptamers for *in vitro* and *in vivo* applications, Dr. Chen managed to map the minimal binding motif that retained PDAC cell-binding affinity and specificity. Aptamer

1501 and aptamer 1502, which account for 14% and 19% of all cloned sequences, respectively, and together one third of the 15<sup>th</sup> round pool, were chosen for further analysis. In addition to their prevalence in the selected 15<sup>th</sup> round, these aptamers can recognize all of the pancreatic cancer cell lines that were tested. Mfold structural analysis showed that these two aptamers possess similar secondary structures with three stem-loop regions. The most notable differences between aptamer 1501 and aptamer 1502 are the base pairing at the 5'-end stem loop and the length of the linker between the stem-loop structures. There are two larger bulges in the 5'-end stem region of aptamer 1501, while only two mismatched bases in the 5'-end stem region of aptamer 1502. Also, the linker of aptamer 1502 is longer than that of aptamer 1501. These differences may lead to lower aptamer 1501 stability and potentially a weaker binding affinity. Based on these observations, Dr. Chen decided to use the three stem-loop structures as a foundation to truncate the aptamers.

While aptamer 1501 was truncated, data for these truncations are not shown here. The truncations, sequence optimization, and characterizations further focused on aptamer 1502 at this point forward. A total of five truncated sequences of aptamer 1502 and full length aptamer 1502 (Figure 1.5A) were prepared by *in vitro* transcription and labeled with Alexa Fluor 488. Truncations were first performed on three different locations on the 5'-end stem region of aptamer 1502 (Figure 1.5B-D). The 3'-end stem-loop of aptamer 1502 was trimmed to generate another truncation (Figure 1.5E). The 3'-end stem-loop structure itself (Figure 1.5F) was also prepared for binding studies. These variations were tested with AsPC-1 cells for binding with flow cytometry. A scrambled sequence (C1), known to have minimal background binding, was used as the control.

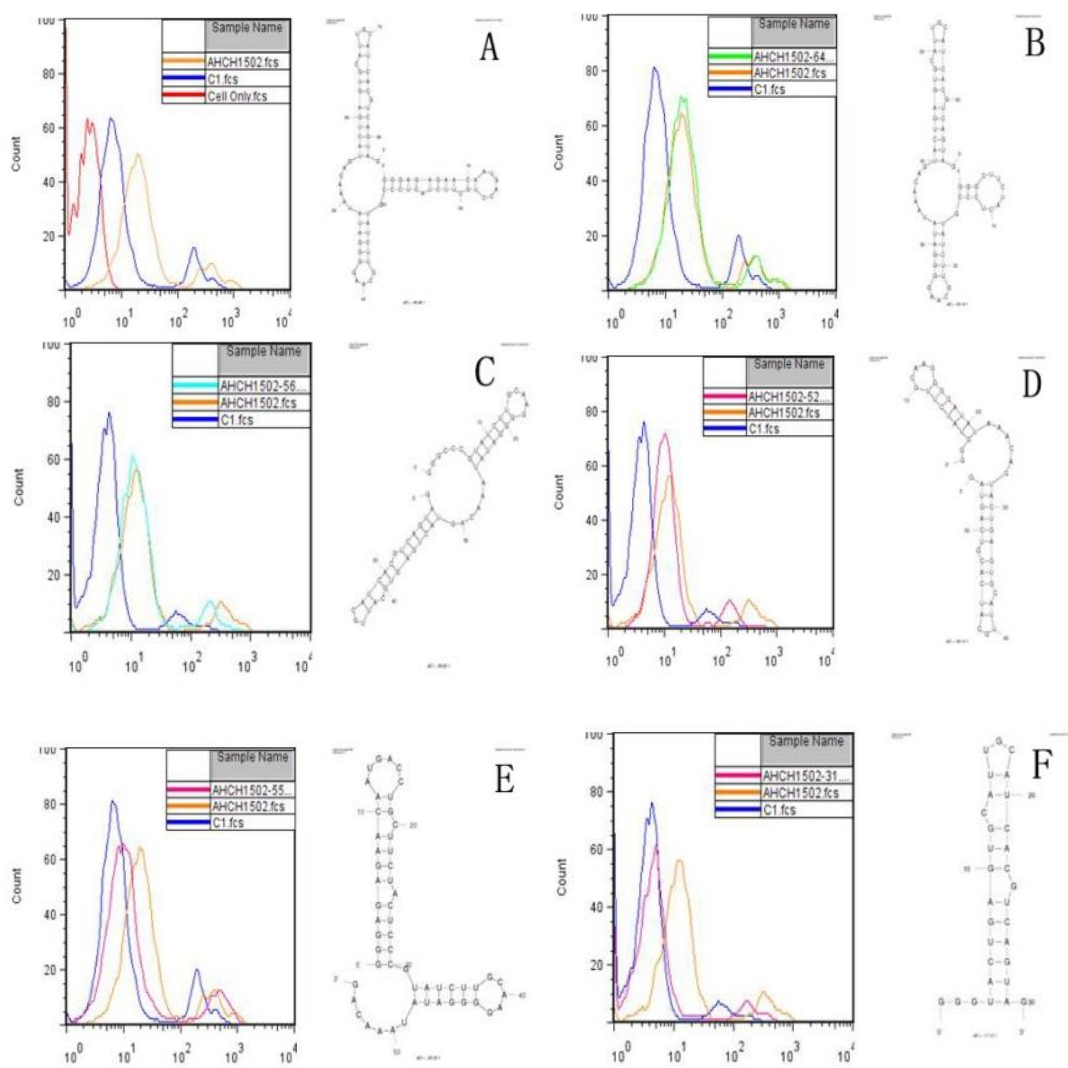


**Figure 1.5** Minimal binding motif study of 2'-F-RNA aptamer. Full length 1502 (A) and five truncated versions of 1502 (B)-(F) were tested for binding with flow cytometry. A scrambled sequence (C1) was used as a control in flow cytometry. Predicated secondary structures of full length 1502 and every truncated aptamer are listed beside flow cytometry results.

As shown by Figure 1.5, all three 5'-end truncations did not diminish the binding capability. The shortest truncated aptamer that retained its binding capability is 52 nucleotides long (Figure 1.5D). These results indicate that the 5'-end stem-loop structure is not critical for the aptamer's binding to the target, and can be removed. Meanwhile, the removal of the 3'-end



stem-loop of aptamer 1502 resulted in dramatically decreased binding affinity (Figure 1.5E), implying that the 3'-end stem-loop is critical for the target recognition of aptamer 1502. When tested by itself, however, the 3'-end stem-loop structure also lost target binding completely (Figure 1.5F). With these truncation results, Dr. Chen reasoned that the central stem-loop structure and 3'-end stem-loop structure are both indispensable for PDAC cell binding of aptamer 1502. Aptamer 1502 can be truncated by up to 31 nucleotides. This shortest aptamer (residues 32-82), containing only the two stem-loops (highlighted in colors), connected by the linker region, retains the PDAC cell-binding affinity and specificity. This length allowed us to chemically synthesize the PDAC-specific aptamer in a large quantity for further characterization and application (seen in Chapters 2-5).

## **1.5 Hypothesis, Aims, and Future Directions**

### **1.5.a. Hypothesis**

Pancreatic ductal adenocarcinoma (PDAC) is one of the most aggressive cancers with a very poor prognosis. One of the reasons that PDAC is so dismal is due to the lack of effective diagnostic tools or therapeutic drugs. It is therefore vital to identify biomarkers specific to PDAC cells as well as ligands that can strongly and selectively bind to these biomarkers. We propose that using a cell target-based selection approach, PDAC-specific ligands can be developed that will hold the promise of targeting fewer normal pancreas and non-pancreatic cells, reducing side effects, and improving the quality of patient's lives.

My dissertation research focused on developing nuclease-resistant PDAC-specific RNA aptamers that were selected using a directed molecular evolution method known as cell-SELEX. The advantage of this method lies in the fact that there is no need for a protein target to be identified, expressed, or purified for the selection to occur. I hypothesized that nuclease-resistant,

partially modified 2'-fluoro aptamers that bind to the cell-surface of PDAC cells without affecting normal pancreas cells and non-pancreatic cells with high specificity can be systematically synthesized and characterized; and that these aptamers can be further applied as targeting ligands for the development of novel diagnostic and therapeutic tools for pancreatic cancer. This project had three specific aims.

### **1.5.b. Specific Aims**

#### **1.5.b.i. Aim 1**

Aim 1 involves the chemical synthesis and characterization of previously selected and truncated highly stable 2'-fluoro RNA aptamers that tightly and specifically bind and recognize PDAC cells but not normal pancreas cells. Previous studies performed in our lab have employed cell-SELEX to identify 2'-fluoro partially modified aptamers that selectively bind to the cell-surface receptors of pancreatic ductal adenocarcinoma cancer (PDAC) cells, but not to normal pancreas cells. With four different types of PDAC cell lines used over 15 increasingly stringent rounds, this cell-SELEX study selected for 13 major classes of aptamers that selectively bind to surface receptors of PDAC cells. We chose to focus our studies on the most prevalent aptamer, termed 1502, for further large scale chemical synthesis, characterization, and application. Truncation of the 5' and 3' ends, done by Dr. Chen, allowed the length of aptamer 1502 to be only 52 nucleotides, from the original 83 nucleotide full length aptamer. Chemical synthesis of aptamer 1502 is possible at this truncated length, and can allow for efficient 3' and 5' modifications at a larger scale. There were several variations of aptamer 1502 synthesized that enabled further characterization and application of subsequent specific aims. In addition to quantitative and qualitative binding affinity characterization, we proposed to thoroughly characterize 1502 for its binding specificity and affinity to various patient derived PDAC tissue

samples. Furthermore, aptamer 1502 was tested for its functional stability and compared to previously selected aptamers to confirm that its cell-surface target is a putative novel biomarker for pancreatic ductal adenocarcinoma.

#### **1.5.b.ii. Aim 2**

In Aim 2 of this research, PEGylated gold nanoparticles were functionalized with aptamer 1502 to further illustrate its ability to target and internalize into AsPC-1 (a PDAC cell line used in selection) and not HPNE cells. Targeted hyperthermia of PDAC cells was performed with an 800 nm IR laser to heat the internalized gold nanoparticles and kill the targeted cells exclusively. The targeted hyperthermia assay allows for the targeting capability and internalization of 1502 to various cell lines to be tested with high sensitivity. Therefore, to further demonstrate the specificity of the selected aptamer against PDAC cell lines, 10 additional PDAC cell lines were tested, along with 3 liver cancer, 1 normal pancreas cell line, and 8 non-pancreatic cancer cell lines. This aim can further characterize the targeting capability and extreme specificity of RNA aptamer 1502.

#### **1.5.b.iii. Aim 3**

Aim 3's mission was to deliver a therapeutic agent specifically to AsPC-1 cells without affecting normal pancreatic cells by functionalizing nanoparticles with aptamer 1502. The specificity of a ligand targeting cancer is critical to avoiding off-targeting side effects of chemotherapies. While the selected and optimized 2'-F RNA aptamer ligands, including aptamer 1502, do not have a known direct therapeutic application, the aptamers do have the specificity to PDAC cell lines. This selectivity can be utilized to deliver therapeutic agents effectively to

PDAC cells without affecting normal pancreatic cells, resulting in selective cell killing. In this aim, hybrid lipid-PLGA (poly-L-glycolic acid) nanoparticles were synthesized, purified, characterized and functionalized with aptamer 1502 that has a 5'-stearyl modification incorporated into the RNA during synthesis. These nanoparticles are biocompatible and can serve as the hydrophobic carriers of cytotoxic small molecule drugs, such as SN-38. Functionalizing drug-carrying nanoparticles with optimized RNA aptamers will not only enable a more effective use of SN-38, but also facilitate targeted therapy of alternative desired therapeutics that can treat pancreatic ductal adenocarcinoma.

### **1.5.c. Ongoing Collaborations and Future Directions**

There are two major goals that are currently being studied and will continue beyond this dissertation research. One is to identify the putative novel aptamer-binding PDAC cell surface biomarker(s) that has great diagnostic and therapeutic potential. This will be done by using a combination of biochemical and proteomic approaches. One of the major reasons that there is an absence of diagnostic and therapeutic tools for pancreatic cancer is due to few number of pancreatic cancer specific biomarkers that have actually been identified. Our cell-SELEX results have shown selected aptamers to bind to cell-surface biomarkers found on PDAC cells. The identity of these novel biomarkers, however, remains unknown. We will utilize the high affinity binding aptamer 1502, characterized and optimized in Aim 1, to form a complex with its protein cell-surface biomarker, facilitating the identification of the binding target. The identification of this biomarker might allow for the discovery of a novel targetable PDAC biomarker that can be used for both targeted diagnosis and therapy.

The second goal is to determine the effects that aptamer 1502 has on *in vivo* targeting against AsPC-1 tumors. We have begun these studies, using an orthotopic PDAC mouse model that we have been using in the Liu lab. Two different delivery platforms will be tested, both utilizing the targeting effects of aptamer 1502. The first platform is aptamer 1502 that is modified on the 5' end with an amino group. This modification can be conjugated to NHS-DOTA and subsequently labeled with copper 64 for tracing with PET imaging. The second platform that we are currently testing is the 1502 functionalized lipid-PLGA nanoparticles. These nanoparticles can carry various hydrophobic dyes initially that can be visualized through IVIS imaging. The long term goal of this delivery system is to encapsulate a small molecule drug that is targeted to the PDAC tumor, allowing for a therapeutic effect against pancreatic ductal adenocarcinoma.

## **1.6 Impact and Innovation**

Given the lack of effective therapies and diagnosis for pancreatic cancer, there is a dire need for researchers to focus their studies on making advancements in these areas. My dissertation research further characterized and applied aptamer 1502, a partially modified 2'-fluoro RNA aptamer selected against pancreatic ductal adenocarcinoma from a cell-SELEX selection. This selection allowed for the discovery of novel nucleic acid ligands that selectively bind to specific biomarkers on PDAC cells. This method has proven successful in previous studies in the Liu lab and through this dissertation research, has been a very effective way to identify promising ligands for diagnostic and therapeutic purposes. In addition, utilizing the cell-SELEX method enables us to identify and further characterize and apply these ligands without their target being known. This is particularly useful when studying pancreatic cancer because

there aren't many pancreatic-cancer specific biomarkers known. We therefore have the capability to synthesize and characterize variations of aptamer 1502 that selectively targets a cell-surface biomarker(s) of pancreatic cancer cells in our first two aims and further apply this aptamer in aim 3. Furthermore, we are currently working on identifying this aptamer's target which could be a novel biomarker of PDAC. The discovery of this cell-surface target would contribute significantly to a type of cancer that currently has an extremely dismal prognosis. Because we were able to continue to develop aptamer 1502 without the target being known, we already have an effective targeting tool for this unknown biomarker that can be used for diagnostic and therapeutic purposes. Ongoing *in vivo* testing will allow for further optimizations of aptamer 1502 against pancreatic ductal adenocarcinoma, and aid in translating these findings into clinical applications.

## **CHAPTER II**

### **CHEMICAL SYNTHESIS AND CHARACTERIZATION OF APTAMER 1502**

#### **2.1 Introduction**

Given the preliminary data from Dr. Chen, we felt that aptamer 1502 was an excellent candidate ligand to further characterize and apply in various cellular studies. We initially designed the necessary characterization and application studies that were necessary to translate this aptamer towards clinical studies. This guided our chemical synthesis plan using the ABI oligosynthesizer. Many researchers utilize the efficient enzymatic systems of PCR and *in vitro* transcription to synthesize RNA aptamers. Even given the partial 2'-F modifications on the pyrimidines, enzymatic synthesis can be done with a commercially available LAR T7 polymerase. For my extensive short-term and long-term application goals, however, chemical synthesis was the more efficient and cost-effective choice. With the truncated length of 52 nucleotides for 1502, it was feasible to synthesize the aptamer on nmol and even  $\mu\text{mol}$  scales. Chemical synthesis is often more reliable than enzymatic transcription for this shorter RNA aptamer length as well. This synthesis approach also allowed for facile 3' or 5' modification with various chemical entities, linkers, or fluorescent tags, which enabled further application and characterization to be done.

For characterization studies, we first wanted to synthesize aptamer 1502 with a fluorescent tag. This allowed for qualitative and quantitative data showing that the newly

synthesized aptamers bind to the cell-surface of AsPC-1 but not HPNE cells, as seen in the enzymatically synthesized aptamers. We also designed variations of 1502 that had mutations in the loop regions of the aptamer, in aims of determining the region(s) of the aptamer that are critical for target binding. Finally, several versions of 1502 were designed with 5' and 3' functional groups that could be useful in applications, as seen in Chapters 3, 4, and 5.

Beyond the synthesis and initial characterization of aptamer 1502 and its binding affinity for the cell-surface receptor of PDAC cells, we wanted to be able to study the clinical potential of aptamer 1502. In this aim, we did that in two different studies. First, we were fortunate to have patient derived xenograft tissue samples from PDAC patients from our collaborator Dr. Jen Jen Yeh. These samples allowed for more clinically relevant testing to be done determining if aptamer 1502 can target pancreatic ductal adenocarcinoma patient tissue in addition to PDAC cell lines. Another important translational aspect of this first aim that was tested was the stability of the aptamer against nuclease degradation. One clinical concern of using RNA aptamers as targeting ligands is that wild type RNA isn't very stable when exposed to nucleases, with an extremely short half-life of only a few minutes. The selected aptamer, 1502 is partially modified with 2'-F pyrimidines, which has shown to have an increased half-time when compared to wild type RNA<sup>25</sup>. Therefore, we wanted to test our synthesized aptamers, which have either 5' or 3' modifications, for stability against nuclease degradation to determine their translational potential when taken *in vivo*.

Finally, this aim looked at comparing aptamer 1502 to two other 2'-F RNA aptamers that were recently selected against PDAC<sup>26,27</sup>. These aptamers, named SQ-2 and M9-5, target newly identified biomarkers, ALPPL-2 and cyclophilin B. The binding specificity of these aptamers to specified (but not all) PDAC cell lines, as reported in the literature, suggests that aptamer 1502



does not bind to the same cell-surface target as aptamers SQ-2 and M9-5. However, to confirm that the biomarker targeted by 1502 is different than the targets of these aptamers, studies were pursued in this aim. Even if the biomarker of 1502 was not identified in this dissertation research, it is important to know if it is the same or different from previously identified biomarkers of pancreatic ductal adenocarcinoma.

## **2.2 Results and Discussion**

### **2.2.a. Chemical synthesis with an 394 ABI Oligosynthesizer**

The RNA and DNA oligos were designed to have varying sequences or modifiers that served a purpose for characterization or application. The RNA aptamer “1502-original” was the original truncated sequence identified by Dr. Hui Chen in the selection that targets pancreatic ductal adenocarcinoma. Throughout this dissertation, this aptamer is also referred to as “1502”. It is important to note that the length of many of the synthesized RNA aptamers was 54 nucleotides, 2 nucleotides longer than the original 52mer, due to the addition of a dT on the 3’ end (to allow for a low volume synthesis column to be used) as well as a modifier on the 5’ end. These additional nucleotides had no effect on the binding of 1502 to PDAC. A scrambled sequence of this aptamer, “1502-scrambled”, was designed to be a non-binding RNA aptamer to PDAC, that shared the secondary structure of the 1502-original sequence. The structure was maintained by keeping consensus stem regions while changing the nucleotides in the loop regions, which are the regions of the oligo that we believe to be directly involved in the aptamer’s binding to its protein target. Additionally, a third variation of aptamer 1502 was designed, called “1502-optimized”. This sequence had minimal differences with “1502-original”, with the intent of strengthening the stem regions with additional A-G base pairing, avoiding any structural changes, with the potential to improve the aptamer’s ability to bind to its target. It is

important to note that this design was a hypothesis, and was not validated in the confocal microscopy binding studies (see below).

There were a series of aptamers that were designed at mutant oligos, with mutations in all of the guanosines in the loop and bulge regions. Six mutants were designed, replacing the guanosines with other nucleotides, so that the replacement did not change the structure of the oligo. These oligos were called, “1502-Mutant7-Sima”, “1502-Mutant11-Sima”, “1502-Mutant24-Sima”, “1502-Mutant38-Sima”, “1502-Mutant41-Sima”, and “1502-Mutant45-Sima”. These oligos, labeled with fluorescent Sima(hex) were tested with the aim of finding a sequence or sequences that didn’t bind to the cell surface of AsPC-1 cells. This could have helped to identify which region of the aptamer contributed to binding interactions with the target. Unfortunately, none of the sequences diminished the binding of the aptamer to the cell surface of AsPC-1, as seen with confocal microscopy (following a similar protocol to methods section 1.4c). Therefore, characterization utilizing the six mutant aptamers was not continued.

The remaining RNA oligos designed for chemical synthesis, were designed for planned application studies, including those discussed in Chapters 2-5. These designs only incorporated the “1502-original” or “1502-scrambled” sequences with varying 5’ or 3’ modifications, with the exception of “1502-ext-phosphoryl”, which was designed for an alternative application. All of the sequences can be seen in Table 2.1 in the methods section below. The additional sequences that were designed for application studies have 3’ and 5’ modifications that include a 5’ alkyne and a 5’ aldehyde. Although these aptamers were synthesized, their application studies were not carried out to completion, and therefore will not be discussed in detail in this dissertation. RNA aptamers that were designed with 5’ and 3’ modifications that were utilized in application studies include the “1502-original-amino” and “1502-scrambled-amino” aptamers, discussed in Aim 2.

Also, the “1502-original-stearyl” and “1502-scrambled-stearyl” aptamers were applied in studies shown in Aim 3. Finally, the biotinylated version of 1502, with the biotin on the 3’ end, “Biotin-1502-original” was applied in the target identification studies that are discussed in Chapter 5.

DNA oligos that were designed included an antisense (44mer) of the 1502 RNA aptamer, as well as a DNA version of the 1502 RNA aptamer (53mer). The antisense was designed to aid in the target identification studies and the DNA version of 1502 was designed as a control sequence for application studies.

Prior to synthesis, the structures of these designed aptamers were predicted using The mfold Web Server from The RNA Institute College of Arts and Sciences at University of Albany, and were based on the  $\Delta G$  of the predicted secondary structures. Each of the oligos synthesized had only one predicted structure, and these structures, without the 3’ and 5’ modifications, can be seen in Figure 2.1.

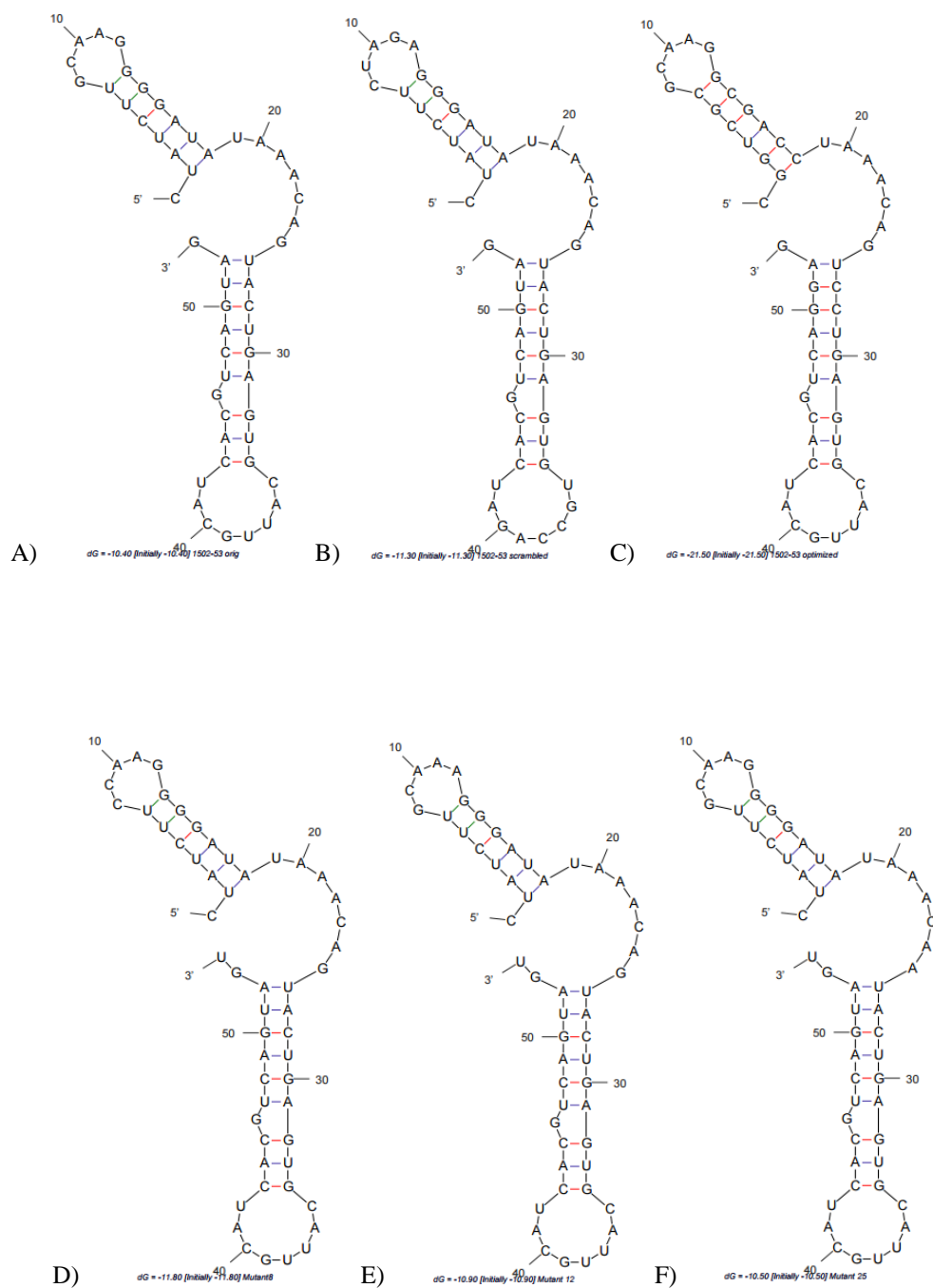


**Figure 2.1** M-fold predicted secondary structures of RNA aptamers A) 1502-original B) 1502-scrambled (negative control) C) 1502-optimized D) 1502-mutant8 E) 1502-mutant12 and F) 1502-mutant25.

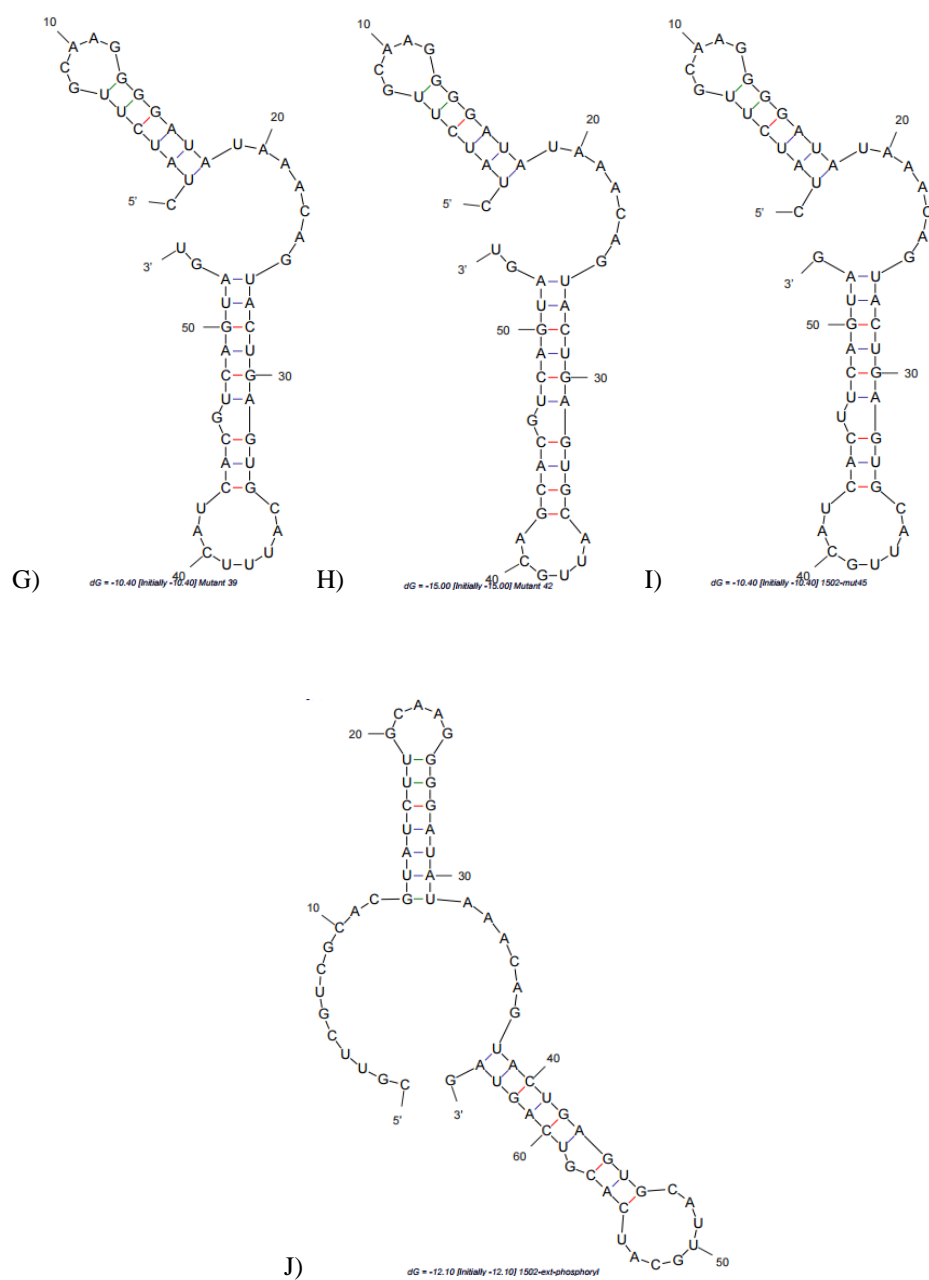


**Figure 2.1 cont.** M-fold predicted secondary structures of RNA aptamers G) 1502-mutant39 H) 1502-mutant42 I) 1502-mutant46 J) 1502-ext-phosphoryl.

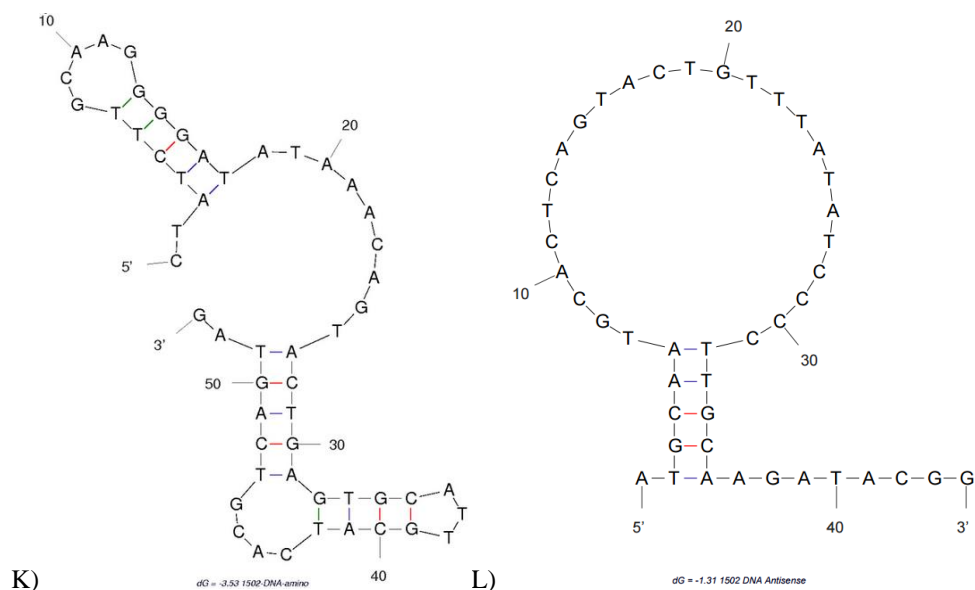


**Figure 2.1 cont.** M-fold predicted secondary structures of DNA aptamers K) 1502-original DNA and L) 1502 DNA antisense.

The sequences that were synthesized are seen in Table 2.1 (shown below in the methods). RNA and DNA aptamers were synthesized with an ABI 394 Oligosynthesizer. Post-synthesis, cleavage, and deprotection, the oligos were purified, and gel electrophoresis was used to quantify the purified oligo. These syntheses were performed on either a 40 nmol or 200 nmol scale. The success of the DNA aptamer syntheses were first confirmed with gel electrophoresis, (data not shown) before continuing with the RNA syntheses. The percent yields, along with the PAGE denaturing gel illustrating the purified RNA aptamers, are portrayed in Figure 2.2.a.-j. This gel analysis would help to confirm fluorescent labeling, if relevant, as well as general size and purification of the aptamer synthesized.

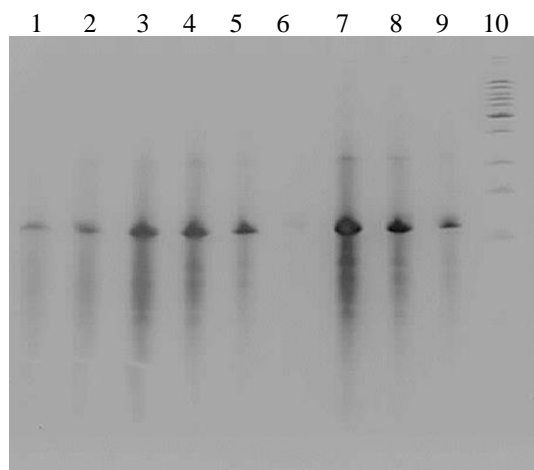


**Figure 2.2.a.** A denaturing urea PAGE gel shows fractions (lanes 1-9) of Biotin-1502-original RNA with a low mw DNA ladder in lane 10, indicating the purity and length of the aptamer. This 1  $\mu$ mol synthesis produced approximately 365 nmol of RNA, or a 36.5% yield.

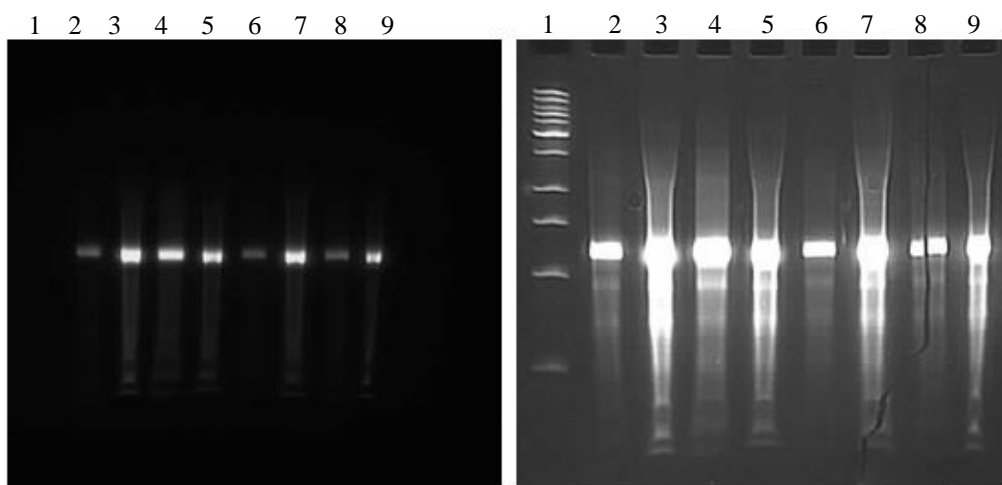


**Figure 2.2.b.** Two denaturing urea PAGE gels show fractions of 1502-original-RNA (lanes 2-9) and the low mw DNA ladder (lane 1), without (left) and with (right) ethidium bromide staining, indicating the presence of a fluorescent Sima and the length of the aptamer. This 40 nmol synthesis produced approximately 19.5 nmol of RNA, or a 48.8% yield.

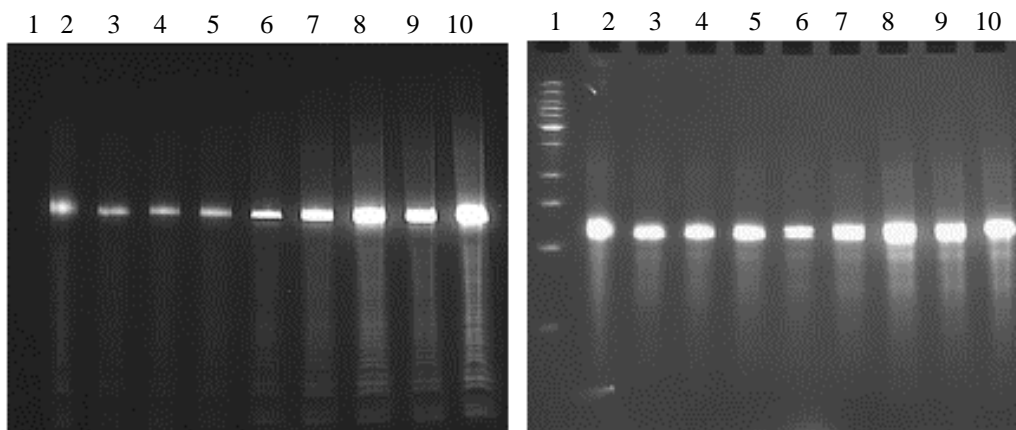


**Figure 2.2.c.** Two denaturing urea PAGE gels shows fractions of Sima-1502-scrambled RNA (lanes 2-6) and Sima-1502-optimized RNA (lanes 7-10), without (left) and with (right) ethidium bromide staining, indicating the presense of a the fluorescent Sima and the length of the aptamer. These 40 nmol syntheses produced approximately 17.7 nmol of RNA for the Sima-1502-scrambled, or a 44.4% yield and approximately 40 nmol of the Sima-1502-optimized RNA, or a 100% yield.

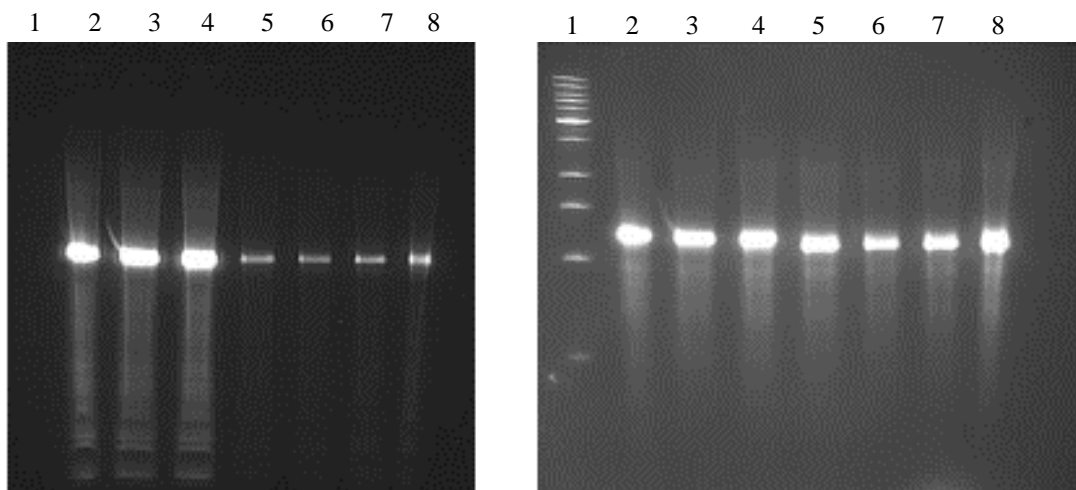


**Figure 2.2.d.** Two denaturing urea PAGE gels shows fractions of Sima-1502-Mutant8 RNA (lanes 2-4) and Sima-1502-Mutant12 RNA (lanes 5-8), without (left) and with (right) ethidium bromide staining, indicating the presense of a the fluorescent Sima and the length of the aptamer. These 40 nmol syntheses produced approximately 18.5 nmol of RNA for the Sima-1502-scrambled, or a 46.4% yield and approximately 39.2 nmol of the Sima-1502-optimized RNA, or a 98.0% yield.



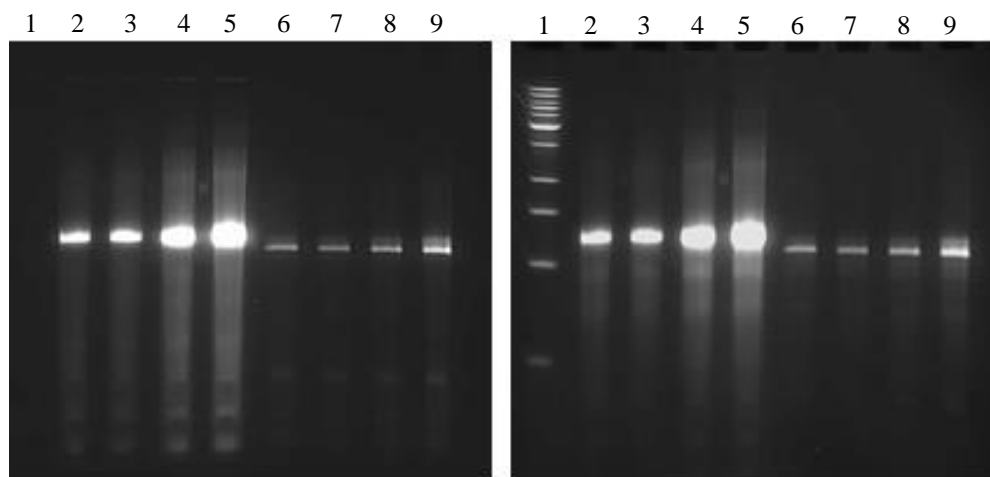


**Figure 2.2.e.** Two denaturing urea PAGE gels shows fractions of Sima-1502-Mutant25 RNA (lanes 2-5) and Sima-1502-Mutant39 RNA (lanes 6-9), without (left) and with (right) ethidium bromide staining, indicating the presense of a the fluorescent Sima and the length of the aptamer. These 40 nmol syntheses produced approximately 10.4 nmol of RNA for the Sima-1502-Mutant25, or a 26.0% yield and approximately 11.1 nmol of the Sima-1502-optimized RNA, or a 27.7% yield.

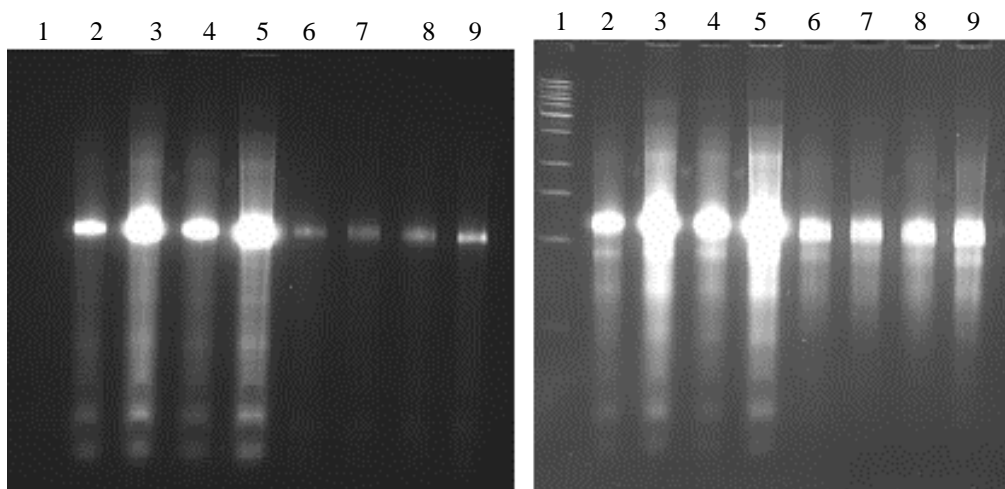


**Figure 2.2.f.** Two denaturing urea PAGE gels shows fractions of Sima-1502-Mutant42 RNA (lanes 2-5) and Sima-1502-Mutant46 RNA (lanes 6-9), without (left) and with (right) ethidium bromide staining, indicating the presense of a the fluorescent Sima and the length of the aptamer. These 40 nmol syntheses produced approximately 28.1 nmol of RNA for the Sima-1502-Mutant25, or a 70.3% yield and approximately 13.3 nmol of the Sima-1502-optimized RNA, or a 33.2% yield.

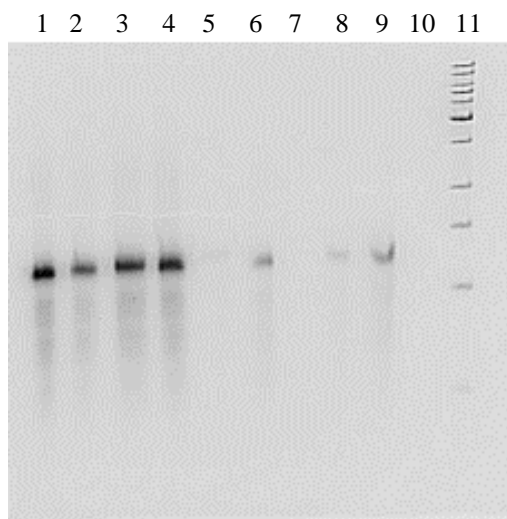


**Figure 2.2.g.** A denaturing urea PAGE gel shows fractions of 1502-original-alkyne RNA (lanes 1-10) with the low mw DNA ladder in lane 11, indicating the purity and length of the aptamer. This 200 nmol synthesis produced approximately 132.3 nmol of RNA for the 1502-original-alkyne, or a 66.1% yield.

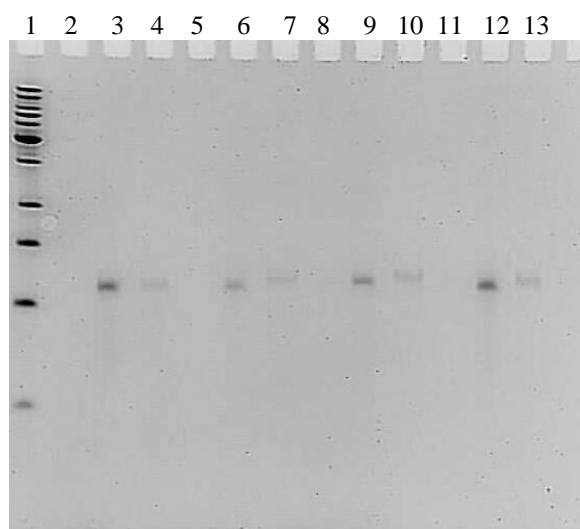


**Figure 2.2.h.** A denaturing urea PAGE gel shows fractions of 1502-scrambled-alkyne RNA (lanes 2-13), with the low mw DNA ladder in lane 1, indicating the purity and length of the aptamer. This 40 nmol synthesis produced approximately 32.4 nmol of RNA for the 1502-scrambled-alkyne, or a 81.1% yield.

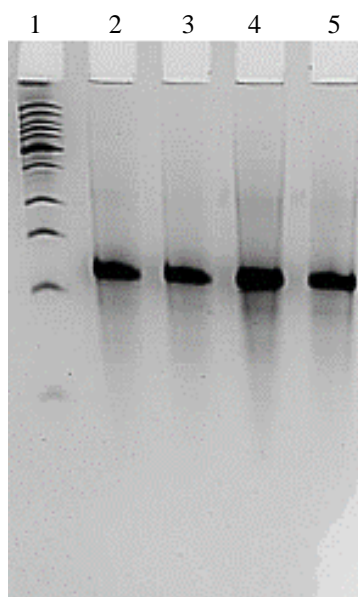


**Figure 2.2.i.** A denaturing urea PAGE gel shows fractions of 1502-original-amino RNA (lanes 2-5), with the DNA low mw ladder in lane 1, indicating the purity and length of the aptamer. This 40 nmol synthesis produced approximately 40 nmol of RNA for the 1502-original-alkyne, or a 100% yield.

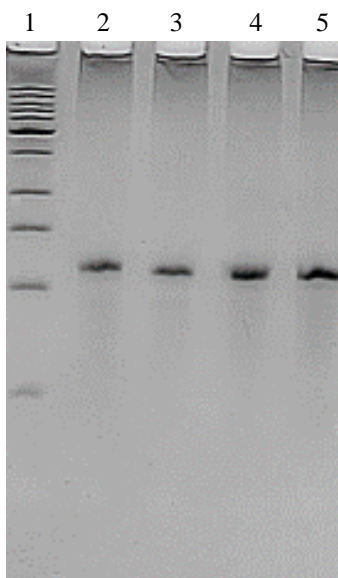


**Figure 2.2.j.** A denaturing urea PAGE gel shows fractions of 1502-original-stearyl RNA (lanes 2-5), with the low mw DNA ladder in lane 1, indicating the purity and length of the aptamer. This 40 nmol synthesis produced approximately 31.7 nmol of RNA for the 1502-original-alkyne, or a 79.3% yield.

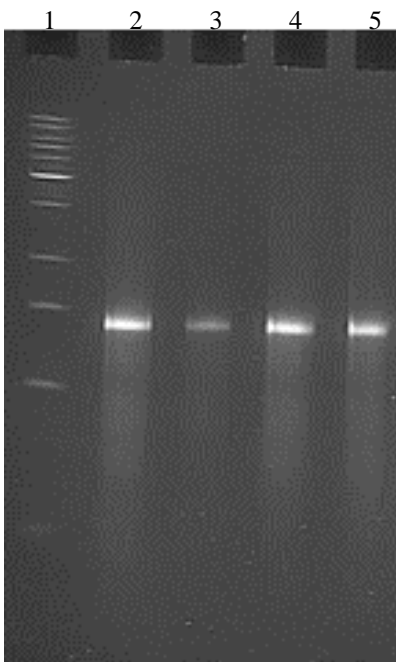


**Figure 2.2.k.** A denaturing urea PAGE gel shows fractions of 1502-ext-phosphoryl RNA (lanes 2-5), with the low mw DNA ladder in lane 1, indicating the purity and length of the aptamer. This 40 nmol synthesis produced approximately 36.2 nmol of RNA for the 1502-original-alkyne, or a 90.5% yield.

### **2.2.b. Qualitative binding of aptamer 1502 with confocal microscopy**

To further analyze the cell surface receptor binding of the selected aptamers for future PDAC targeting applications, we utilized the chemically synthesized 1502 aptamers 1502 that contained a 5' fluorescent Sima (hex) group to visualize binding (or non-binding) properties of the aptamers. These properties were first analyzed by confocal microscopy for a qualitative assessment of the aptamer binding to the cell surface of PDAC cells. Figure 2.3A illustrates that 1502-original-Sima, but not its scrambled version, shown in Figure 2.3B bound to the surface of AspC-1 cells when the binding was performed at 4°C for 30 min. No binding was observed when HPNE normal pancreas cells were used. When 1502-original-Sima was tested on HepG2 (liver

cancer) cells, a bright fluorescence was observed around the cell's surface, similar, if not brighter in nature to 1502's binding to AsPC-1 cells.

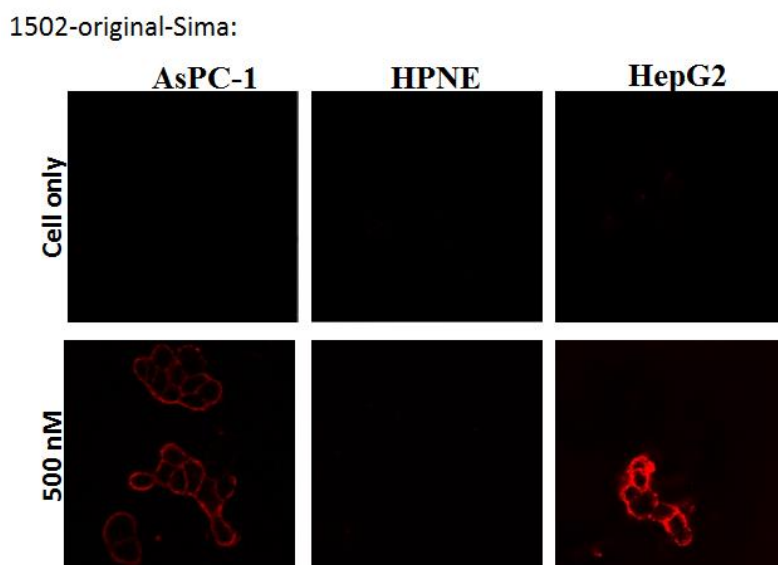


**Figure 2.3A** Binding of the 1502-original-Sima aptamer with AsPC-1 PDAC, HNPE normal pancreas, or HepG2 liver cancer cells visualized with confocal microscopy illustrates binding of the aptamer to AsPC-1 and HepG2.

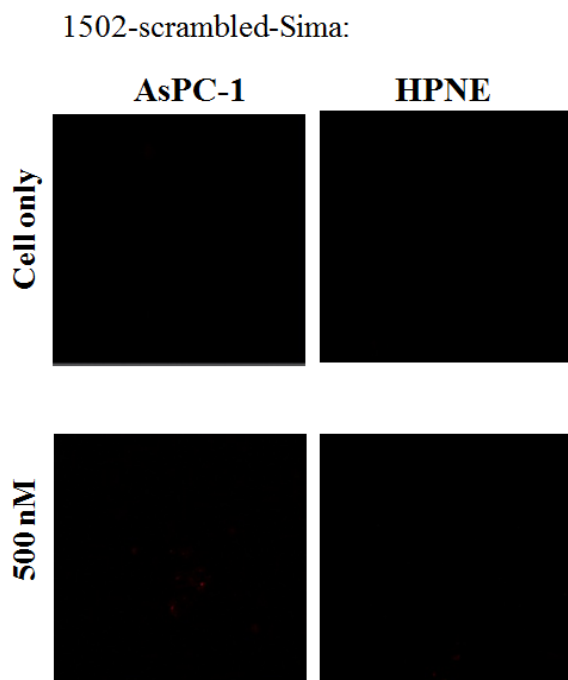


**Figure 2.3B** Binding of the 1502-scrambled-Sima version with AsPC-1 PDAC or HPNE normal pancreas control cells demonstrates a non-binding sequence seen with confocal microscopy.

1502-optimized-Sima was tested on AsPC-1 and HPNE cells to visualize binding comparative to 1502-original-Sima. An identical approach to the characterization of 1502-original-Sima and 1502-scrambled-Sima was taken to test the cell surface binding of this potentially optimized aptamer. Results (not shown) demonstrated binding to the cell surface of AsPC-1 and not HPNE cells, however the relative fluorescence was not brighter and therefore did not indicate an “optimized” aptamer. It was then determined that further characterization and application studies were to be done with the “original” selected sequence.

As described in the synthesis of the RNA aptamers, six mutant aptamers were synthesized with a 5' Sima group and tested for binding to AsPC-1 vs. HPNE cells. If one of the mutant aptamers observed diminished or a lack of binding to AsPC-1 cells, further binding studies were planned to study the interactions of aptamer 1502 to the potential target. The cell binding assay was done at 4°C for 30 min, as done previously. The binding of these mutant sequences, data not shown, was not affected by the mutations that were designed into the sequences. Because of these results, no further studies were done with the six mutated 1502 sequences.

### **2.2.c. Quantitative binding of aptamer 1502 with flow cytometry**

Flow cytometry was used to determine the binding affinity of aptamer 1502-original-Sima to AsPC-1, HPNE (control), and HepG2 (liver) cells. The cell-binding affinity was determined by measuring the fluorescent signal associated with the three different cell lines. It was found that 1502 showed a  $K_d$  of  $125 \text{ nM} \pm 4.95 \text{ nM}$  to AsPC-1 cells, whereas its binding with HPNE normal pancreas cells was not measurable. Additionally, aptamer 1502 showed binding to HepG2 cells with a  $K_d$  around  $60 \text{ nM} \pm 1.72 \text{ nM}$ . The binding affinity ( $K_d$ ) was

calculated on CellQuest software. These results confirm that the chemically synthesized aptamer 1502 binds strongly to the target cell line AsPC-1 and not the normal pancreas control cell line, HPNE. Additionally, the strong binding of HepG2 can be useful in identifying the unknown potentially novel target of aptamer 1502.

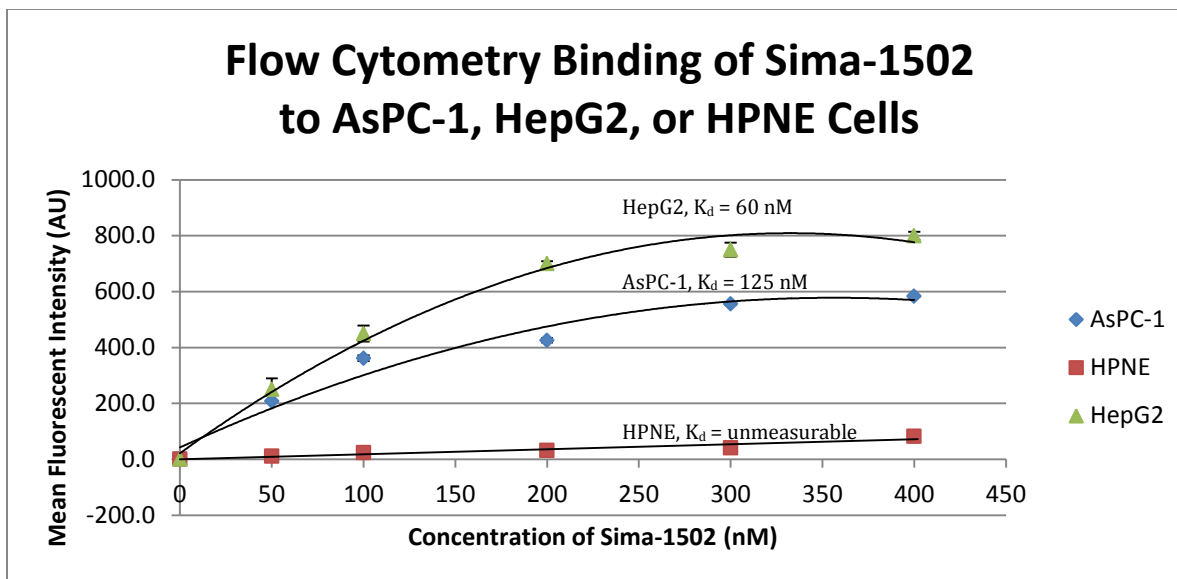


**Figure 2.4** Mean fluorescent intensity (AU) was determined by flow cytometry when varying with concentrations (nM) of aptamer 1502 labeled with Sima were incubated with AsPC-1, HPNE, and HepG2 cells. AsPC-1 and HepG2 demonstrated binding of  $125 \text{ nM} \pm 4.95 \text{ nM}$  and  $60 \text{ nM} \pm 1.72 \text{ nM}$ , with no measurable binding from HPNE.

#### 2.2.d. Immunohistochemistry of 1502 with Tumor Tissues from Patient Derived Xenograft PDAC Mouse

Prior to any meaningful translational applications, it is critical to examine whether the putative novel receptor that is recognized by 1502 is present on patient pancreatic cancer tissue. To address the question, we performed immunohistochemical studies by incubating TAMRA-labeled 1502 with tumor tissue samples from the Patient-Derived Xenograft (PDX) mice, in which different patient tumors had been engrafted as tumor fragments into immunocompromised mice. As shown in Figure 2.5, strong binding signal was observed in all the three tissue samples derived from different human patients, as well as in the AsPC-1 tumor tissue sample. These

results suggest that the putative 1502-binding biomarker that is highly specific to PDAC cells is very likely present on patient PDAC tissue. The results also demonstrated that the TAMRA-labeled 1502 did not target the control A375 (malignant melanoma) tissue. While this sample set is small, it is an indication of the translational application of 1502 to target and identify not only PDAC cells, but PDAC patient tissue as well.

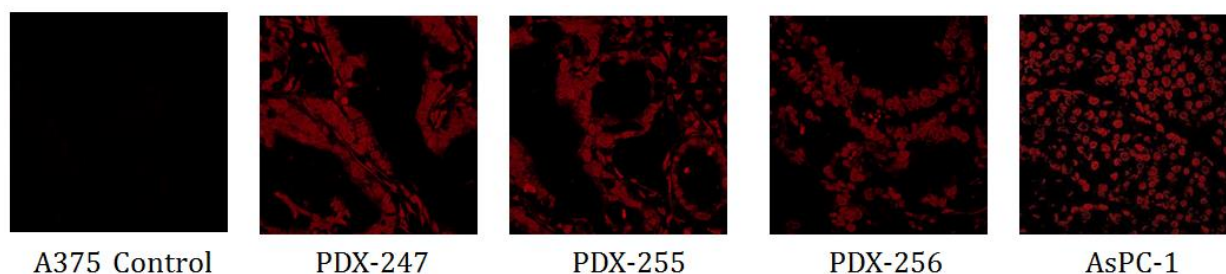


**Figure 2.5** Immunohistochemistry studies on the binding of TAMRA-labeled 1502 to PDX tissue samples of pancreatic ductal adenocarcinoma.

#### 2.2.e. Serum stability assay

With evidence that aptamer 1502 can bind to PDX tissue samples, in addition to cell lines, it would be beneficial to further test the translational application potential of aptamer 1502. The stability of the aptamer in mouse serum, tested through a serum stability assay, could help to predict how stable the aptamer may be *in vivo*. 2'-F partially modified RNA aptamers typically have an increased stability when compared to WT aptamers, however a decreased stability when compared to fully modified RNA aptamers, as shown previously in our lab<sup>28</sup>. We tested three of the synthesized 2'-F partially modified RNA aptamers in 10 or 50% mouse serum for time points ranging from 0 min to 24 h. The aptamers tested were 1502-ext-phosphoryl and 1502-original-amino. The 1502-ext-phosphoryl was predicted to have a similar stability to other unmodified 2'-F partially modified aptamers and was therefore considered to be a standard for the assay. The



1502-original-amino aptamer is further applied in Aim 2, and it is an aptamer that has translational *in vivo* application, as seen in Chapter 5. It was predicted that this aptamer would have a similar stability to 1502-ext-phosphoryl.

The results of this assay can be seen in Figure 2.6. The 1502-ext-phosphoryl aptamer did degrade over time in both the 10% and 50% mouse serum, with less than 25% of the aptamer remaining after 24 h in 50% serum. This was to be expected for this aptamer. The 1502-original-amino aptamer, however, seemed to have an increased stability in 10 and 50% serum, with the only noticeable degradation occurring at 24 h in 50% serum. This was an unexpected result, although promising when considering utilizing the aptamer *in vivo*. Both aptamer's assays were repeated 3 times to confirm the findings. It is believed that the 5' amino modifier may have provided stability to the aptamer against nuclease degradation.

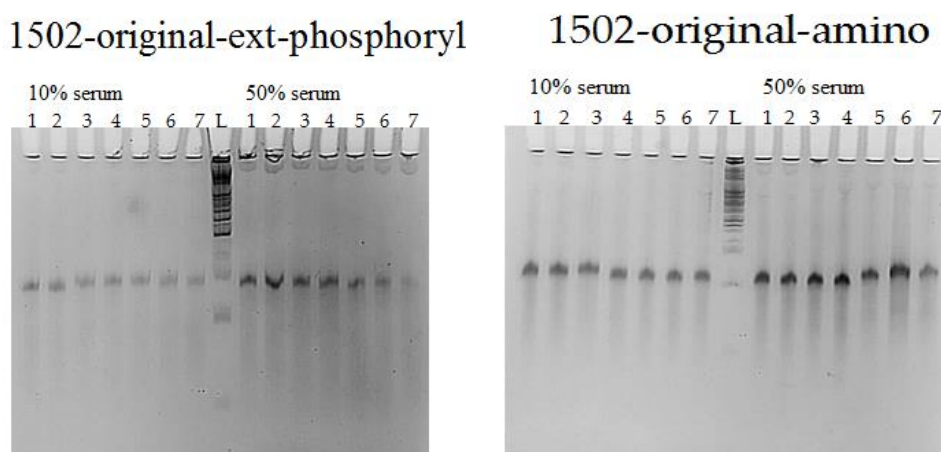


**Figure 2.6** Preliminary results demonstrate that 1502-ext-phosphoryl degrades with 10 and 50% mouse serum, and is at least 75% degraded by 24 h in 50% serum. 1502-original-amino, however, does not appear to degrade in 10% serum and only exhibits slight degradation in 50% serum at 24 h. Lanes correspond to time of incubation in mouse serum; 1-0 min, 2-5 min, 3-2 h, 4-4 h, 5-8 h, 6-12 h, and 7-24 h.

## 2.2.f. Determining if known PDAC-targeted aptamers have the same target as 1502

Recently published in the literature, are two 2'-F partially modified RNA aptamers that were selected against pancreatic ductal adenocarcinoma cells lines<sup>26,27</sup>. Post-selection, these

researchers determined the target proteins of their aptamer to be cyclophilin B for RNA aptamer M9-5, and ALPPL-2 for aptamer SQ-2. Based on the differences in cell binding of these aptamers against tested cell lines seen in the literature, there is an indication that aptamers M9-5 and SQ-2 have differing binding properties when compared to our selected 2'-F RNA aptamer, 1502. In Chapter 3, a comprehensive cell-binding study is done with 20+ cell lines to validate 1502's specificity. However, because 1502's target has yet to be identified, we would like to further confirm that 1502 does not bind to the same target as either aptamer M9-5 or SQ-2.

With the M9-5 aptamer, there were technical difficulties in synthesizing the RNA aptamer by transcription. Both Klenow and PCR were attempted with various designed primers, however the RNA transcription was too low to be useful for labeling. Fortunately, I was able to enzymatically synthesize the full length SQ-2 aptamer, which had a non-functional 3'-end that was reported in the literature. The Lee group utilized this non-functional end for labeling with a tamra-antisense oligo, an approach that I took to label the SQ-2 aptamer. With a 3'-antisense oligo labeled with tamra, I could anneal the SQ-2 RNA to the antisense for a fluorescent labeling of the aptamer, an approach also taken by the Lee group to demonstrate cellular binding.

Initially, a competition of 1502 against SQ-2 was done on AsPC-1 cells. In this experiment, Sima-labeled 1502 was mixed with unlabeled SQ-2 at a 1:1, 1:3, and 1:6 ratio. The mixture was incubated with AsPC-1 cells to test if the presence of the SQ-2 aptamer, especially when in excess, interfered or inhibited the binding of 1502 to the cell surface of AsPC-1 cells. The results were visualized with confocal microscopy. Figure 2.7 demonstrated that even at a 1:6 ratio of Sima-1502 to unlabeled SQ-2, there was no obvious inhibition of binding visualized by the fluorescent signal observed by Sima-1502 binding to AsPC-1 cells.

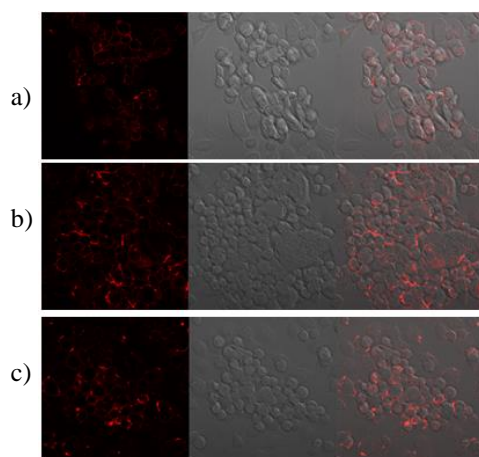


**Figure 2.7** Competition study with Sima-1502 and unlabeled aptamer SQ-2 at 1:1(top images), 1:3 (middle images), and 1:6 (bottom images) molar ratios of 1502:SQ-2.

After labeling aptamer SQ-2 with the tamra-antisense oligo, I further demonstrated that the SQ-2 aptamer that I synthesized could bind to the cell lines tested in the paper, including ALPPL-2 expressing Capan-1, AsPC-1, and Panc-1 cell lines, without binding to low expressing HPNE, CFPAC-1, and MiaPaca-2 cells. Sima-labeled 1502 was tested on these same cell lines, which illustrated differences in binding. Figure 2.8a shows the binding similarities and more significantly, differences, between 1502 and SQ-2 with the tested PDAC and non-PDAC cell lines. The differences seen with these aptamers indicate that the aptamers likely bind to different targets.

Finally, it was important to additionally test cell lines that are known to have a high expression of ALPPL-2. The aim was to confirm that SQ-2 is functional and 1502 is not functional against these cell lines. Although the ALPPL-2 protein is not completely understood, we were able to identify cell lines that have a higher expression of the protein through the Broad-Novartis Cancer Cell Line Encyclopedia<sup>29</sup>. We found that the colorectal adenocarcinoma cell line, LoVo cells, have a relatively high mRNA expression that corresponds to ALPPL-2 expression. Additionally, a rectal adenocarcinoma cell line, SW837, also have a relatively high

mRNA expression according the Broad-Novartis Encyclopedia. We tested these cell lines with tamra-labeled SQ-2 and Sima-labeled 1502, data seen in Figure 2.8b. These results illustrate that 1502 does not bind to cell lines with a known higher expression of ALPPL-2, again suggesting that aptamer 1502 does not bind to ALPPL-2. The tamra-labeled SQ-2 aptamer demonstrated binding to both LoVo and SW837 cell lines; results that further supported the aptamer's binding to ALPPL-2.

Although at this time, the M9-5 aptamer was not successfully synthesized, we know its target has been proven to be cyclophilin B. We again used the Broad-Novartis Cancer Cell Encyclopedia to determine cancer cell lines that have high mRNA expression that correlates to higher cyclophilin B gene expression <sup>29</sup>. Two cell lines demonstrate relatively higher levels of cyclophilin B expression include a lung carcinoma, A549, as well as a breast adenocarcinoma cell line, MCF7. It was also seen from this database, that A549 has some ALPPL-2 expression as well, although not as high as LoVo or SW837 cells. We tested the A549 and MCF7 cell lines against Sima-1502 to determine if 1502 bound to cell lines with a high expression of cyclophilin B. If 1502 targeted this receptor, the Sima-labeled aptamer would likely show this binding through fluorescent microscopy. As seen in Figure 2.8.a.-j., 1502 did not illustrate binding to either A549 or MCF7 cells, cell lines with higher cyclophilin B expression, suggesting that this aptamer does not bind to cyclophilin B. While it would be best to have the M9-5 aptamer to further demonstrate the differences in the two aptamer's targets, these results suggest that 1502's target is not the previously identified cyclophilin B.

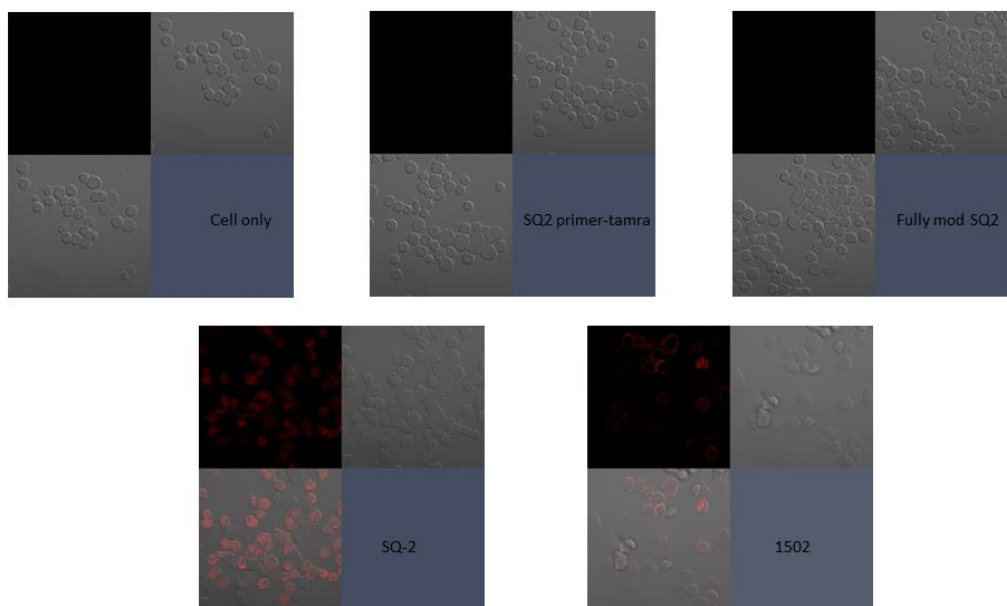


**Figure 2.8.a.** Aptamers SQ-2 (tamra labeled) and 1502 (sima labeled) at a 300 nM concentration, were tested against AsPC-1 cells at 4°C for 30 min. As expected from the literature and from our previous testing, binding was observed for SQ-2 and 1502. Cell only, the tamra-antisense oligo, and a fully modified non-functional labeled SQ-2 aptamer were used as controls and showed no binding to AsPC-1 cells.

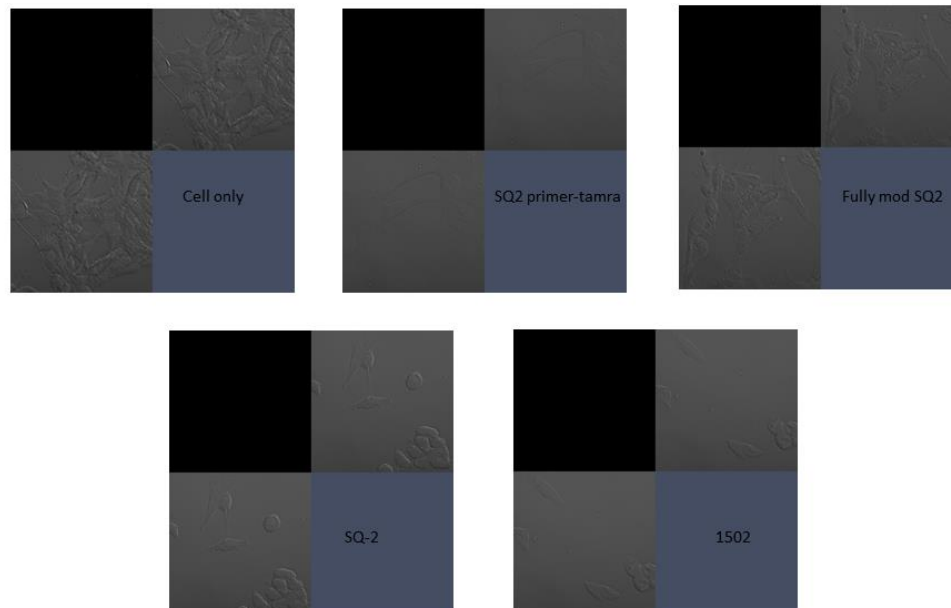


**Figure 2.8.b.** Aptamers SQ-2 (tamra labeled) and 1502 (sima labeled) at a 300 nM concentration, were tested against HPNE cells at 4°C for 30 min. As expected from the literature and from our previous testing, binding was not observed for SQ-2 and 1502, as seen with the controls: cell only, the tamra-antisense oligo, and a fully modified non-functional labeled SQ-2 aptamer.

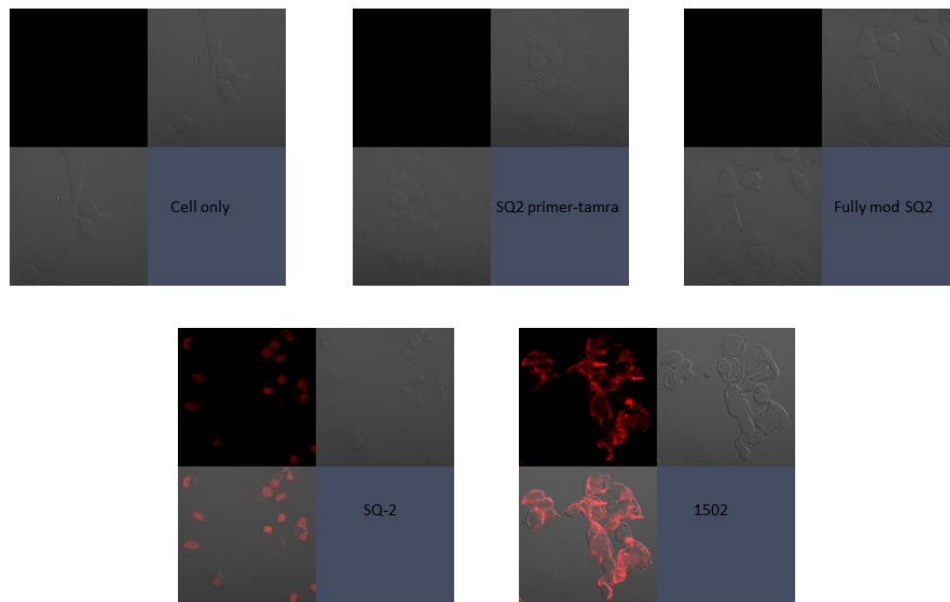


**Figure 2.8.c.** Aptamers SQ-2 (tamra labeled) and 1502 (sima labeled) at a 300 nM concentration, were tested against Panc-1 cells at 4°C for 30 min. As expected from the literature and from our previous testing, binding was observed for SQ-2 and 1502. Cell only, the tamra-antisense oligo, and a fully modified non-functional labeled SQ-2 aptamer were used as controls and showed no binding to Panc-1 cells.

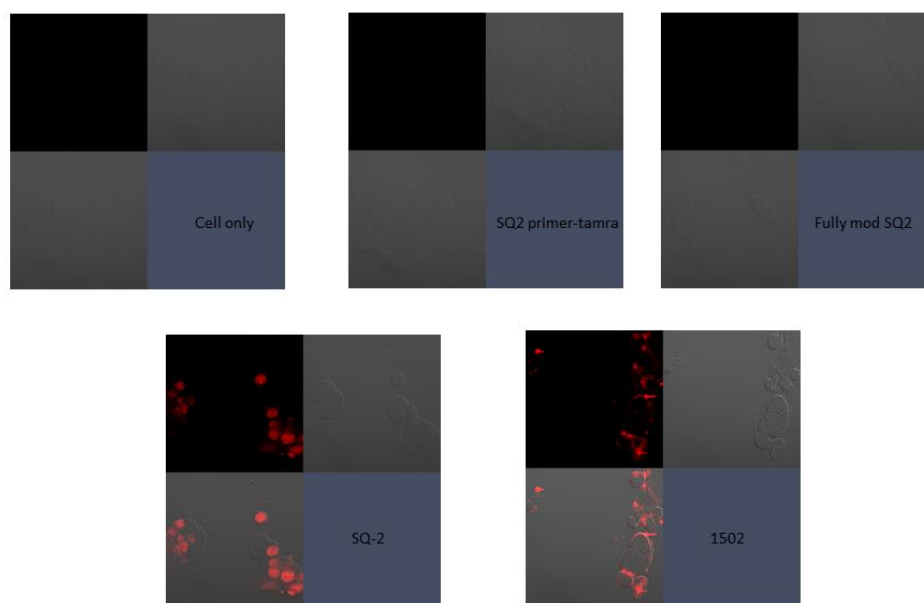


**Figure 2.8.d.** Aptamers SQ-2 (tamra labeled) and 1502 (sima labeled) at a 300 nM concentration, were tested against Capan-1 cells at 4°C for 30 min. As expected from the literature and from our previous testing, binding was observed for SQ-2 and 1502. Cell only, the tamra-antisense oligo, and a fully modified non-functional labeled SQ-2 aptamer were used as controls and showed no binding to Capan-1 cells.

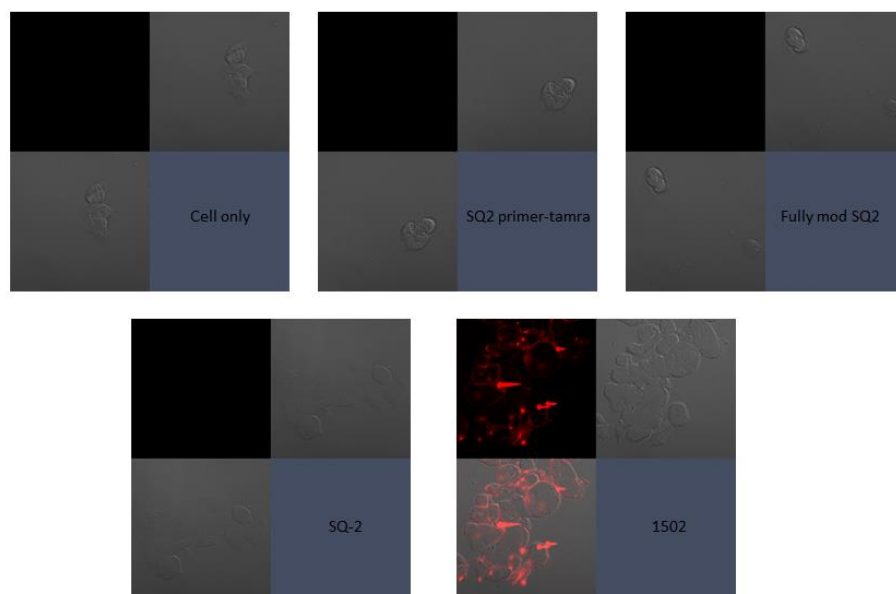


**Figure 2.8.e.** Aptamers SQ-2 (tamra labeled) and 1502 (sima labeled) at a 300 nM concentration, were tested against CFPAC-1 cells at 4°C for 30 min. As expected from the literature and from our previous testing, binding was observed 1502 but not for SQ-2, an indication of different cell surface targets. Cell only, the tamra-antisense oligo, and a fully modified non-functional labeled SQ-2 aptamer were used as controls and showed no binding to CFPAC-1 cells.

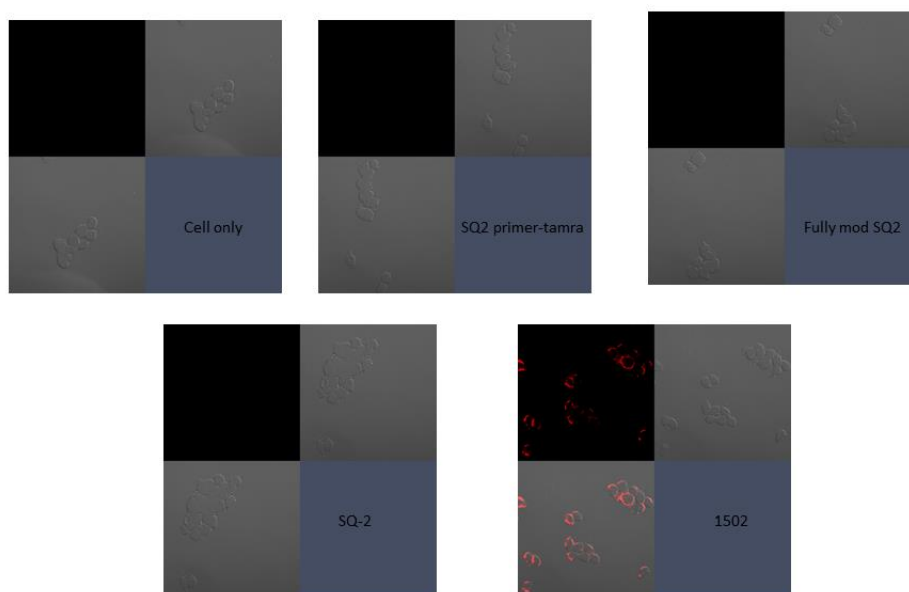


**Figure 2.8.f.** Aptamers SQ-2 (tamra labeled) and 1502 (sima labeled) at a 300 nM concentration, were tested against MiaPaca-2 cells at 4°C for 30 min. As expected from the literature and from our previous testing, binding was observed 1502 but not for SQ-2, an indication of different cell surface targets. Cell only, the tamra-antisense oligo, and a fully modified non-functional labeled SQ-2 aptamer were used as controls and showed no binding to MiaPaca-2 cells.

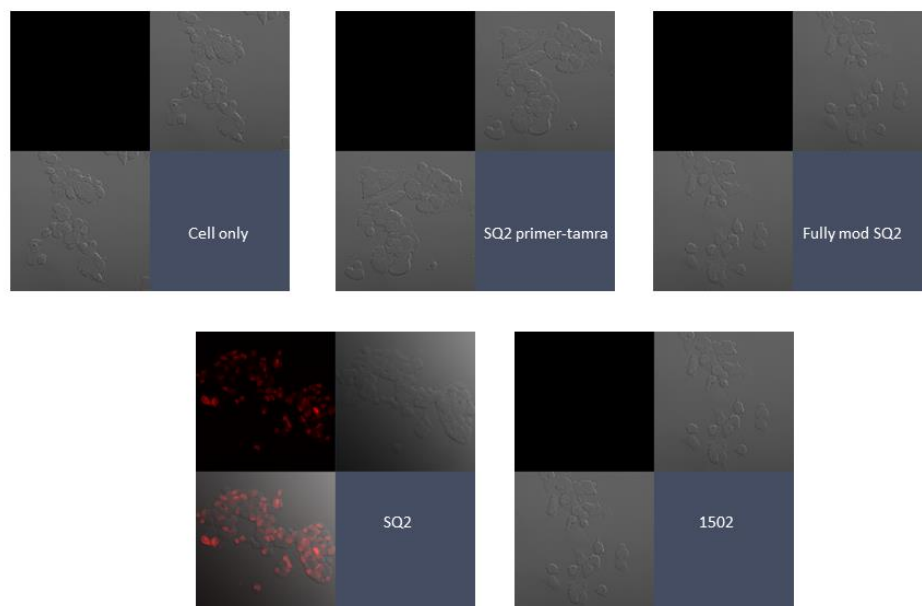


**Figure 2.8.g.** Aptamers SQ-2 (tamra labeled) and 1502 (sima labeled) at a 300 nM concentration, were tested against LoVo cells at 4°C for 30 min. The literature indicates that LoVo has a high ALPPL-2 expression and it was therefore expected that binding was observed for SQ-2. When tested, binding was not observed for 1502, however, suggesting that 1502 does not have a strong binding affinity for ALPPL-2. Cell only, the tamra-antisense oligo, and a fully modified non-functional labeled SQ-2 aptamer were used as controls and showed no binding to LoVo cells.

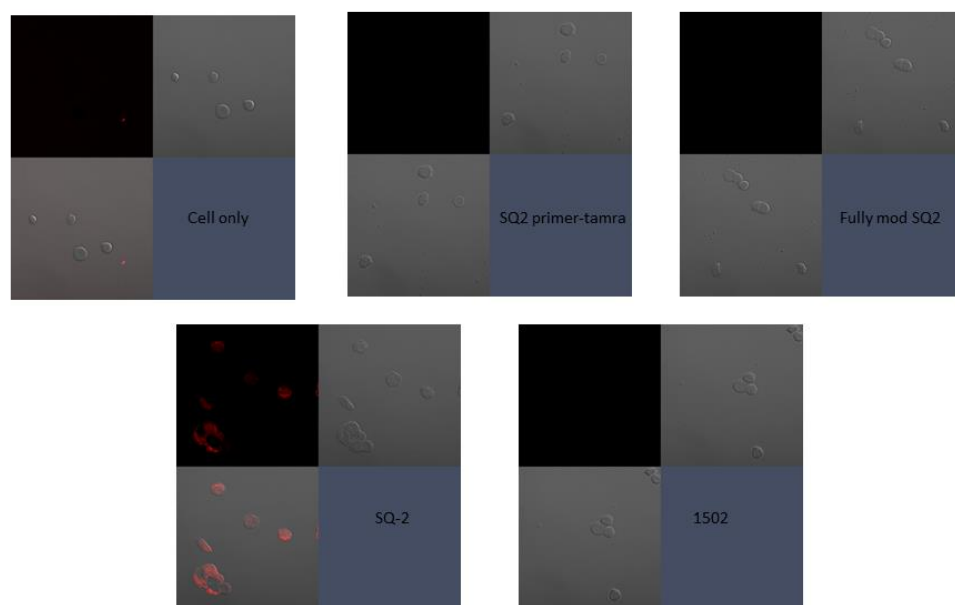


**Figure 2.8.h.** Aptamers SQ-2 (tamra labeled) and 1502 (sima labeled) at a 300 nM concentration, were tested against SW837 cells at 4°C for 30 min. The literature indicates that SW837 has a high ALPPL-2 expression and it was therefore expected that binding was observed for SQ-2. When tested, binding was not observed for 1502, however, suggesting that 1502 does not have a strong binding affinity for ALPPL-2. Cell only, the tamra-antisense oligo, and a fully modified non-functional labeled SQ-2 aptamer were used as controls and showed no binding to SW837 cells.



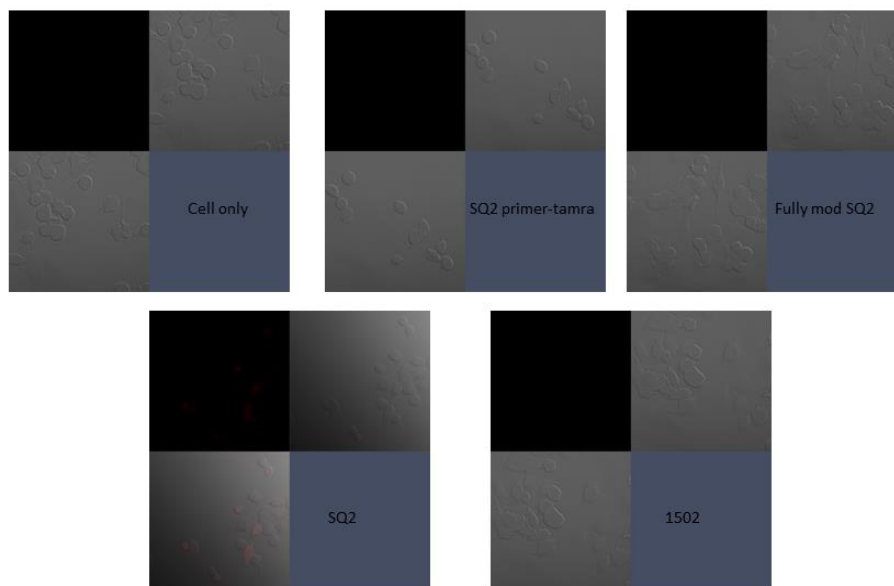


**Figure 2.8.i.** Aptamers SQ-2 (tamra labeled) and 1502 (sima labeled) at a 300 nM concentration, were tested against A549 cells at 4°C for 30 min. The literature indicates that A549 cells have a slightly elevated ALPPL-2 expression and it was therefore expected that there would be some binding observed for SQ-2. It is also suggested by the literature that A549 has a high expression of cyclophilin B. Aptamer 1502, as well as controls, cell only, the tamra-antisense oligo, and a fully modified non-functional labeled SQ-2 aptamer showed no binding to A549 cells, suggesting that cyclophilin B is not the unknown target of 1502.

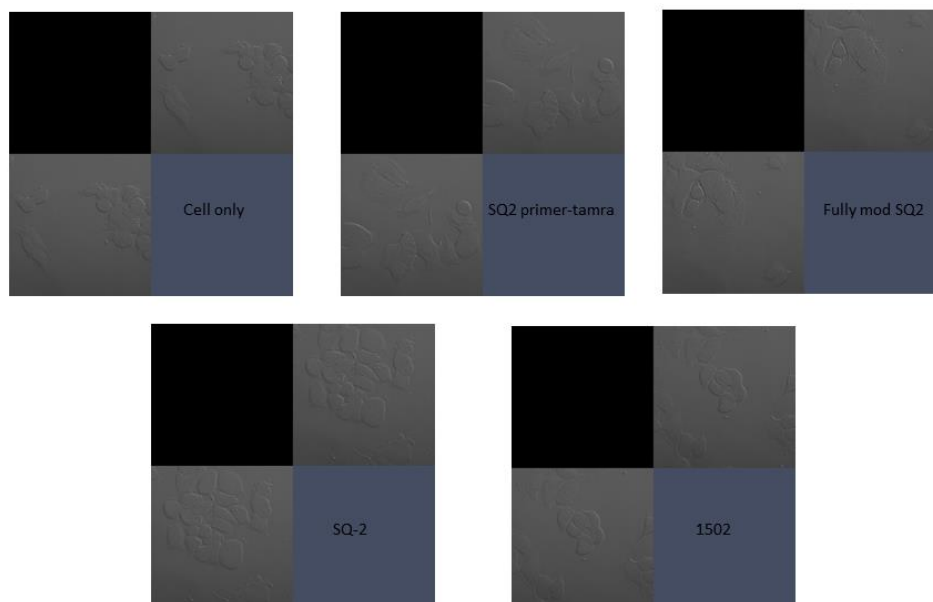


**Figure 2.8.j.** Aptamers SQ-2 (tamra labeled) and 1502 (sima labeled) at a 300 nM concentration, were tested against MCF7 cells at 4°C for 30 min. The literature indicates that MCF7 cells have a low expression of ALPPL-2 and a relatively high expression of cyclophilin B. There was no observed binding of aptamers SQ-2 or 1502, as well as controls, cell only, the tamra-antisense oligo, and a fully modified non-functional labeled SQ-2 aptamer showed no binding to A549 cells, suggesting that cyclophilin B is not the unknown target of 1502.

By testing Sima-1502 against targeted PDAC cell lines, non-binding normal pancreas HPNE, ALPPL-2 positive non-PDAC cell lines, and cyclophilin B positive non-PDAC cell lines, and comparing the qualitative binding of 1502 to ALPPL-2 targeting aptamer SQ-2, the results suggest that aptamer 1502 does not target the PDAC biomarkers ALPPL-2 or cyclophilin B. Because the target of 1502 is still unknown, it was important to test for its binding to recently proven biomarkers of pancreatic adenocarcinoma. We believe that aptamer 1502 could be targeting a novel biomarker overexpressed specifically on PDAC cell lines, and that this target can be therefore very useful in further diagnostic and therapeutic development.

### **2.3 Concluding Remarks**

This chapter highlights the extensive chemical synthesis and characterization of 2'-F RNA aptamer 1502. The synthesis was done on an ABI oligosynthesizer that was rebuilt and reprogrammed to facilitate low volume DNA and RNA solid-phase oligo synthesis. Cleavage, deprotection, and purification was customized and performed successfully for over 20 DNA and RNA variations of 1502, as seen by the PAGE denaturing gel analysis and quantification. The large scale synthesis and straight forward 3' and 5' modifications allowed for extensive characterization and application of these aptamers in subsequent studies, something that would be much more difficult with enzymatic synthesis.

The initial binding affinity characterization that was done with Sima-labeled 1502 proved that this aptamer does bind to the cell surface of AsPC-1 and not HPNE cells. Quantification of this binding affinity with flow cytometry indicated a slightly stronger binding affinity of 1502 to AsPC-1 with 125 nM binding, with no observable binding to HPNE. A liver cancer cell line, HepG2 was tested based on the knowledge that these two cell lines have shared biomarkers, and

that 1502 may be binding to one of these cell-surface proteins. Indeed, there was observable cell-surface binding of Sima-labeled 1502 to HepG2, seen with confocal microscopy and flow cytometry. These results will be useful when continuing the biomarker identification studies and was utilized in the targeted hyperthermia experiments, seen in Chapter 3.

## **2.4 Materials and Methods**

### **2.4.a. Chemical synthesis with an 394 ABI Oligosynthesizer**

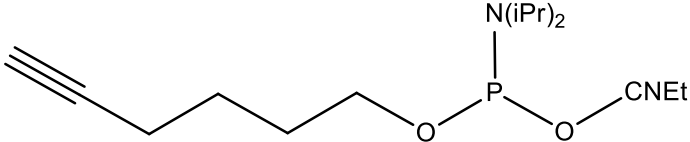
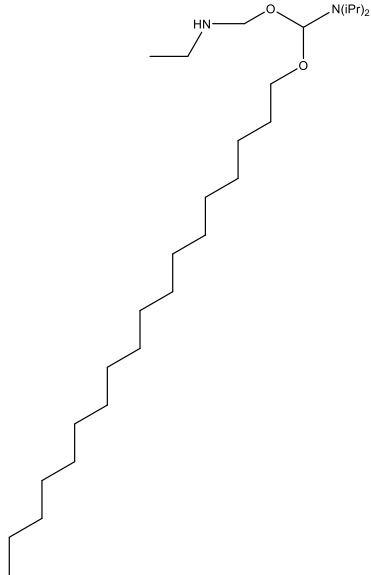
The optimized truncated RNA aptamers were chemically synthesized with an ABI 394 Oligosynthesizer (Table 2.1). These aptamers were modified on the 3' or 5' end with various linkers, fluorescent groups, and functional chemistries. A comprehensive list of these modifiers can be found in Table 2.2. To facilitate deprotection under relatively milder conditions, we used TBDMS-protected ultra-mild phosphoramidites and reagents (Chem Genes and Glen Research) for the oligosynthesis. Table 2.3 illustrates the full list of reagents used for both DNA and RNA synthesis. For DNA aptamers, the cycle used was a normal volume CE cycle, synthesizing at either a 40 nmol or 200 nmol scale. For the RNA aptamers synthesized, the cycle was programmed to have longer coupling times with lower volumes of reagents needed, using low volume polystyrene columns (Glen Research). Oligos were synthesized with DMT on, a manual deprotection, and could be monitored throughout by trityl reports. Aptamer synthesis took anywhere from 4 to 16 h, depending on the length of the oligo and the nature of the cycle.

Synthesized Aptamers	Sequence (5' to 3')	Synthesis Cycle	Scale
1502-original-Sima (Hex)	Sima- CUAUCUUGCAAGGGGAUAUAAACAGUAC UGAGUGCAUUGCAUCACGUCAGUAGdT	LV40RNAA LL	40 nmol
1502-scrambled-Sima (Hex)	Sima- CUAUCUUCUAGAGGGGAUAUAAACAGUAC UGAGUGUGCCAGAUCACGUCAGUAGdT	LV40RNAA LL	40 nmol
1502-optimized-Sima	Sima- CUAUCUUGCAAGGGGAUAUAAACAGUAC UGAGUGCAUUUCAUCACGUCAGUAGdT	LV40RNAA LL	40 nmol
1502-mutated7-Sima	Sima- CUAUCUUGCAAGGGGAUAUAAACAGUAC UGAGUGCAUUGCAUCACUUCAGUAGdT	LV40RNAA LL	40 nmol
1502-mutated11-Sima	Sima- CUAUCUUGCAAGGGGAUAUAAACAGUAC UGAGUGCAUUGCAGCACGUCAGUAGdT	LV40RNAA LL	40 nmol
1502-mutated24-Sima	Sima- CUAUCUUCUAGAGGGGAUAUAAACAGUAC UGAGUGUGCCAGAUCACGUCAGUAGdT	LV40RNAA LL	40 nmol
1502-mutated38-Sima	Sima- CGGUCGCGCAAGGCGACCUAAACAGUCC UGAGUGCAUUGCAUCACGUCAGGAGdT	LV40RNAA LL	40 nmol
1502-mutated41-Sima	Sima- CUAUCUCCAAGGGGAUAUAAACAGUAC UGAGUGCAUUGCAUCACGUCAGUAGdT	LV40RNAA LL	40 nmol
1502-mutated45-Sima	Sima- CUAUCUUGCAAAGGGGAUAUAAACAGUAC UGAGUGCAUUGCAUCACGUCAGUAGdT	LV40RNAA LL	40 nmol
Biotin-1502-original	CUAUCUUGCAAGGGGAUAUAAACAGUAC UGAGUGCAUUGCAUCACGUCAGUAG- Biotin	LV200RNA ALL	0.2 µmol, 1 µmol
1502-original-amino	Amino- CUAUCUUGCAAGGGGAUAUAAACAGUAC UGAGUGCAUUGCAUCACGUCAGUAGdT	LV40RNAA LL, LV200RNA ALL	40 nmol 1.0 µmol
1502-scrambled-amino	Amino- CUAUCUUCUAGAGGGGAUAUAAACAGUAC UGAGUGUGCCAGAUCACGUCAGUAGdT	LV200RNA ALL	0.2 µmol
1502-original-extension-phosphoryl	Phosphoryl- CGUUCGUCGCACGUAUCUUGCAAGGGGA UAUAAACAGUACUGAGUGCAUUGCAUCA CGUCAGUAGdT	LV40RNAA LL	40 nmol
1502-original-aldehyde	Aldehyde- CUAUCUUGCAAGGGGAUAUAAACAGUAC UGAGUGCAUUGCAUCACGUCAGUAGdT	LV40RNAA LL	40 nmol
1502-original-alkyne	Alkyne- CUAUCUUGCAAGGGGAUAUAAACAGUAC UGAGUGCAUUGCAUCACGUCAGUAGdT	LV200RNA ALL	0.2 µmol
1502-scrambled-alkyne	Alkyne- CUAUCUUCUAGAGGGGAUAUAAACAGUAC UGAGUGUGCCAGAUCACGUCAGUAGdT	LV40RNAA LL	40 nmol
1502-original-stearyl	Stearyl- CUAUCUUGCAAGGGGAUAUAAACAGUAC	LV200RNA ALL	0.2 µmol, 1.0 µmol

	UGAGUGCAUUGCAUCACGUCAGUAGdT		
1502-scrambled-stearyl	Stearyl- CUAUCUUCUAGAGGGGAUUA AACAGUAC UGAGUGUGCCAGAUCACGUCAGUAGdT	LV200RNA ALL	0.2 µmol
1502-antisense (DNA)	ATGCAATGCACTCAGTACTGTTTATATCC CCTTGCAAGATACGG	0.2 µmol CE	0.2 µmol
1502-aldehyde (DNA)	Aldehyde- CTATCTTGCAAGGGGATATAAACAGTACT GAGTGCATTGCATCACGTCAGTAG	0.2 µmol CE	0.2 µmol
1502-amino (DNA)	Amino- CTATCTTGCAAGGGGATATAAACAGTACT GAGTGCATTGCATCACGTCAGTAG	0.2 µmol CE	0.2 µmol

**Table 2.1** Chemically synthesized truncated RNA and DNA aptamers and their sequences.

Modifier	Structure
Sima (hex) phosphoramidite	
3'Biotin-TEG CPG	
5' –Amino-Modifier C6-PDA	
Chemical Phosphorylation Reagent II	
5'-Aldehyde-Modifier C2 Phosphoramidite	

5'-Hexynyl Phosphoramidite	
Stearyl Phosphoramidite	

**Table 2.2** Chemical modifiers synthesized on the 3' and 5' ends (Glen Research).

General Oligosynthesis Reagents	DNA Oligosynthesis Reagents	RNA Oligosynthesis Reagents
LV polystyrene columns (dT), (dG)	dG-CE-phosphoramidite	iPr-Pac-G-CE Phosphoramidite
0.02M I <sub>2</sub> in THF/Pyridine/H <sub>2</sub> O	dC-CE-phosphoramidite	2'-F-Ac-C-CE Phosphoramidite
Dichloromethane	dT-CE-phosphoramidite	2'-F-U-CE Phosphoramidite
Acetonitrile	0.45 M Tetrazole in Acetonitrile	0.25M 5-Ethylthio-1H-tetrazole in Acetonitrile
Deblocking Mix (3% TCA/DCM)	Cap Mix A (THF/Pyridine/Ac <sub>2</sub> O)	Cap Mix A (THF/Pyridine/Pac20)

**Table 2.3** List of oligosynthesis reagents used for DNA and RNA synthesis.

#### **2.4.b. Cleavage, deprotection, and purification of aptamers**

For the DNA control aptamers, the oligos were cleaved and base-deprotected with 30% ammonium hydroxide (Sigma) for 16 h at 55°C. The supernatant was dried and resuspended in TE with 50 mM NaCl.

The RNA oligos were cleaved and base-deprotected with a fresh 1:1 solution of 30% ammonium hydroxide and 40% methylamine (AMA) at room temperature for 2 h. The supernatant was dried to a pellet, and the RNA was resuspended in 100 µL anhydrous DMSO. If necessary, the oligo was heated to 65°C for 5 min to get it into solution. To deprotect the 2'-silyl groups, triethylamine trihydrofluoride (TEA.3HF) was added to the sample and the mixture was heated to 65°C for 2.5 h. The deprotected oligo was desalted by a Nap 5 column or ethanol precipitation. The concentration was measured by NanoDrop and the aptamer length was confirmed by a PAGE denaturing gel. The RNA aptamers were stored in DEPC-treated water at -20°C.

To purify the aptamers, the oligos with MMT on the 5' end, were flushed through a GlenPak DNA cartridge (Glen Research) to remove abortive sequences, followed by cleavage of the MMT protecting group to result in a purified full-length oligo.

#### **2.4.c. Cell culture**

AsPC-1 (pancreatic ductal adenocarcinoma), PANC-1 (pancreatic ductal adenocarcinoma), CAPAN-1 (pancreatic ductal adenocarcinoma), CFPAC-1 (pancreatic ductal adenocarcinoma), hTERT-HPNE (pancreatic ductal epithelial cell), LNCaP (prostate adenocarcinoma), BxPC-3 (pancreatic ductal adenocarcinoma), HPAF-II (pancreatic ductal adenocarcinoma), Hs766T (pancreatic ductal adenocarcinoma), SW1990 (pancreatic ductal



adenocarcinoma), COLO 587 (pancreatic ductal adenocarcinoma), Mia-Paca-2 (pancreatic carcinoma), Hep3B (hepatocellular carcinoma), PC-3 (prostate adenocarcinoma), DU 145 (prostate carcinoma), A549 (lung carcinoma), SK-OV-3 (ovarian adenocarcinoma), MCF7 (breast adenocarcinoma), HT-29 (colorectal adenocarcinoma), A431 (epidermoid carcinoma), MCF7 (breast adenocarcinoma), SW837 (rectal adenocarcinoma), and LoVo (colon adenocarcinoma) were purchased from the Tissue Culture Facility at Lineberger Cancer Center, UNC. These cells originated from the American Type Culture Collection (ATCC) cell repository and were therefore validated through this source. HepG2 (hepatocellular carcinoma) and Huh7 (hepatocellular carcinoma) were acquired through a collaborator. Cell culture was maintained at 37°C and 5% CO<sub>2</sub> in various mediums which included RPMI 1640, EMEM with NEAA, McCoy's 5a, DMEM/F12, Leibovitz's L-15, IMDM, F-12K, or DMEM medium supplemented with 10% heat-inactivated fetal bovine serum, FBS (GIBCO) and 100 units/ml penicillin–streptomycin (Cellgro), along with additional supplements when necessary.

#### **2.4.d. Confocal microscopy**

The binding of selected pools and individual aptamers to target cells was evaluated by fluorescence confocal imaging. Cells tested included AsPC-1, HPNE (control), and two additional liver cancer cell lines, HepG2 and Huh7. Cells were incubated with various concentrations, ranging from 0 to 1000 nM, of Sima-labeled aptamers in 200 µL binding buffer (1x PBS with 5 mM Ca<sup>2+</sup> and 1 mM Mg<sup>2+</sup>) at 4°C for 30 minutes. The Sima-labeled aptamers tested included Sima-original 1502, Sima-scrambled 1502 (control), and Sima-optimized 1502. After washing, cells were fixed with 1.5% paraformaldehyde (PFA), for 10 min in the dark at room temperature. The cover glass containing the cells and sample was transferred to a slide with

cell-adhesion solution (company) for examination with a confocal microscope. Fluorescence confocal imaging was performed on a Zeiss LSM 700 confocal microscope in the UNC School of Medicine Microscopy Services Laboratory. The objective used for imaging was a 40X oil-immersion objective.

#### **2.4.e. Flow cytometry**

To monitor the enrichment of aptamers along with the progress of SELEX and quantify the cell-binding of individual aptamers, Sima-labeled aptamer, Sima-original-1502, which is also termed 1502, was incubated with  $1 \times 10^6$  cells in 400  $\mu$ L binding buffer at 4°C for 30 min. Similar to the confocal microscopy testing, the cell lines tested included AsPC-1, HPNE (control), and two additional liver cancer cell lines, HepG2 and Huh7. Cells were washed twice after incubation and analyzed by flow cytometry. Flow cytometry was performed on a FACScan cytometer with CellQuest software (Becton Dickinson).  $K_d$  was calculated by this software using the following equation:  $Y = B_{\max} * X / (K_d + X)$ . Nonspecific binding was also calculated using cell only controls and subtracted from the tested samples.

#### **2.4.f. Immunohistochemistry with (Patient-Derived Xenograft) PDX Tissue Samples**

Patient derived xenograft tissue samples from 3 patients were tested to determine if aptamer 1502 could bind to human tissue. AsPC-1 tumor tissue were tested as a positive control, and A375 tumor (melanoma) tumor tissue was the negative control. Paraffin embedded tissue samples were prepared by the UNC Histology Core. Staining wells were filled with xylene to remove the paraffin, and tissue samples were soaked in the wells for 10 min. This was done a second time with fresh xylene. Tissue samples were rinsed in various ethanol in water

preparations (100%, 95%, 70%, 50%, and 30%) for 2 min each to continue this process. Tissue plates were rinsed with PBS and kept in a 1 M Tris buffer, pH 8.0 which was heated to 95°C for 15 min. Plates were saturated with the RNA binding buffer at room temperature in a humidified chamber. Finally, 500 nM of TAMERA-labeled 1502, previously prepared by Dr. Hui Chen, was added to the plates at 4°C for 30 min in the dark. The aptamer was then removed and plates washed with the binding buffer 2X, and the plates were left to dry in the dark at room temperature overnight. A BX-61 microscope, with a 10X objective lens, was used to take images of the tissue samples.

#### **2.4.g. Serum stability assay**

Three synthesized 2'-F RNA aptamers were tested for their stability in mouse serum (Life Technologies). This included three 1502 RNA aptamers with 5' modifications; 1502-original-stearyl, 1502-original-amino, and 1502-original-phosphoryl. 5 pmol of the aptamers was incubated with either 10 or 50% mouse serum at 37°C for varied time points (0, 5 min, 2, 4, 8, 12, and 24 h). This experiment was repeated 3X for reproducibility. All samples were examined by PAGE gel electrophoresis.

#### **2.4.h. Determining if known PDAC-targeted aptamers have the same target as 1502**

To determine if aptamer 1502 has the same target as recently selected PDAC aptamers, M9-5 (that targets cyclophilin B) and SQ-2 (that targets ALPPL-2), it is important to compare the binding of the three aptamers *in vitro*. Primers were designed to assemble and synthesize M9-5 and SQ-2 DNA sequences. The DNA was transcribed into partially modified 2'-F C/U RNA using LAR T7 polymerase. It is important to note that aptamer M9-5 has not been efficiently

transcribed to date, and therefore the cell binding studies have been limited. However, cell binding studies confirmed the targeting and non-targeting properties of aptamers SQ-2 and 1502 against cell lines that have higher expression levels of ALPPL-2, as well as binding studies for aptamer 1502 against cell lines with a higher expression of cyclophilin B. Additionally, a competition study was initially performed between aptamer 1502 and aptamers SQ-2 to determine if their targeting of PDAC competed with one another.

#### **2.4.i. Enzymatic synthesis of RNA aptamers M9-5 and SQ-2**

##### **2.4.i.i. Primer design**

5' and 3' primers were designed for DNA assembly for both the M9-5 and SQ-2 RNA aptamers.

SQ-2's 5' primer – 5'

TTCTAATACGACTCACTATAGGGAGATACCAGCTTATTCAATTGCCTGAAAAGCTAT  
CGCCCAATTCGCAGT 3' containing the T7 promoter (underlined) and the 3' primer - 5'  
AGATTGCACTTACTATCTTAAAGGATATCACTGCGAATTGGGCGATAGCTTTTC 3'  
was designed for Klenow.

M9-5's 5' primer – 5'

TTCTAATACGACTCACTATAGGGAGGACGATGCGGGGACCTATGCAGTAGCCAGTG  
TGGACT

3' containing the T7 promotor (underlined) and the 3' primer - 5'

AGATTGCACTTACTATCTTAAAAATTCGGGCGAGTCGTCTGGGGGGGGCAGCC  
CAGTCCACACTGGCTACTGCAT 3' was designed for assembly PCR or Klenow.

#### **2.4.i.ii. PCR/Klenow and *in vitro* transcription**

The DNA template for M9-5 was assembled through PCR. Briefly, PCR reactions contained 0.2 mM dNTPs (each), 0.2  $\mu$ M of each 5' and 3' primer, 1X Taq polymerase buffer, and 1.25 U/50  $\mu$ L reaction Taq polymerase (NEB). Through PCR titrations, 15 rounds of PCR was determined to be optimal. PCR parameters consisted of 2 min of Taq activation at 94°C, and 15 cycles of PCR at 94°C for 30 s, 58°C for 30 s, 72°C for 30 s, followed by 10 min of extension at 72°C. For SQ-2, the DNA template was assembled and amplified through a Klenow reaction. The 5' and 3' primers, at concentrations of 1.5 and 1.0  $\mu$ M respectively, were annealed by heating to 80°C followed by slow cooling to room temperature. 1X NEBuffer 2 (NEB), 0.2 mM dNTPs, and 2.5U/50  $\mu$ L reaction Klenow Fragment (3' to 5' exo-) (NEB) were added and the reaction was kept at 37°C for 1.5 h. The quality of PCR amplification and Klenow reactions were confirmed by agarose gel electrophoresis and visualized by ethidium bromide staining. Both DNA templates were purified with phenol/chloroform extraction, followed by ethanol precipitation, and resuspended in TE buffer with 5 mM NaCl.

*In vitro* transcription was performed with mutant LAR T7 polymerase (made in-house). Briefly, the transcription reactions contained 200 nM DNA template, 1X LAR T7 buffer, 1.5 mM rNTPs, including 2'-F U and 2'-F C, 6.25 mM MgCl<sub>2</sub>, 10 mM DTT, 0.8 U/100  $\mu$ L thermostable inorganic pyrophosphatase (NEB), and 0.8 U/100  $\mu$ L LAR T7 polymerase. The reactions were done at 37°C for 20 h. RNA transcripts were treated with DNase for 2 h at 37°C and EDTA at 70°C for 10 min. The RNA aptamers were purified by ethanol precipitation and resuspended in DEPC-treated water.

#### **2.4.j. Labeling of RNA aptamers with a tamra-labeled antisense oligo**

A tamra-labeled antisense sequence was designed to complement the 3' non-functional tail that is present in the SQ-2 RNA aptamer. This primer's sequence is as follows – 5' tamra-AGATTGCACTTACTATCTTAAA 3'. The SQ-2 aptamer and the tamra-antisense oligo were combined at a 1:20 molar ratio. The mixture was heated to 80°C for 3 mins, followed by a slow cooling to room temperature to anneal the antisense oligo to the RNA aptamer. The resulting aptamer was diluted in 1x PBS with 5 mM  $\text{Ca}^{2+}$  and 1 mM  $\text{Mg}^{2+}$ , to the desired concentration for the cell binding and competition studies.

#### **2.4.k. Competition study between aptamer 1502 and SQ-2**

To determine if aptamer 1502 competes with aptamer SQ-2 in binding to ALPPL-2, Sima-labeled 1502 was mixed with unlabeled SQ-2 at a 1:1, 1:3, and 1:6 molar ratio with a 200 nM 1502 concentration. These mixtures were incubated with AsPC-1 cells for 30 min at 4°C. Sima-1502 was also tested on AsPC-1 cells to confirm it's functionality of binding to AsPC-1. The cells were washed once with 1X PBS and transferred to slides with cell-adhesion solution. The Zeiss 700 confocal microscope with a 40X objective oil lens was used to visualize cell-surface binding.

#### **2.4.l. Binding of aptamers 1502 and SQ-2 to targeted and non-targeted cell lines**

The functionality of the tamra-labeled aptamer, SQ-2 was confirmed by incubation at a 300 nM concentration with AsPC-1 and HPNE (control) cells at 4°C for 30 min. Sima-1502 was also tested at 300 nM to confirm it's functionality. The cells were washed once with 1X PBS and

transferred to slides with cell-adhesion solution. The Zeiss 700 confocal microscope with a 40X objective oil lens was used to visualize cell-surface binding.

To continue the comparison of binding to differing PDAC cell lines, tamra-labeled SQ-2 and Sima-1502 aptamers were tested against some of these PDAC and non-pancreatic cancer cell known to have high or low expression of ALPPL-2. The demonstrated binding of these aptamers, visualized with confocal microscopy, can help to indicate if 1502 binds to SQ-2's PDAC target, ALPPL-2. Cell lines were initially chosen based on the literature for PDAC cell lines tested with aptamer SQ-2. The SQ-2 binding cell lines included Capan-1, Panc-1, and AsPC-1. The non-binding cell lines included HPNE, MiaPaca-2, and CFPAC-1. The aptamers were incubated with the cell lines separately at 300 nM at 4°C for 30 min. Additional controls included cell only, tamra-antisense oligo only, and a fully modified non-functional SQ-2 aptamer, labeled with the tamra oligo. The cells were washed once with 1X PBS and transferred to slides with cell-adhesion solution. The Zeiss 700 confocal microscope with a 40X objective oil lens was used to visualize cell-surface binding.

To complete the study, we introduced different cell lines that are known to have a higher expression of ALPPL-2, a colorectal adenocarcinoma, LoVo, and a rectal adenocarcinoma, SW837. The same conditions and controls, as listed above, were applied.

Finally, although we didn't have the M9-5 aptamer synthesized, we tested Sima-labeled 1502 against two cell lines that are known to have a higher expression of cyclophilin B. These cell lines included lung carcinoma cells, A549 (which also has some expression of ALPPL-2), and a breast adenocarcinoma cell line, MCF7. The same controls and conditions, as performed for the PDAC cell lines seen above, applied for the cyclophilin B experiment.

## **CHAPTER III**

### **TARGETED HYPERTHERMIA APPLICATION OF 1502 FUNCTIONALIZED GOLD NANOPARTICLES DEMONSTRATES THE SPECIFICITY OF 1502 TO PANCREATIC DUCTAL ADENOCARCINOMA**

#### **3.1 Introduction**

We know from the selection performed by Dr. Chen, and the additional characterization done in Aim 1, that aptamer 1502 does bind to the cell surface of PDAC cell line, AsPC-1, and not normal pancreas, HPNE. We also know that aptamer 1502 can bind to one liver cancer cell line tested, HepG2. This could aid in the biomarker identification and is reasonable considering that liver cancer and PDAC are known to share characteristic molecular indicators<sup>30-32</sup>.

However, this finding could call into question the specificity of aptamer 1502 to pancreatic ductal adenocarcinoma, the type of cancer that the series of aptamers were selected against. It is therefore critical to further identify aptamer 1502's specificity against pancreatic cancer, liver cancer, and non-pancreatic cancer. To do so, we need to develop a sensitive and accurate platform that can identify the targeted cell lines over the cell lines that are not targeted by aptamer 1502.

In addition to further characterizing the targeting capabilities of aptamer 1502 against PDAC and non-PDAC cell lines, it would be useful to develop an assay that could take advantage of the internalization properties of aptamer 1502, which was observed when the aptamer was incubated with AsPC-1 cells at 37°C (seen in the preliminary data from Chapter 1).



Although the mechanism of action has not been proven, we hypothesize that 1502 targets a cell-surface receptor and subsequently internalizes through receptor-mediated endocytosis. If we could characterize this delivery to other PDAC or non-PDAC cell lines, it could be extremely beneficial for targeted therapeutic delivery via aptamer 1502. This goal is a part of Aim 3 and is discussed in detail in Chapter 4.

We chose to develop a targeted hyperthermia assay by functionalizing PEGylated gold nanoparticles with aptamer 1502. We have functionalized gold nanoparticles in previous studies in our lab and know it to be a very sensitive ligand-directed cell-killing assay that would take advantage and further characterize the internalization capabilities of aptamer 1502<sup>33-34</sup>. Gold nanoparticles, and other types of plasmonic metal nanoparticles, have the capability to produce hyperthermia in cells after internalization. The theory behind this approach is that the gold nanoparticles, PEGylated for stability in salted buffers, will be directed to the cell-surface of cell lines that contain the biomarker which is targeted by 1502. The aptamer and the conjugated gold nanoparticles will be internalized by receptor mediated endocytosis (our hypothesis). A near infrared (NIR) laser at 800 nm will be used to localize radiation heat to the gold nanoparticles to an average temperature of 42°C, which is too hot for the cells to survive. This targeted hyperthermia has shown to be a non-invasive approach for cancer treatment, especially when used in conjunction with chemotherapy delivery<sup>35</sup>. This type of targeted hyperthermia allows for selective delivery of heat to only the cells that are targeted by the ligand conjugated to the nanoparticle. The gold nanoparticles are particularly efficient in this approach due to their enhanced localized surface plasmon resonance and their surface chemistry, facilitating the conjugation of biomolecules such as RNA aptamer 1502<sup>36,37</sup>.

This assay would allow for a sensitive specificity screen to be done across several cell lines, and would also selectively kill the cells targeted by aptamer 1502. The variation of aptamer 1502 that was synthesized with a 5' amino group can be converted fairly easily to a 5' dithiocarbamate with carbon disulfide and an alkaline buffer. This modification will have two thiol groups that can conjugate to the gold's surface, functionalizing the nanoparticle to target cell lines that overexpress the RNA ligand's unknown biomarker.

## **3.2 Results and Discussion**

### **3.2.a. Characterization with the zeta sizer**

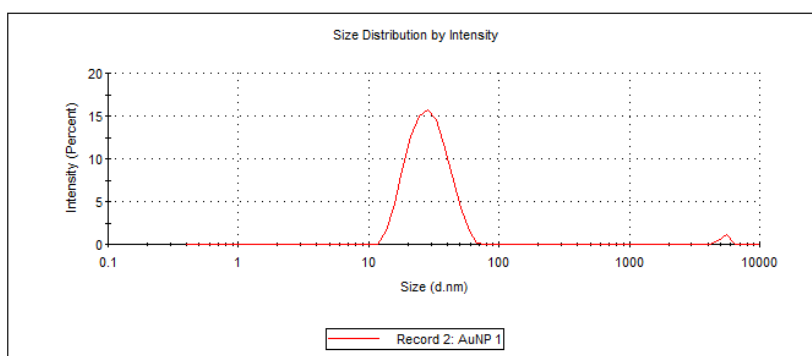
While the 30 nm citrate coated gold nanoparticles are commercially available, and were purchased and quality controlled by Nanocomposix, it is important to validate their size, polydispersity index, and zeta potential and to further characterize the 1502 aptamer functionalized gold nanoparticle. The Zeta Sizer was used for this characterization, with measurements taken for three samples, 3X and averaged with a standard deviation. The results for size, PDI, and zeta potential for the gold nanoparticle and aptamer functionalized gold nanoparticle can be seen in Figure 3.1. The gold nanoparticle measured an average size of  $27.81 \pm 9.986$  nm and a PDI of 0.251. The 1502 functionalized gold nanoparticle measured an average size of  $47.61 \pm 7.328$  nm and a PDI that was a little higher at 0.413. With the 1502 aptamer measuring approximately 8 nm in length, this increase in size is what we would expect. This increase in size also indicates that the aptamer successfully conjugated to the gold nanoparticles. The zeta potential measurements were taken of the same group of samples, and measured to be  $-48.8$  mV  $\pm 9.2$  for the gold nanoparticle and  $-52.3$  mV  $\pm 10.1$  for the 1502-gold nanoparticle.

These values are within the expected values for gold nanoparticles and aptamer functionalized gold nanoparticles.

A)

### 30 nM Gold Nanoparticle

	Size (d.nm):	% Intensity:	St Dev (d.nm):
<b>Z-Average (d.nm):</b> 27.81	<b>Peak 1:</b> 29.56	98.5	9.986
<b>Pdl:</b> 0.251	<b>Peak 2:</b> 5357	1.5	340.3
<b>Intercept:</b> 0.907	<b>Peak 3:</b> 0.000	0.0	0.000
<b>Result quality :</b> Good			



B)

### 1502-Gold Nanoparticle

	Size (d.nm):	% Number:	St Dev (d.nm):
<b>Z-Average (d.nm):</b> 47.61	<b>Peak 1:</b> 25.84	100.0	7.328
<b>Pdl:</b> 0.413	<b>Peak 2:</b> 0.000	0.0	0.000
<b>Intercept:</b> 0.865	<b>Peak 3:</b> 0.000	0.0	0.000
<b>Result quality :</b> Good			

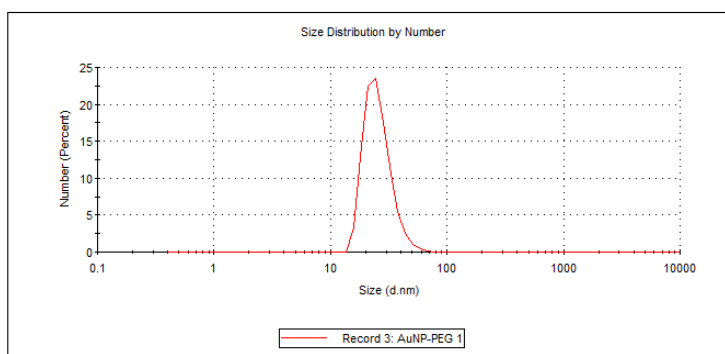


**Figure 3.1** Gold nanoparticle size and polydispersity index of A) 30 nm gold nanoparticles and B) 1502-gold nanoparticles measured with a Malvern Zeta Sizer.

### **3.2.b. Hyperthermia Studies Using Gold nanoparticles targeted with 1502**

The presence of the putative 1502-binding receptor in PDX tumors prompted us to take advantage of this aptamer for more detailed specificity studies on the whole panel of PDAC cell lines. We first tested whether this 1502 could be immobilized on the surface of gold nanoparticles (AuNPs) to target the killing of bound cancer cells using the AuNP-mediated hyperthermia effect.

To introduce aptamer 1502 to AuNPs, we synthesized the aptamer with a 5' amino group, which can react with carbon disulfide to form a dithiocarbamate, a functional group that has been reported to adsorb much more strongly onto gold nanoparticles (AuNPs) than monothiols. Using a modified protocol based on that in the literature<sup>38</sup>, we were able to generate PEGylated AuNPs targeted against PDAC with aptamer 1502.

There was some trial and error to stabilize the citrate coated gold nanoparticles against aggregation, a common potential issue with metallic nanoparticles. For this formulation, the optimal protocol that allowed for nanoparticle stability, was to add 1000:1 molar ratio of PEG-2000-thiol (to the gold nanoparticles) first to a 1X PBS buffer, followed by the nanoparticles. This allowed for the negatively charged citrate coated gold nanoparticles to stabilize in the 1X PBS buffer and prevented significant aggregation as well. The aptamer, at varying molar ratios, as seen below, was added last after the nanoparticles were stabilized.

### **3.2.c. Optimization of Aptamer to Gold Nanoparticle Ratio**

Since aptamers can interact with each other by base-pairing and abolish the desired target-binding function when they are present closely in space, it is of great importance to tune the density of the aptamer on the AuNPs surface. The ratio of aptamer to gold nanoparticle was

optimized based on the effective cell-killing of AsPC-1 in the targeted hyperthermia assay by examining the 1502:gold nanoparticle molar ratio at  $\leq 1000:1$ ,  $\leq 400:1$ ,  $\leq 200:1$ ,  $\leq 20:1$ , and  $\leq 2:1$ , respectively. We chose these ratios to initially test a wide range of aptamer to nanoparticle ratios. The values weren't chosen or optimized based on the conjugation efficiency of the aptamer to nanoparticle, but on the relative cell-killing effect, as mentioned above.

Due to the sensitive nature of the nanoparticle's stability in the 1X PBS buffer, free aptamer 1502 could not be removed without nanoparticle aggregation. Several methods were tried, however it appeared that the aptamer present in solution (whether conjugated or free) helped to stabilize the nanoparticles further and could not be removed. The ratio values have therefore been listed as  $\leq$  because it represents the input of the aptamer compared to the gold nanoparticle. We believe that at higher ratios, there may be more unconjugated 1502 in solution due to the decreased surface area available on the nanoparticles as well as the increased steric interactions of the aptamers that were conjugated. These steric interactions would make it difficult for 1502 to fold into its functional secondary structure, and therefore have less effective targeting than ratios that allowed for proper aptamer folding.

Each ratio was tested on AsPC-1, HepG2, and HPNE (data not shown) cell lines to determine the optimal formulation for effective targeting and subsequent cell killing through the targeted hyperthermia assay. After treatment with live/dead cell assay dyes, samples were visualized with confocal microscopy, as seen in Figure 3.2.

While all of the ratios had some cell killing effect, it appeared that  $\leq 20:1$  was the most effective in targeted cell death of AsPC-1 cells, whereas the negative control (the DNA version of the aptamer) did not show any targeting or cell-killing effect. The ratio of  $\leq 2:1$  had a cell

killing effect as well, however it was not as strong as the  $\leq 20:1$  ratio. It is this aptamer to gold nanoparticle ratio that was used in subsequent targeted hyperthermia studies.

It is worth mentioning that the DNA aptamer 1502 with a 5'-amino was used in this study because the 1502-scrambled-RNA sequence wasn't synthesized until this study was already complete. While the DNA aptamer was a negative control, the 1502-scrambled-RNA is a more relevant control and could be conjugated to the gold nanoparticle and tested on the various cell lines to further confirm the results.

It is interesting to note the differences of AsPC-1 and HepG2. The most effective ratio for HepG2 appears to be  $\leq 400:1$ . This optimized ratio suggests that more aptamers are needed for the targeting and internalization of the gold nanoparticle into HepG2 cell lines; results that conflict with the binding affinity of 60 nM seen in Chapter 2. AsPC-1 has a slightly lower binding affinity, and yet in this study, the best conditions for AsPC-1 was  $\leq 20:1$ , suggesting that this cell line needs less aptamer's on the gold nanoparticle to have the same targeting, internalization, and cell-killing effect. These differing results could be due to the varying target expression profiles and internalization properties of AsPC-1 and HepG2. Additionally, there is a chance that aptamer 1502 binds to different targets on AsPC-1 and HepG2, which would mean that the two cell lines couldn't be directly compared for the aptamer's binding affinity.

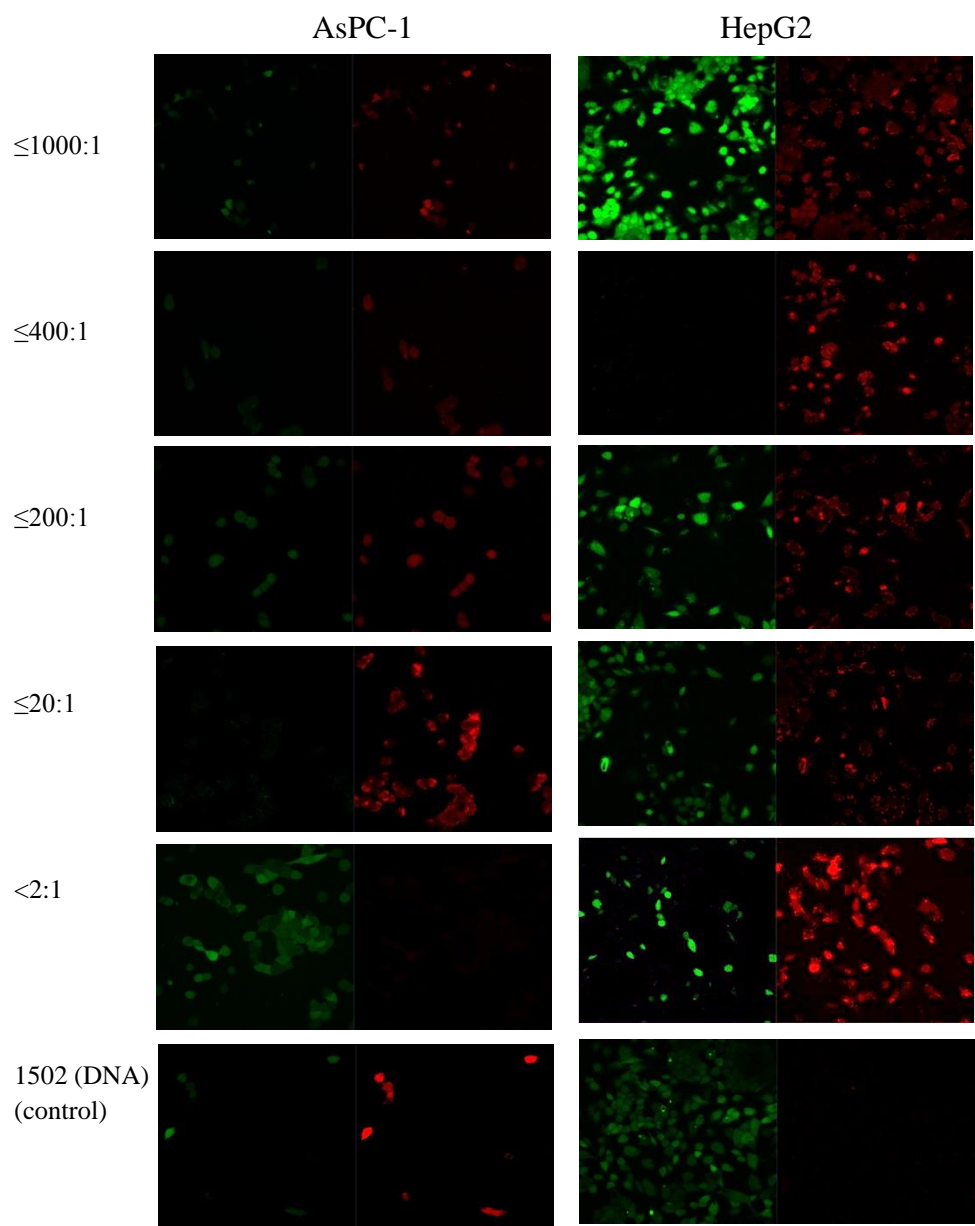


**Figure 3.2** The hyperthermia cell killing effect of AuNPs with different molar ratios of 1502 aptamer:AuNPs.

Although the 1502-gold nanoparticles were prepared in predicted ratios of  $\leq 20:1$ , there was a need to determine actual loading of the aptamer to the gold nanoparticles to further quantify this targeted hyperthermia effect. After centrifugation of the 1502-gold nanoparticles at the varying aptamer:gold nanoparticle ratios, the NanoDrop was used to measure the aptamer concentration of the resuspended gold nanoparticle pellets.. These measurements were compared to a standard curve of the input concentrations to determine the actual concentration of 1502 conjugated to the gold nanoparticles at each tested ratio.

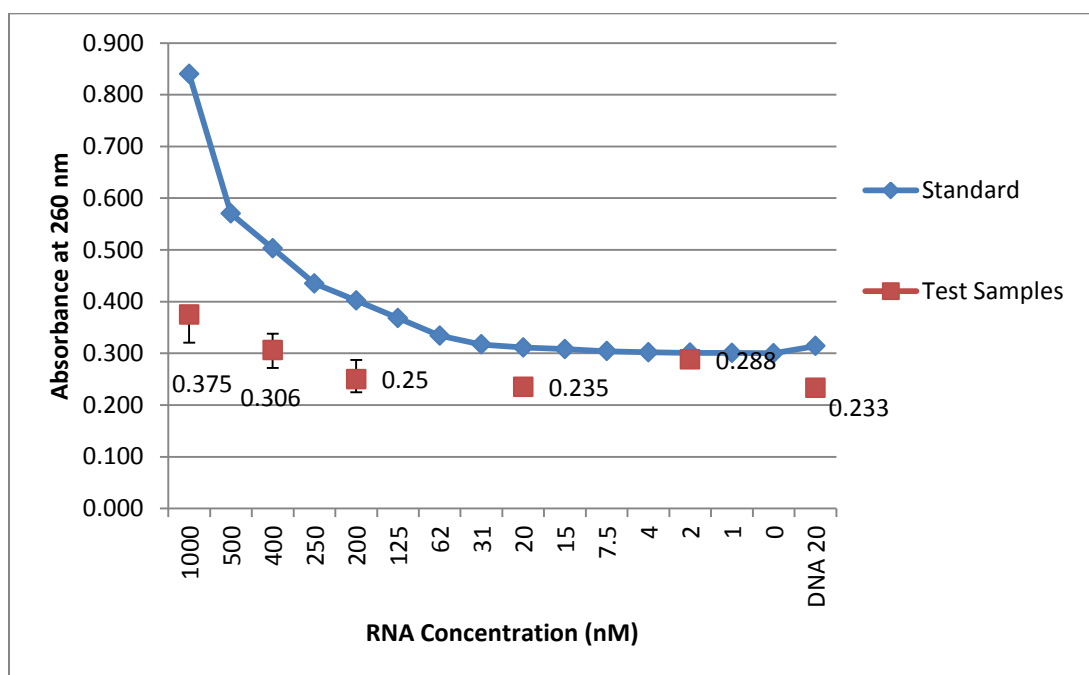


**Figure 3.3** This graph represents the raw absorbance data at 260 nm (observed for RNA) for both the standard concentrations of 0 to 1000 nM of 1502 RNA, seen in blue, and the tested 1502:gold nanoparticles in red, with free 1502 removed.



Input Aptamer for Labeling (nM)	Actual Labeling (nM)	Conjugation Efficiency (%)
2	1.91	95.7
DNA 20	14.8	74.2
20	15.1	75.6
200	124	62.2
400	243	60.8
1000	446	44.6

**Table 3.1** This table shows the calculated actual labeling concentration of 1502 when compared to the input concentration. The overall conjugation efficiency of 1502 to the gold nanoparticle is seen on the right.

The decreased loading and conjugation efficiency with increasing input concentration is understandable due to the steric and charge limitations of the aptamers on the surface of the nanoparticles. The targeted hyperthermia data, seen in Figure 3.2, further supports this conclusion. Although there is a higher concentration of 1502, the cell killing effect is not improved with concentrations above 20 nM for AsPC-1 cells. Even if a higher concentration of aptamers can be conjugated to the gold nanoparticle, as seen in Table 3.1, all of the aptamers may not be functional, resulting in a decrease in binding affinity and internalization.

### 3.2.d. Targeted Hyperthermia Assay against PDAC and Non-PDAC Cell Lines

We first tested the targeted hyperthermia assay with the two cell lines used for the original selection, AsPC-1 and HPNE. Controls included PBS (positive), methanol (negative), (data not shown), and IR laser only. Additionally, a non-targeting PEYylated gold nanoparticles (AuNPs) and the DNA version of 1502 were tested to determine if there was non-specific uptake of AuNPs with these two cell lines. Images were taken of both the center of the cell plate exposed to the near IR laser, and the outer edge of the plate which was not exposed. Figure 3.4 shows that only the RNA 1502-AuNP-PEG, when treated with the IR laser, can target, subsequently internalize into AsPC-1 cells, and cause cell death. This aptamer, as well as the controls, has no such effect on HPNE cells.

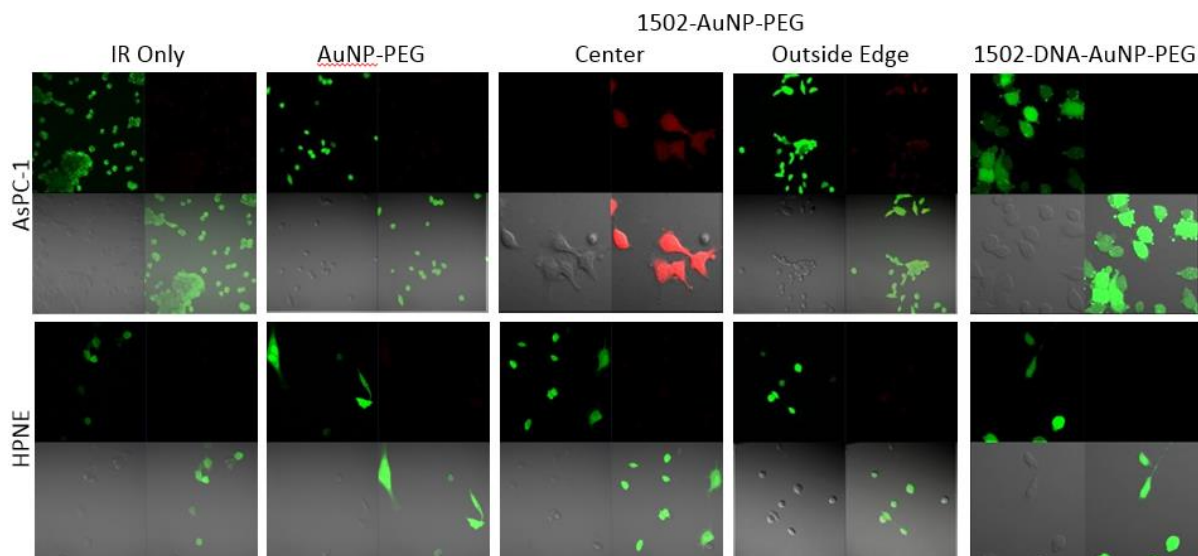


**Figure 3.4** Confocal microscopy images show effective cell killing only when the AuNPs-PEG were targeted by the aptamer ligand to AsPC-1 cells, but not normal pancreas (HPNE) cells.

The optimized conditions were applied to the hyperthermia treatment on all the 11 PDAC cell lines that are available to us, 3 liver cancer cell lines, in addition to 7 non-pancreatic cancer cell lines, that we had at our disposal, representing various organ systems. As illustrated in Figure 3.5.a.-u., it appears that 1502 is extremely specific to PDAC and pancreatic cancer cells, and not to normal pancreas, or most of non-pancreatic cell lines. It is evident that this aptamer has a specific affinity for a cell-surface biomarker that is expressed on PDAC and pancreatic carcinoma cells, and can be subsequently internalized for targeted hyperthermia treatment by a near IR laser. When this aptamer was tested on other cancer cell lines, derived from various organ systems including liver, prostate, lung, ovary, breast, colon, and skin, there was no such effect. These results indicate that our selected aptamer, 1502 is likely binding to a cell-surface biomarker that is overexpressed on the surface of pancreatic cancer but not on many other cancer or normal pancreatic cells.

### AsPC-1: Pancreatic ductal adenocarcinoma

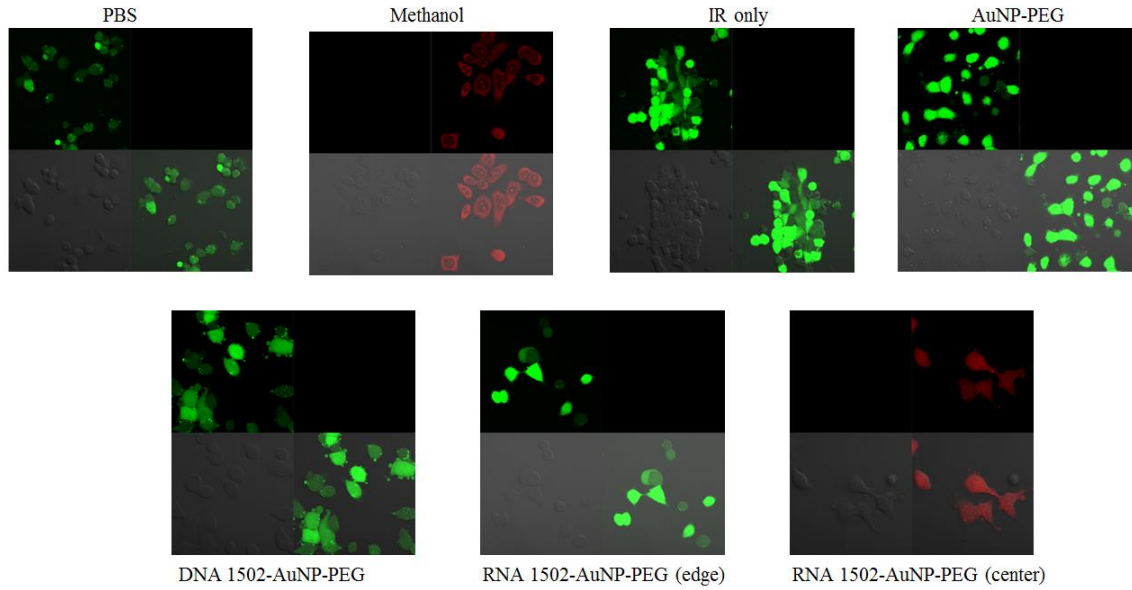


**Figure 3.5.a.** When conjugated to a PEGylated AuNP and treated with an IR laser, RNA aptamer, and not DNA aptamer 1502 can explicitly target, internalize, and subsequently kill AsPC-1 cells. Controls, including AuNP-PEG do not have a targeted hyperthermia on AsPC-1 cells.

### HPNE: Normal Pancreas

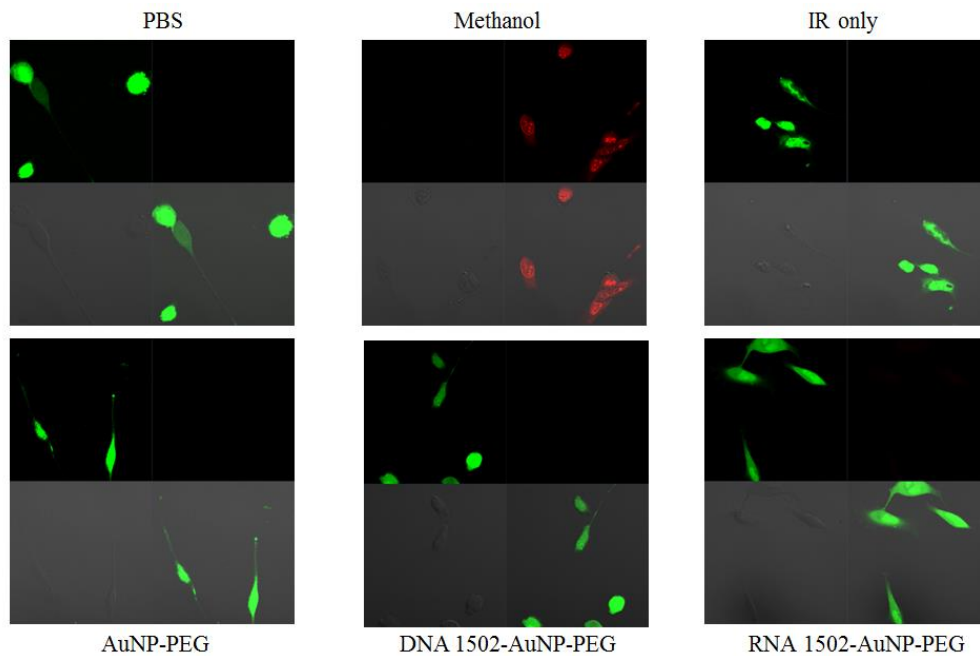


**Figure 3.5.b.** When conjugated to a PEGylated AuNP and treated with an IR laser RNA aptamer and DNA aptamer 1502, as well as AuNP-PEG has no targeted hyperthermia effect on HPNE cells.

### Capan-1: PDAC

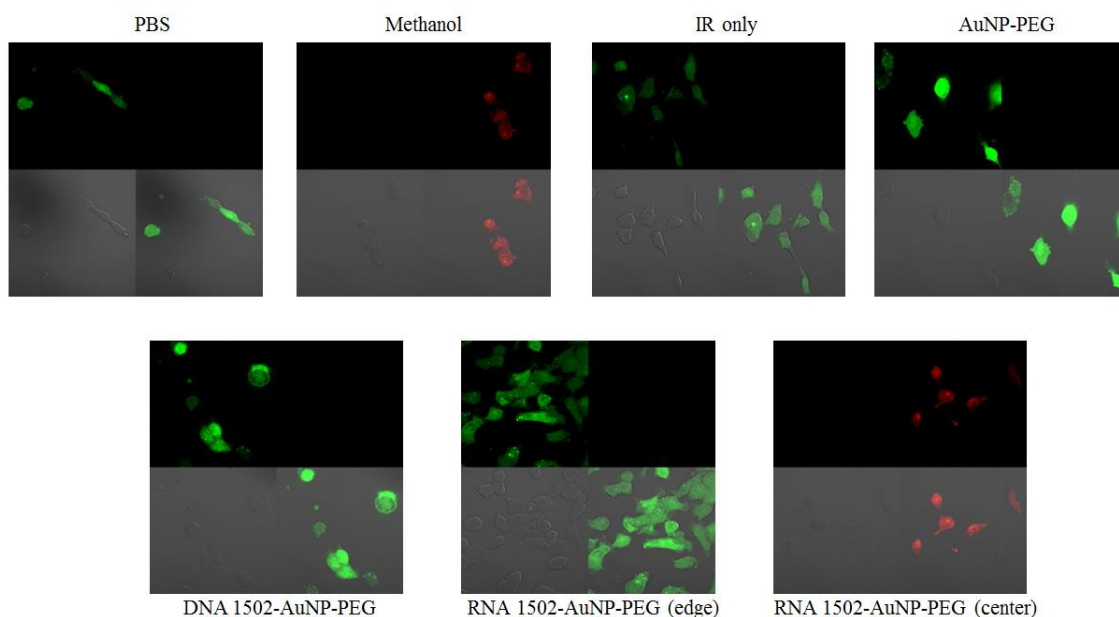


**Figure 3.5.c.** When conjugated to a PEGylated AuNP and treated with an IR laser, RNA aptamer, and not DNA aptamer 1502 can explicitly target, internalize, and subsequently kill Capan-1 cells. Controls, including AuNP-PEG do not have a targeted hyperthermia on Capan-1 cells.

### Capan-2: PDAC

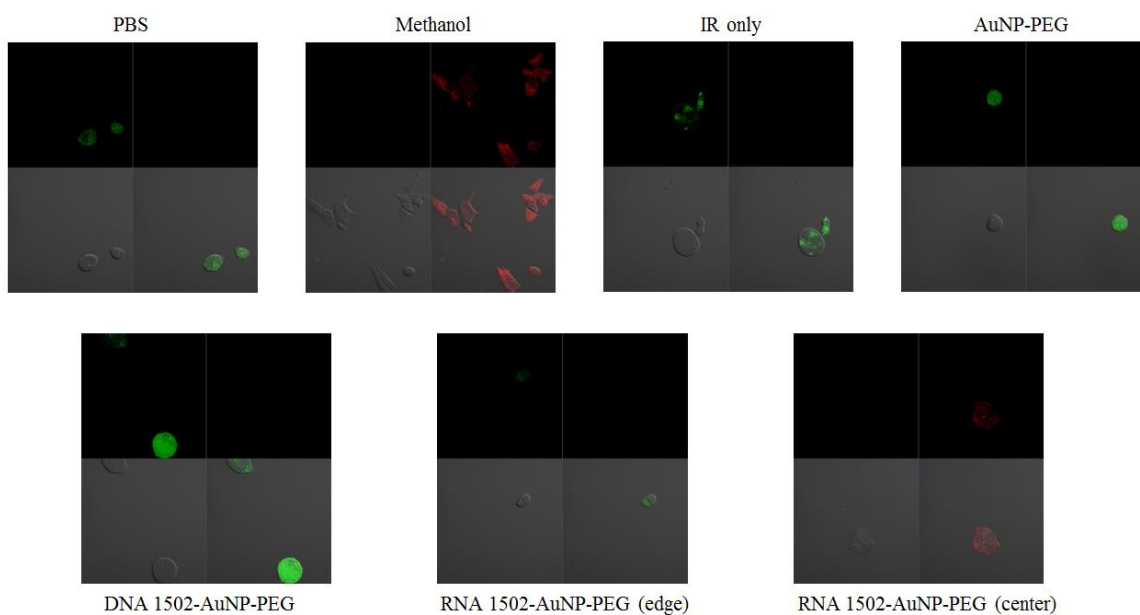


**Figure 3.5.d.** When conjugated to a PEGylated AuNP and treated with an IR laser, RNA aptamer, and not DNA aptamer 1502 can explicitly target, internalize, and subsequently kill Capan-2 cells. Controls, including AuNP-PEG do not have a targeted hyperthermia on Capan-2 cells.

### CFPAC: PDAC

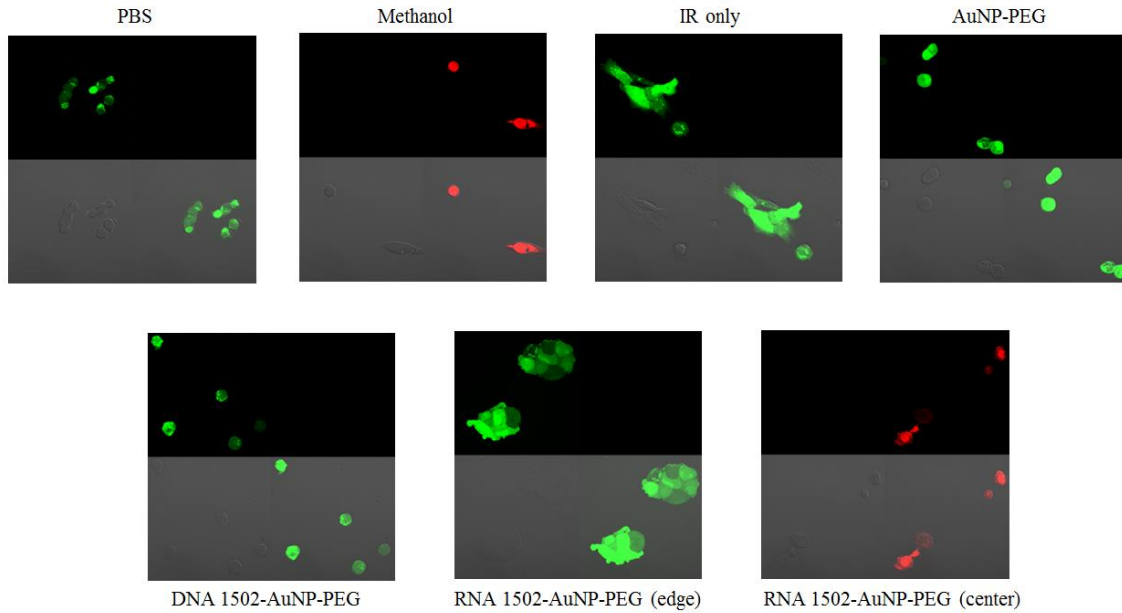


**Figure 3.5.e.** When conjugated to a PEGylated AuNP and treated with an IR laser, RNA aptamer, and not DNA aptamer 1502 can explicitly target, internalize, and subsequently kill CFPAC cells. Controls, including AuNP-PEG do not have a targeted hyperthermia on CFPAC cells.

### Panc-1: PDAC

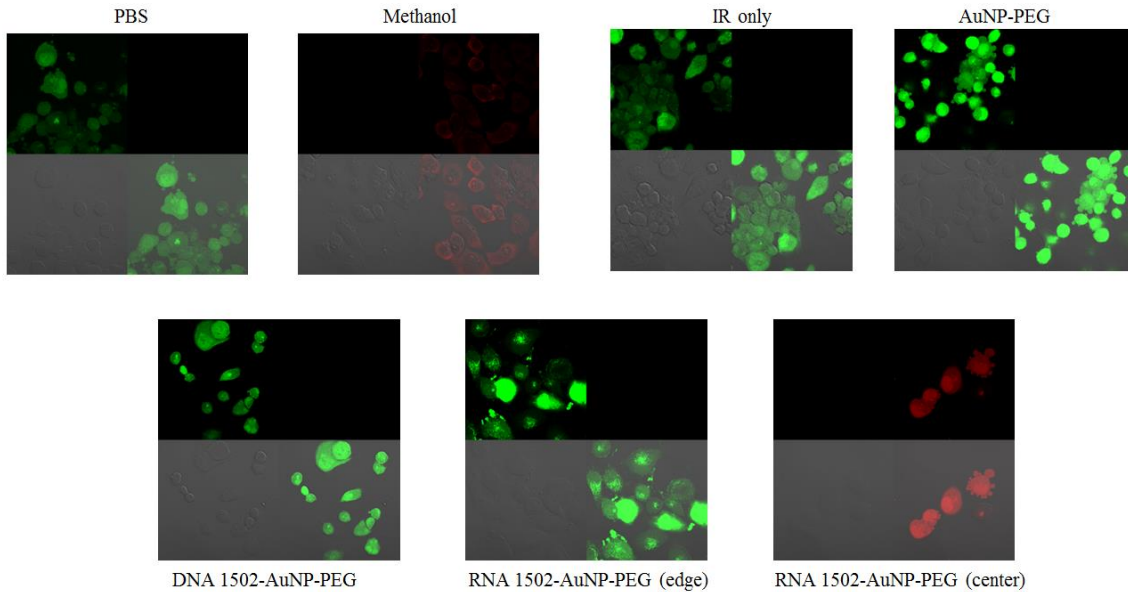


**Figure 3.5.f.** When conjugated to a PEGylated AuNP and treated with an IR laser, RNA aptamer, and not DNA aptamer 1502 can explicitly target, internalize, and subsequently kill Panc-1 cells. Controls, including AuNP-PEG do not have a targeted hyperthermia on Panc-1 cells.

### BX-PC3: PDAC

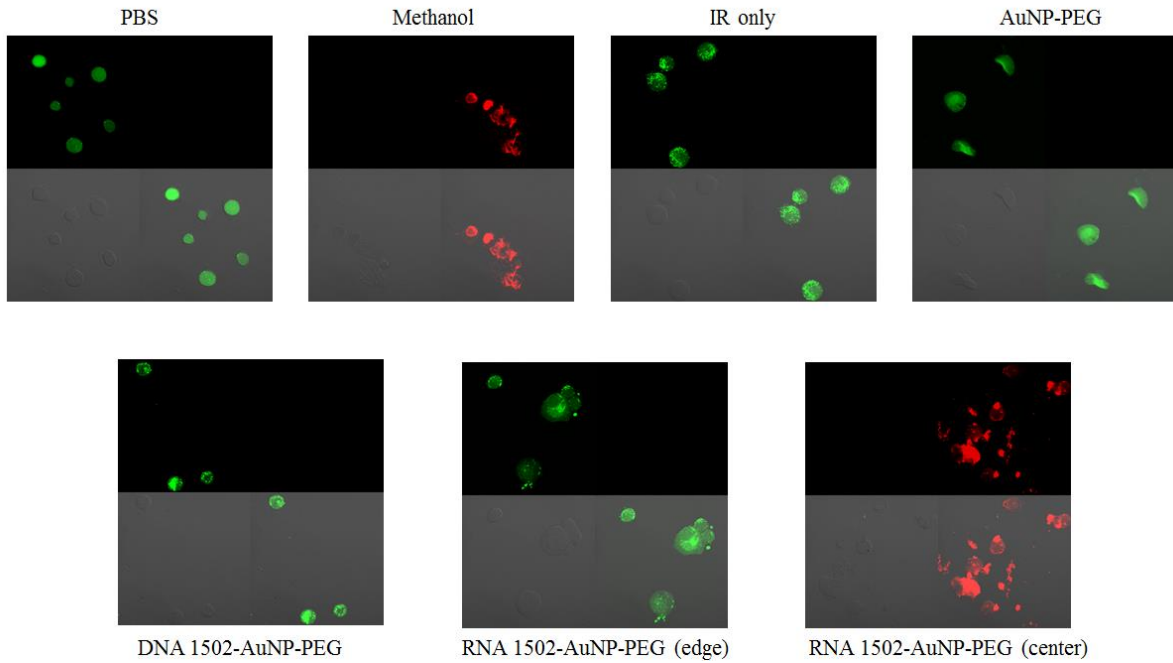


**Figure 3.5.g.** When conjugated to a PEGylated AuNP and treated with an IR laser, RNA aptamer, and not DNA aptamer 1502 can explicitly target, internalize, and subsequently kill BX-PC3 cells. Controls, including AuNP-PEG do not have a targeted hyperthermia on BX-PC3 cells.

### HPAF-II: PDAC

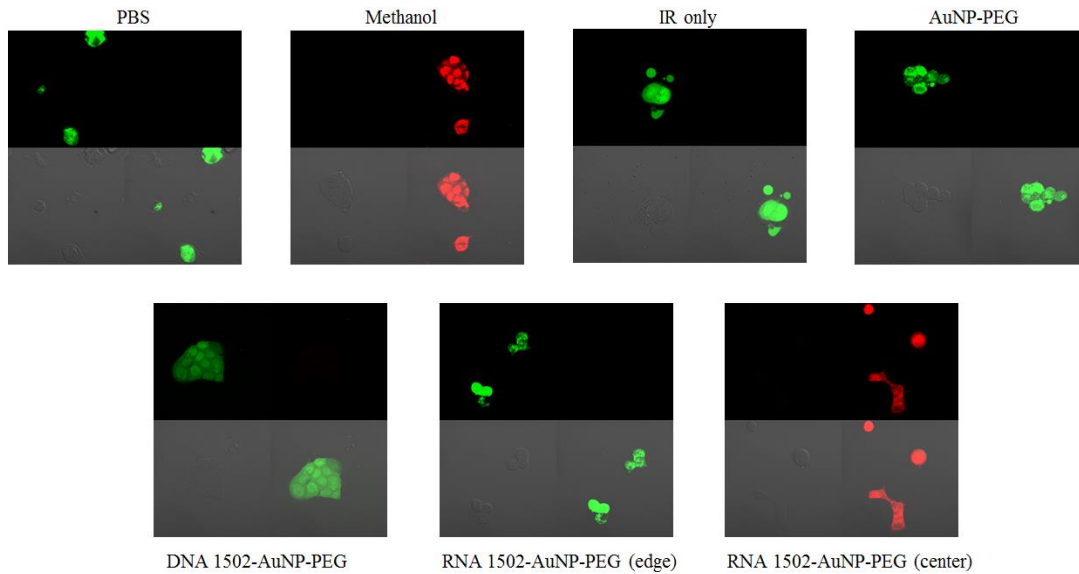


**Figure 3.5.h.** When conjugated to a PEGylated AuNP and treated with an IR laser, RNA aptamer, and not DNA aptamer 1502 can explicitly target, internalize, and subsequently kill HPAF-II cells. Controls, including AuNP-PEG do not have a targeted hyperthermia on HPAF-II cells.

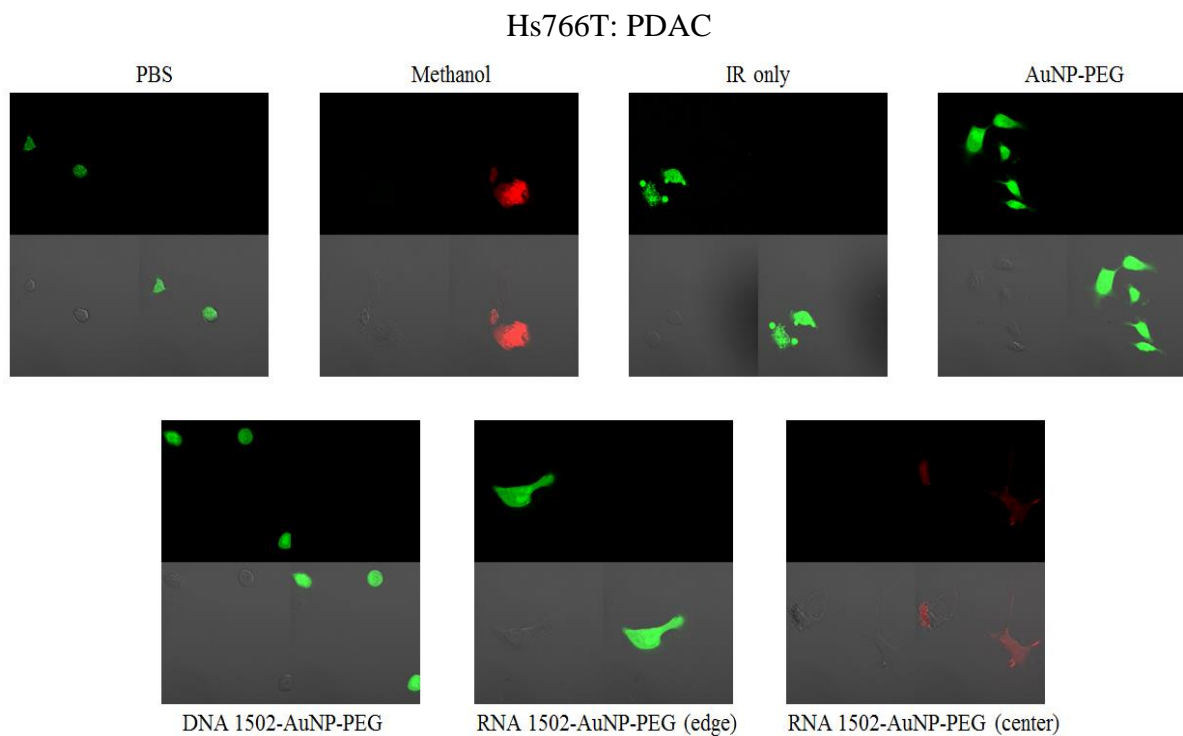


**Figure 3.5.i.** When conjugated to a PEGylated AuNP and treated with an IR laser, RNA aptamer, and not DNA aptamer 1502 can explicitly target, internalize, and subsequently kill Hs766T cells. Controls, including AuNP-PEG do not have a targeted hyperthermia on Hs766T cells.

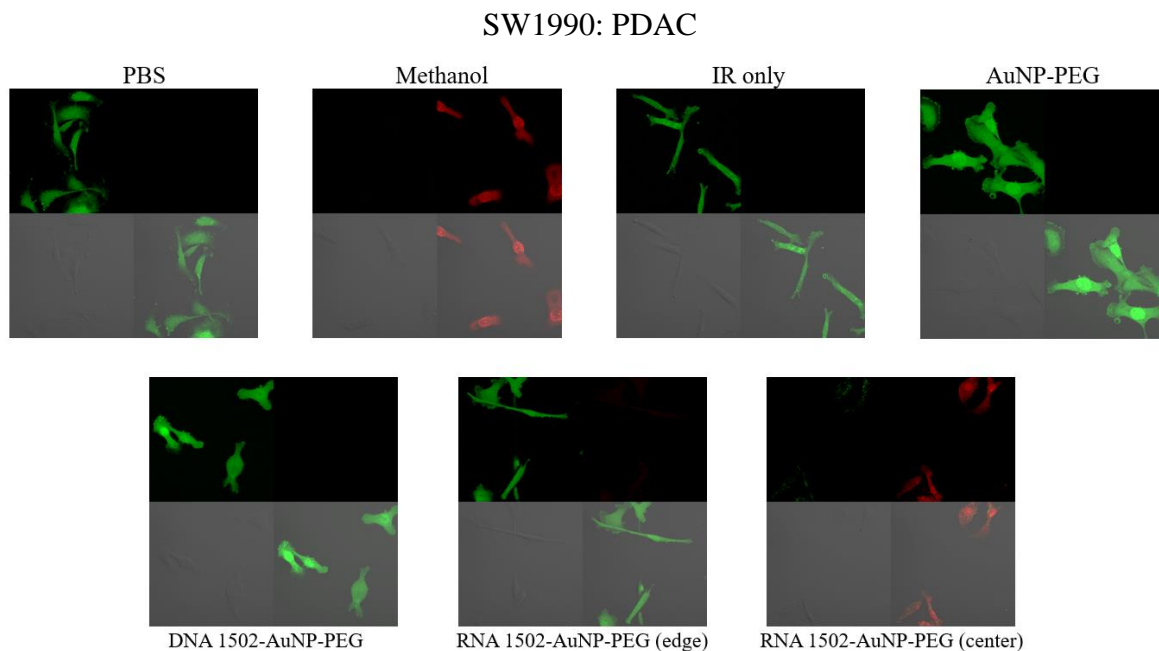


**Figure 3.5.j.** When conjugated to a PEGylated AuNP and treated with an IR laser, RNA aptamer, and not DNA aptamer 1502 can explicitly target, internalize, and subsequently kill SW1990 cells. Controls, including AuNP-PEG do not have a targeted hyperthermia on SW1990 cells.



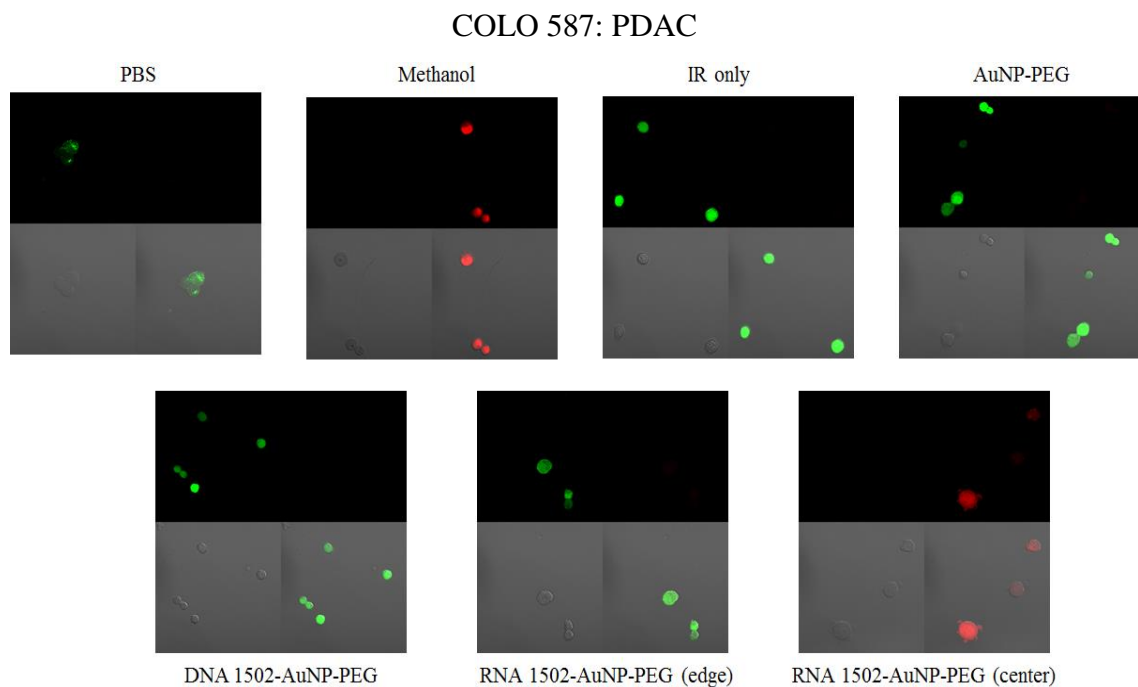


**Figure 3.5.k.** When conjugated to a PEGylated AuNP and treated with an IR laser, RNA aptamer, and not DNA aptamer 1502 can explicitly target, internalize, and subsequently kill COLO 587 cells. Controls, including AuNP-PEG do not have a targeted hyperthermia on COLO 587 cells.

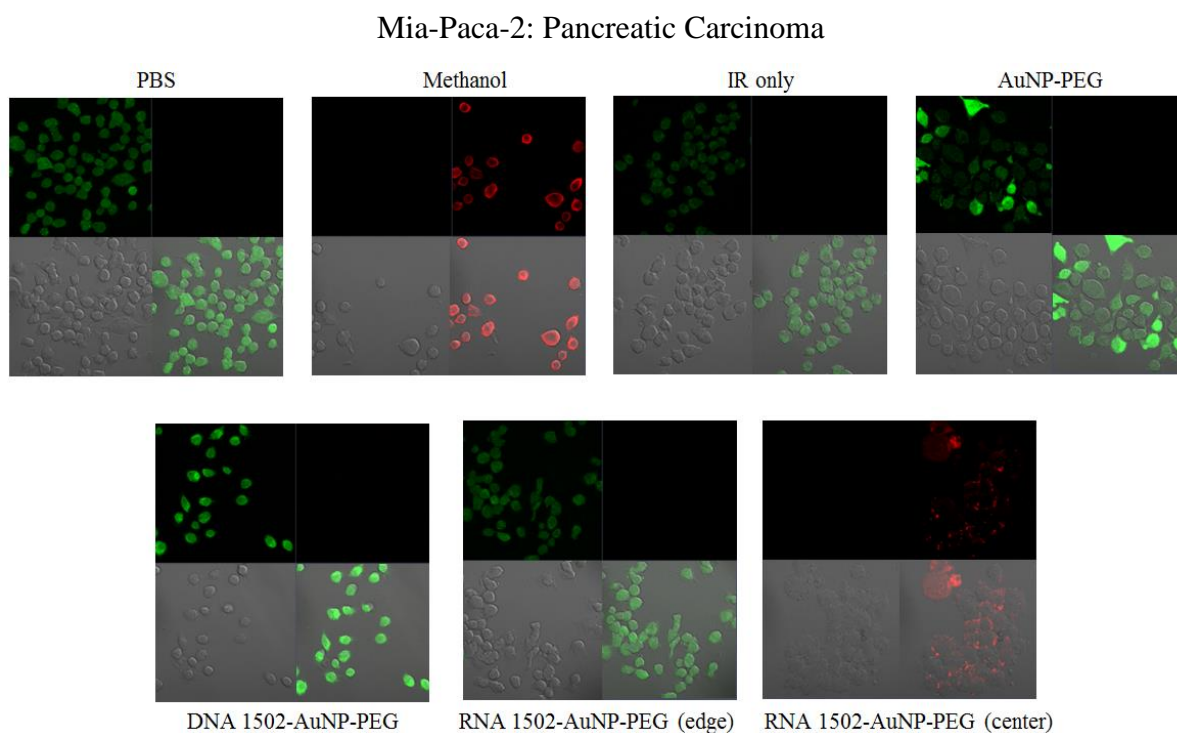


**Figure 3.5.l.** When conjugated to a PEGylated AuNP and treated with an IR laser, RNA aptamer, and not DNA aptamer 1502 can explicitly target, internalize, and subsequently kill Mia-Paca-2 cells. Controls, including AuNP-PEG do not have a targeted hyperthermia on Mia-Paca-2 cells.



### HepG2: Liver Cancer

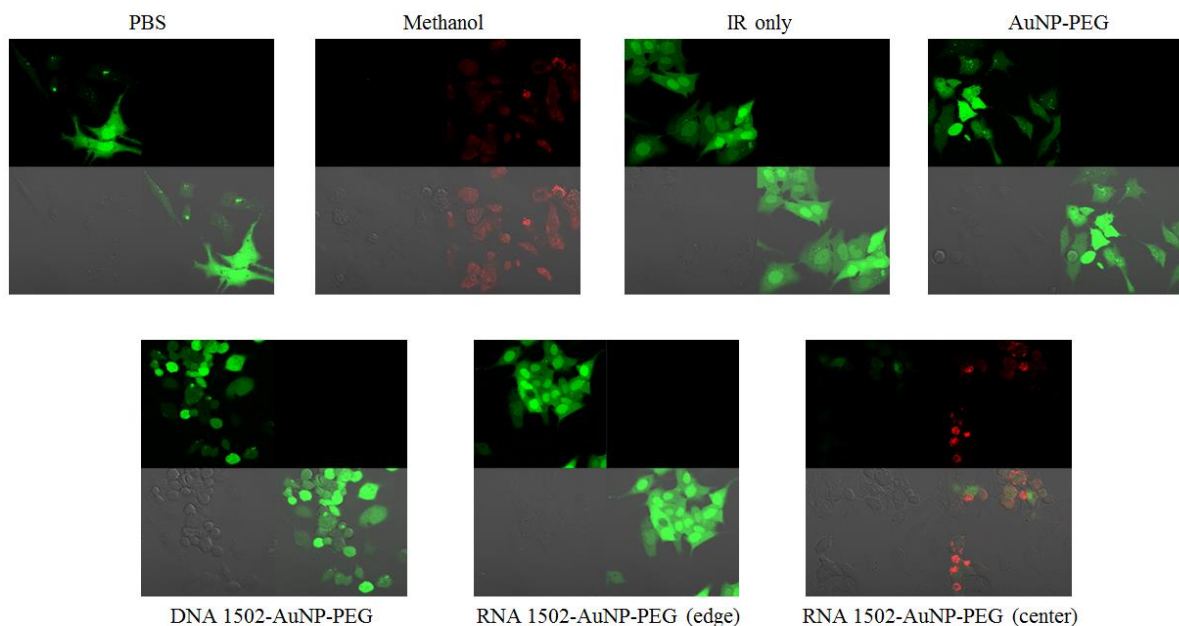


**Figure 3.5.m.** When conjugated to a PEGylated AuNP and treated with an IR laser, RNA aptamer, and not DNA aptamer 1502 can explicitly target, internalize, and subsequently kill HepG2 cells. The cell killing effect isn't as pronounced as it is in PDAC cell lines, however there is a noticeable cell killing effect. Controls, including AuNP-PEG do not have a targeted hyperthermia on HepG2 cells.

### Hep3B: Liver Cancer

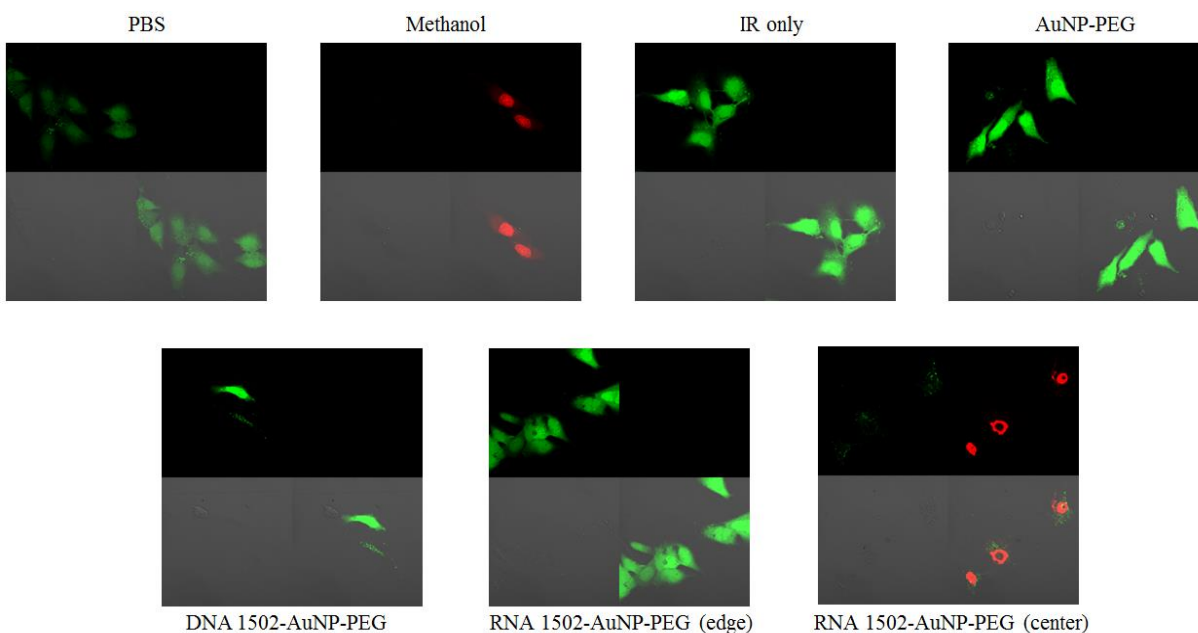


**Figure 3.5.n.** When conjugated to a PEGylated AuNP and treated with an IR laser, RNA aptamer, and not DNA aptamer 1502 can explicitly target, internalize, and subsequently kill Hep3B. The cell killing effect isn't as pronounced as it is in PDAC cell lines, however there is a noticeable cell killing effect. Controls, including AuNP-PEG do not have a targeted hyperthermia on Hep3B cells.

### Huh7: Liver Cancer

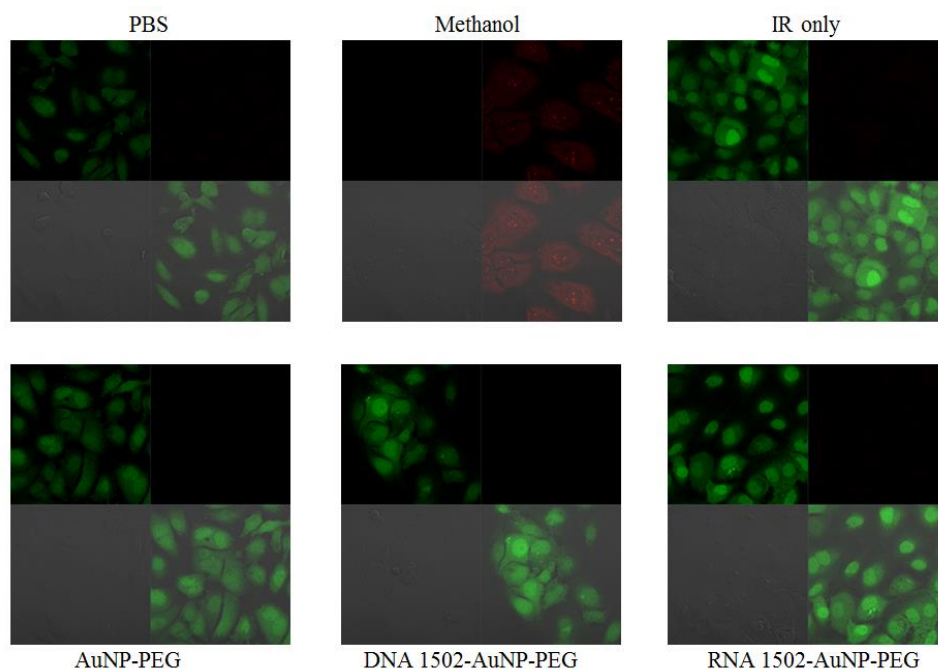


**Figure 3.5.o.** When conjugated to a PEGylated AuNP and treated with an IR laser RNA aptamer and DNA aptamer 1502, as well as AuNP-PEG has no targeted hyperthermia effect on Huh7 cells.

### PC-3: Prostate Cancer

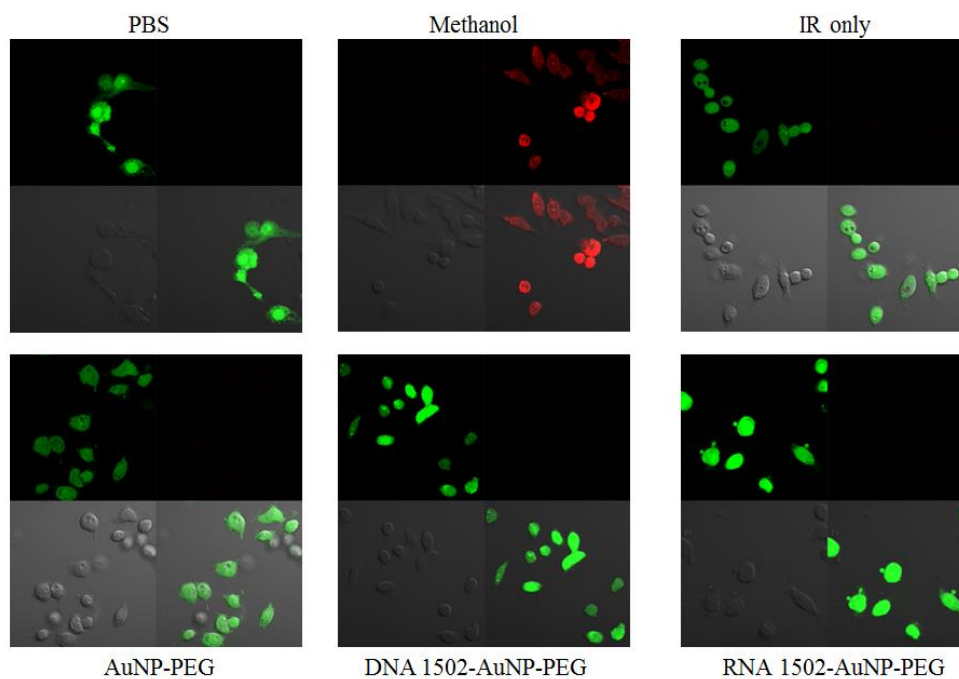


**Figure 3.5.p.** When conjugated to a PEGylated AuNP and treated with an IR laser RNA aptamer and DNA aptamer 1502, as well as AuNP-PEG has no targeted hyperthermia effect on PC-3 cells.

### DU 145: Prostate Cancer

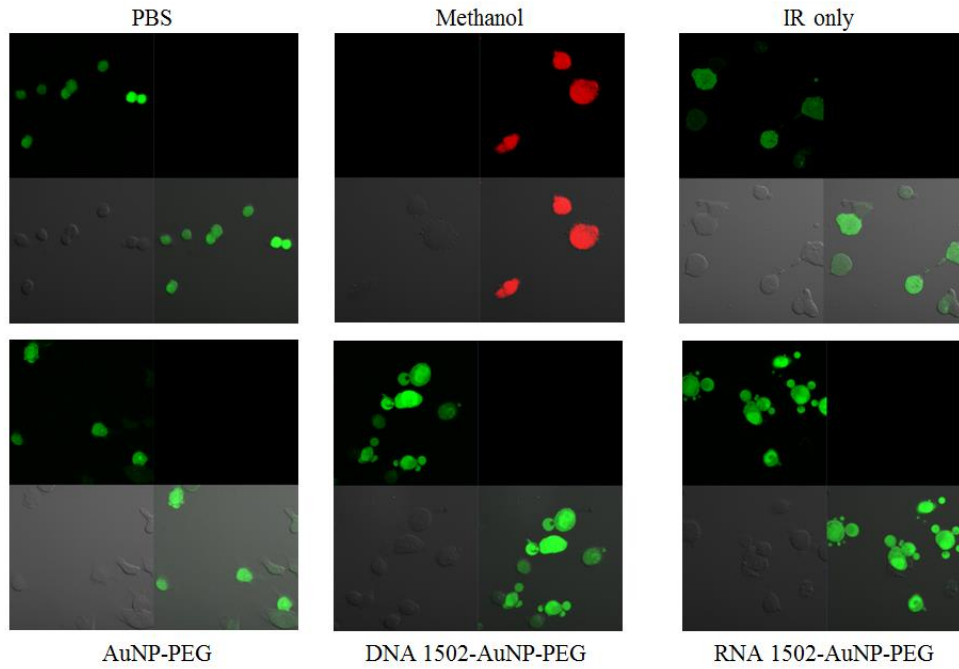


**Figure 3.5.q.** When conjugated to a PEGylated AuNP and treated with an IR laser RNA aptamer and DNA aptamer 1502, as well as AuNP-PEG has no targeted hyperthermia effect on DU 145 cells.

### A549: Lung Cancer

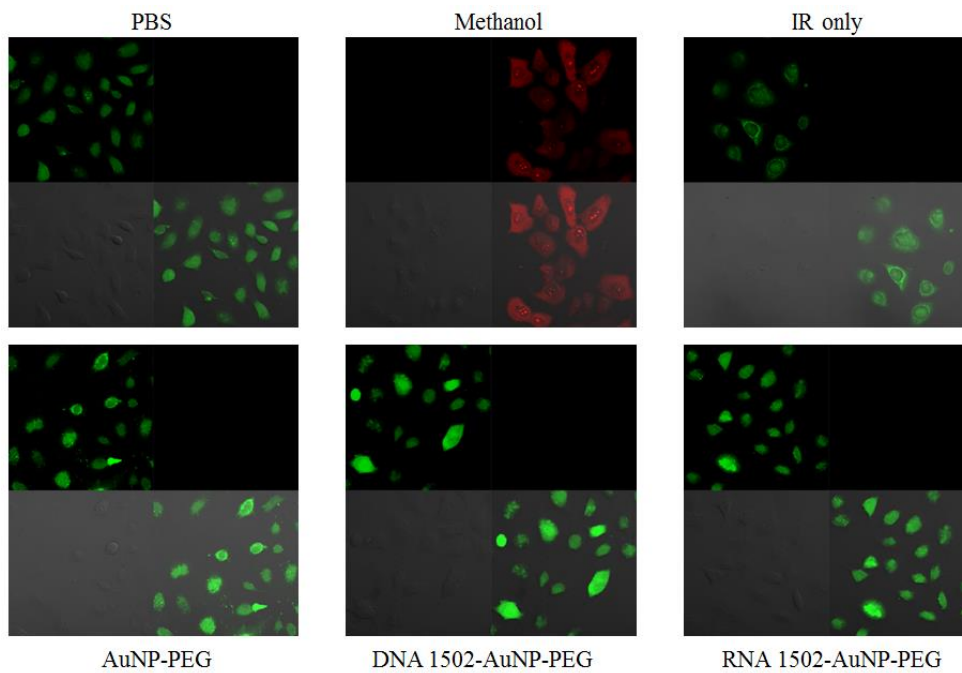


**Figure 3.5.r.** When conjugated to a PEGylated AuNP and treated with an IR laser RNA aptamer and DNA aptamer 1502, as well as AuNP-PEG has no targeted hyperthermia effect on A549 cells.

### SKOV-3: Ovarian Cancer

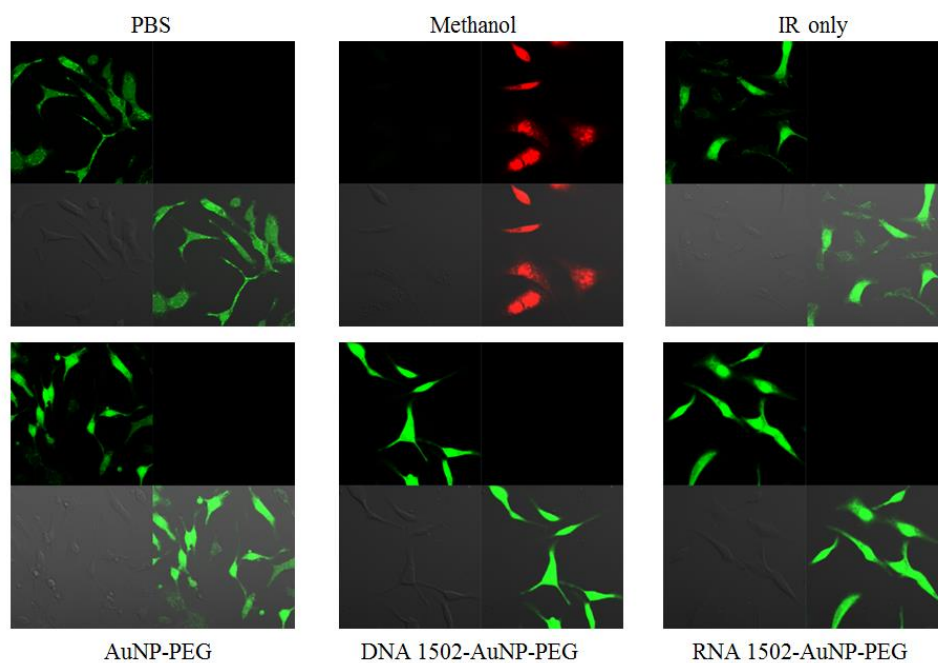


**Figure 3.5.s.** When conjugated to a PEGylated AuNP and treated with an IR laser RNA aptamer and DNA aptamer 1502, as well as AuNP-PEG has no targeted hyperthermia effect on SKOV-3 cells.

### MCF7: Breast Cancer

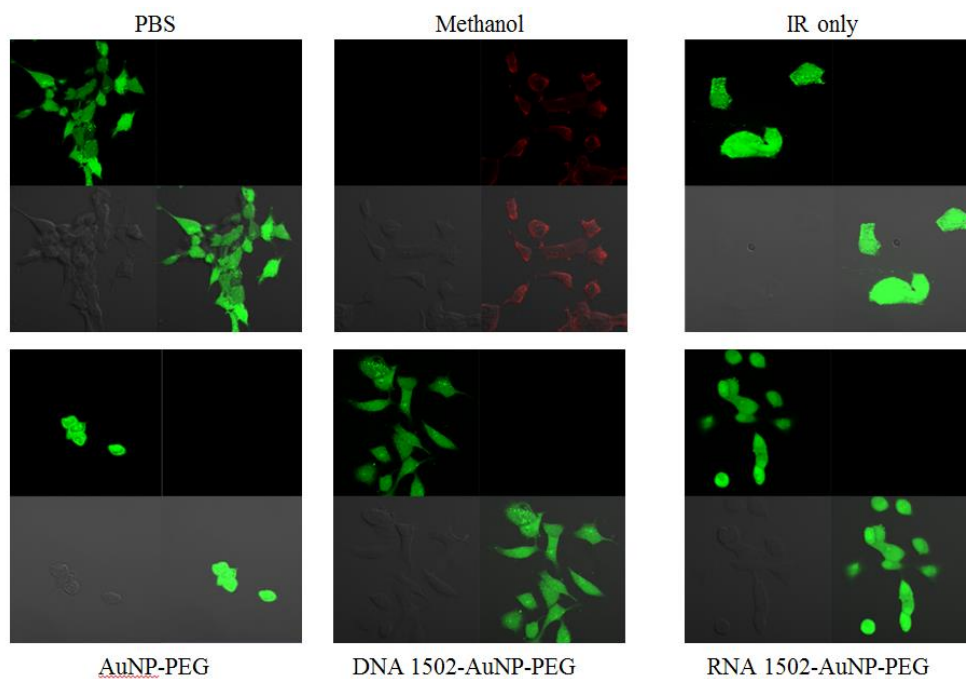


**Figure 3.5.t.** When conjugated to a PEGylated AuNP and treated with an IR laser RNA aptamer and DNA aptamer 1502, as well as AuNP-PEG has no targeted hyperthermia effect on MCF7 cells.

### HT29: Colon Cancer

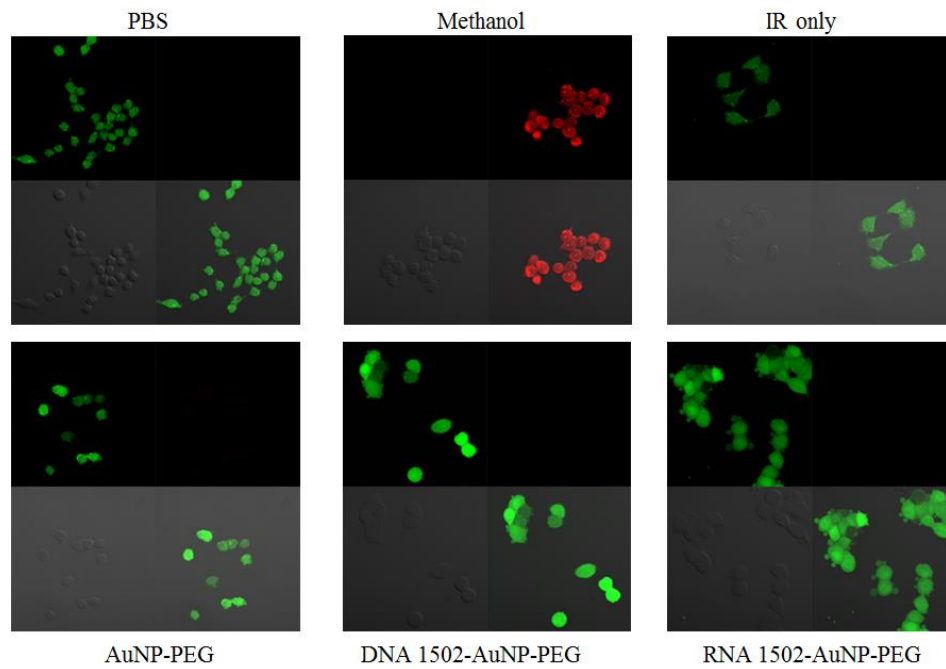


**Figure 3.5.u.** When conjugated to a PEGylated AuNP and treated with an IR laser RNA aptamer and DNA aptamer 1502, as well as AuNP-PEG has no targeted hyperthermia effect on HT29 cells.

### A431: Skin Cancer

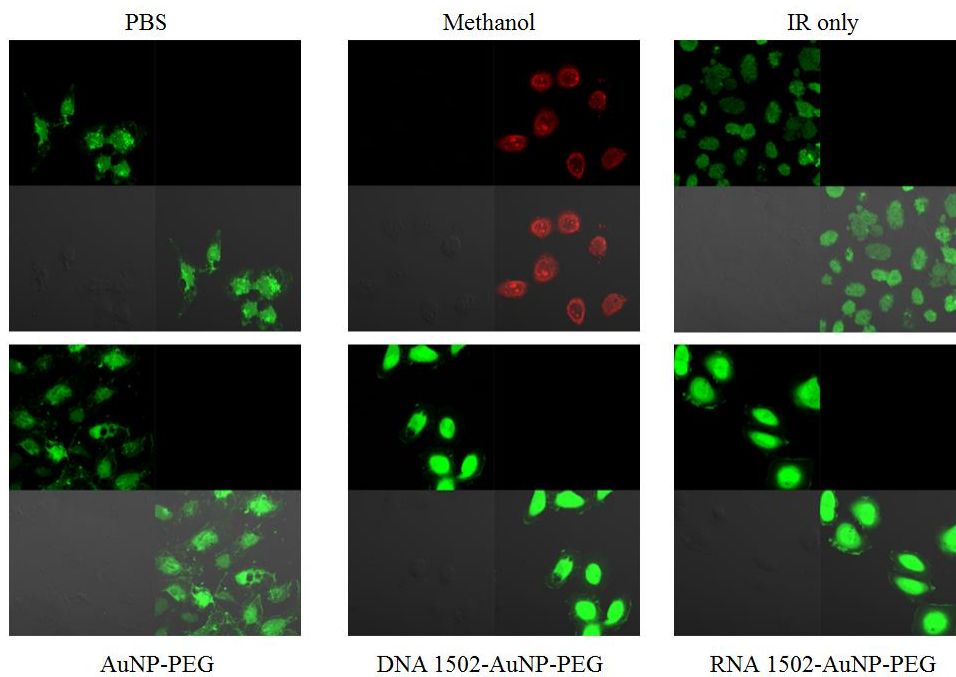


**Figure 3.5.v.** When conjugated to a PEGylated AuNP and treated with an IR laser RNA aptamer and DNA aptamer 1502, as well as AuNP-PEG has no targeted hyperthermia effect on A431 cells.

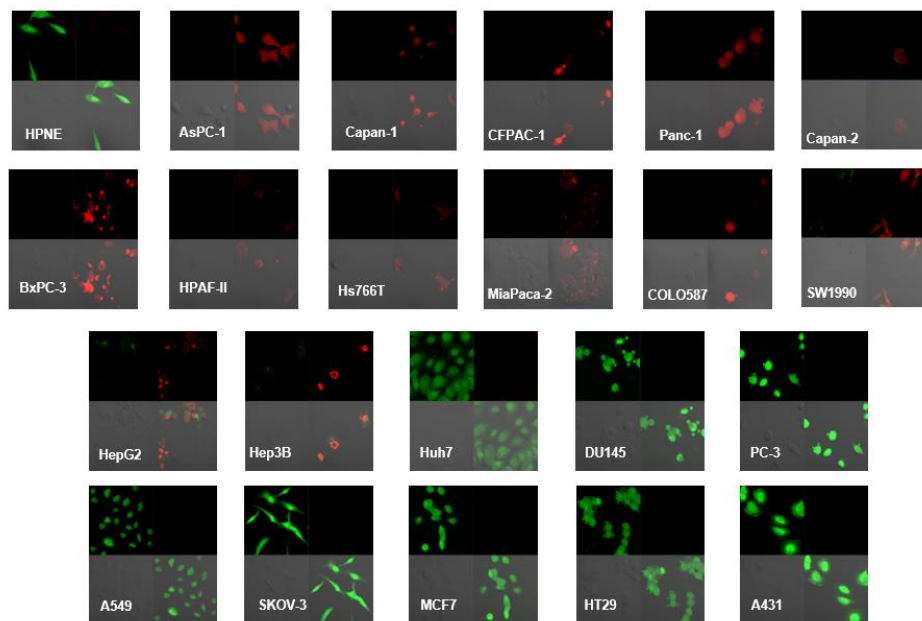


**Figure 3.6** A summary of the targeted hyperthermia study, depicted by confocal microscopy images, demonstrates extreme selectivity of 1502 to PDAC cell lines (11 tested), and 2 liver cancer cell lines, and not normal pancreas or non-pancreatic cancer cells (8 tested). These images are of the 1502-AuNP treated with the IR laser.

The comprehensive list of cell lines tested with this assay, along with the summarized assay results, can be seen in Table 3.2.

Cell Line	Tissue/Disease Type	Targeted Hyperthermia Induced Cell Killing Effect Observed (Yes/No)
hTERT-HPNE	Normal pancreas	No
AsPC-1	PDAC	Yes
Capan-1	PDAC	Yes
Capan-2	PDAC	Yes
CFPAC-1	PDAC	Yes
Panc-1	PDAC	Yes
BxPC-3	PDAC	Yes
HPAF-II	PDAC	Yes
Hs766T	PDAC	Yes
SW1990	PDAC	Yes
COLO 587	PDAC	Yes
Mia-Paca-2	Pancreatic carcinoma	Yes
HepG2	Hepatocellular carcinoma	Yes (although not as effective)
Hep3B	Hepatocellular carcinoma	Yes (although not as effective)
Huh7	Heptatocellular carcinoma	No
PC-3	Prostate adenocarcinoma	No
DU 145	Prostate carcinoma	No
A549	Lung carcinoma	No
SK-OV-3	Ovarian adenocarcinoma	No
MCF7	Breast adenocarcinoma	No
HT-29	Colorectal adenocarcinoma	No
A431	Epidermoid Carcinoma	No

**Table 3.2** The targeted hyperthermia assay using 1502-AuNP was done on 1 normal pancreas cell line, 11 PDAC and pancreatic carcinoma cell lines, 3 liver cancer cell lines, and 7 non-pancreatic cancer cell lines.

### 3.3. Concluding Remarks

One of the overarching goals of this aim was to further define the specificity of aptamer 1502 against pancreatic ductal adenocarcinoma. Aptamer 1502's ability to internalize into AsPC-1 cells when incubated at 37°C vs. cell-surface binding at 4°C suggested that the ligand had a mechanism allowing for this internalization. We predict that 1502 is internalizing through receptor mediated endocytosis, however this was never confirmed in our studies. Given this property of aptamer 1502, we developed an assay that could not only sensitively identify if the

aptamer was targeting a cell line, but also if the aptamer was internalizing, directing a gold nanoparticle with it.

The gold nanoparticles were PEGylated, and variation of 1502 that was synthesized with a 5' amino was converted to a 5' dithiocarbamate to react with the gold surface. Titrated ratios of 1502 to gold nanoparticle were tested to ensure efficient targeting to AsPC-1 cells, and the targeted hyperthermia assay conditions were optimized. The initial targeted hyperthermia tests demonstrated that aptamer 1502 conjugated to PEGylated gold nanoparticles could target, internalize, and subsequently kill AsPC-1 cells after treatment with a NIR laser, heating the gold nanoparticles to 42°C. When tested on HPNE cells, the aptamer-gold nanoparticle platform did not have a cell killing effect, indicating that the normal pancreas cell line wasn't targeted by 1502. Testing with HepG2 cells, which were previously shown to be targeted by aptamer 1502, gave similar results to AsPC-1 cells. The 1502-gold nanoparticle targeted and internalized into HepG2 cells, and after treatment with an NIR laser, induced cell death for this liver cancer cell line.

Given the success of the 1502 functionalized gold nanoparticle, with the included controls, we felt confident that the targeted hyperthermia assay could be used to further characterize the specificity of aptamer 1502 against other pancreatic ductal adenocarcinoma cell lines. We tested 11 of the 14 pancreatic cancer cell lines that are available, every cell line that was available to our lab. Additionally, we tested two other liver cancer cell lines, in hopes of further defining the binding affinity and specificity of 1502 to liver cancer. Finally, we tested eight non-pancreatic cancer cell lines, which had some differences to the original non-pancreatic cancer cell lines tested by Dr. Chen during the selection. This gave us a diverse panel of



cancerous cells that could help to define aptamer 1502's specificity to the cell-surface biomarkers present on a series of cancer cell lines.

The targeted hyperthermia assay results indicated that aptamer 1502 is highly specific to pancreatic ductal adenocarcinoma cell lines, demonstrating a cell killing effect with eleven of eleven pancreatic cancer cell lines tested. It is important to note that Mia-Paca-2 experiences a slightly decreased cell killing effect, which may be due to the fact that it is a pancreatic carcinoma and not a pancreatic ductal adenocarcinoma. The only other cell line that was targeted by aptamer 1502 was two of the three tested liver cancer cell lines, HepG2 and Hep3B. The cell killing effect does not seem to be as strong for these cell lines as it was for PDAC cell lines, however there is noticeable cell death to HepG2 and Hep3B after treatment with 1502-gold nanoparticles and the NIR laser. Interestingly, Huh7, which is also a liver cancer cell line, was not affected by this platform. It is hypothesized that this cell line has derived from HepG2 and Hep3B and overexpresses differing biomarkers on its cell surface. Finally, the normal pancreas and eight non-pancreatic cancer cell lines tested with the aptamer 1502-gold nanoparticle and NIR laser hyperthermia treatment did not experience a cell-killing effect. This data further confirmed aptamer 1502's extreme specificity to pancreatic cancer, which could be very useful for clinical application as a diagnostic or therapeutic tool against the disease.

### **3.3 Materials and Methods**

#### **3.4.a. Cell culture**

AsPC-1 (pancreatic ductal adenocarcinoma), PANC-1 (pancreatic ductal adenocarcinoma), CAPAN-1 (pancreatic ductal adenocarcinoma), CFPAC-1 (pancreatic ductal adenocarcinoma), hTERT-HPNE (pancreatic ductal epithelial cell), BxPC-3 (pancreatic ductal adenocarcinoma), HPAF-II (pancreatic ductal adenocarcinoma), Hs766T (pancreatic ductal adenocarcinoma),

SW1990 (pancreatic ductal adenocarcinoma), COLO 587 (pancreatic ductal adenocarcinoma), Mia-Paca-2 (pancreatic carcinoma), HepB3 (hepatocellular carcinoma), PC-3 (prostate adenocarcinoma), DU 145 (prostate carcinoma), A549 (lung carcinoma), SK-OV-3 (ovarian adenocarcinoma), MCF7 (breast adenocarcinoma), LNCaP (prostate adenocarcinoma), HT-29 (colorectal adenocarcinoma), and A431 (epidermoid carcinoma) were purchased from American Type Culture Collection (ATCC). Huh7 (hepatocellular carcinoma) and HepG2 (hepatocellular carcinoma) were acquired from a collaborator. Cell culture was maintained at 37°C and 5% CO<sub>2</sub> in various mediums which included RPMI 1640, EMEM with NEAA, McCoy's 5a, DMEM/F12, Leibovitz's L-15, IMDM, or DMEM medium supplemented with 10% heat-inactivated fetal bovine serum (FBS) (GIBCO) and 100 units/ml penicillin–streptomycin (Cellgro).

### **3.4.b. Developing the functionalized gold nanoparticle**

#### **3.4.b.i. Reacting 1502-amino with CS<sub>2</sub>**

To allow for a reaction of the gold nanoparticle with 1502, the 5' modified 1502-amino was reacted with carbon disulfide in a borate buffer, pH 9.0 for 2 h at room temperature. The buffer was changed back to DEPC water using a 5K column, 3X at 13500 rpm, room temperature. After the reaction, the 5' end of 1502 was a dithiocarbamate, which could be reacted with the gold nanoparticle. The same was done with the DNA aptamer with the 5'-amino.

### **3.4.b.ii. Functionalizing the nanoparticle**

Aqueous, citrate-coated, 30 nm gold nanoparticles (Nanocomposix) were used for a targeted hyperthermia treatment of PDAC cells. To functionalize these nanoparticles, they were first incubated in PBS with 1000X molar excess of PEG-2000-thiol (Sigma) by spinning for 2 h at room temperature. The aptamer was added, at various ratios to the gold nanoparticle, spinning overnight at room temperature.

A schematic of this process is shown in Figure 3.7. Stock, PEGylated, and functionalized nanoparticles were characterized for zeta size and potential to confirm successful functionalization of the nanoparticle.

### **3.4.b.iii. Determining the best conditions for a PEGylated gold nanoparticle functionalized with 1502**

Because gold nanoparticles can be sensitive to their surrounding buffer, the protocol for PEGylation and functionalization of the gold nanoparticle needed to be optimized to avoid nanoparticle aggregation. Varying molar ratios of PEG-2000-thiol to gold nanoparticle were tried, and conditions of immobilization were tested until a reproducible, stable, and functional gold nanoparticle was formulated. The optimal conditions for this formulation included reacting a 1000:1 molar ratio of PEG-2000-thiol:gold nanoparticle in PBS (adding the PEG first for stability) at room temperature for 2 h, followed by incubation with varying molar ratios of aptamer 1502 that contains a 5'-dithiocarbamate at room temperature for 2 h. If necessary, the AuNPs were sonicated to resuspend nanoparticles that had adhered to the Eppendorf tube sidewall.

### **3.4.c. Characterization with the zeta sizer**

#### **3.4.c.i. Size, PDI, and zeta potential**

The size and polydispersity index of the gold nanoparticles, before and after functionalization with aptamer 1502, was tested by the Malvern Zeta Sizer three times with a disposable cuvette. The sample was transferred to a folded capillary cell for zeta potential measurement, also measured three times for each sample.

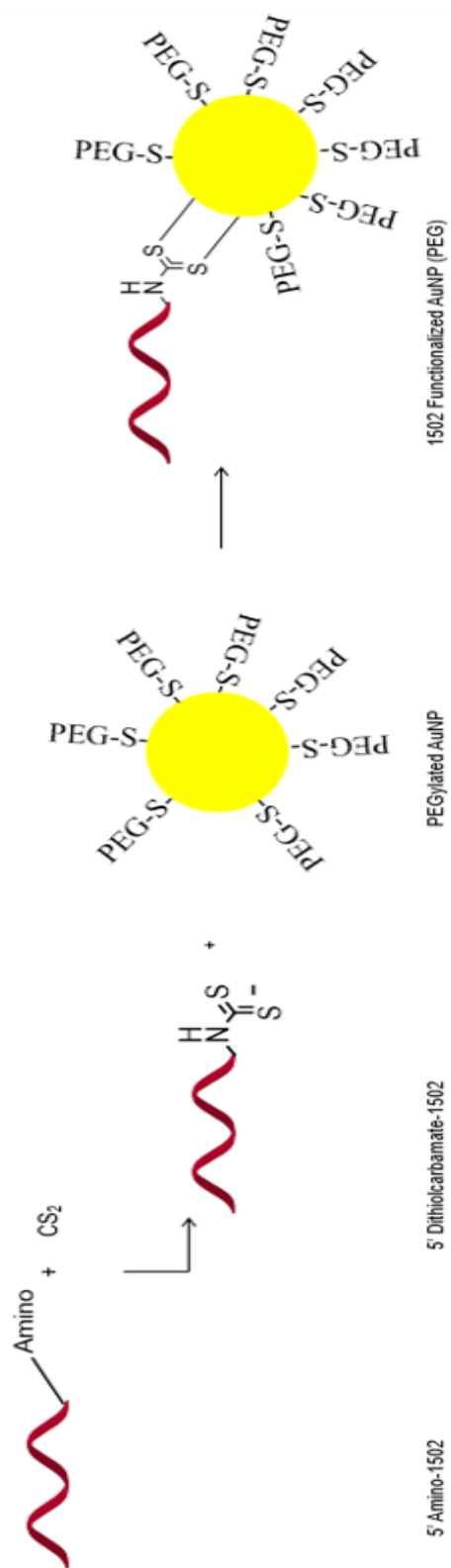


**Figure 3.7** Schematic illustration of efficient immobilization of PDAC-specific aptamer to PEGylated gold nanoparticles (AuNPs).

#### **3.4.d. Optimization of aptamer 1502 to gold nanoparticle ratio**

The PEGylated gold nanoparticles were immobilized with varying molar ratios of aptamer 1502. This included a  $\leq 1000:1$ ,  $\leq 400:1$ ,  $\leq 200:1$ ,  $\leq 20:1$ , and  $\leq 2:1$  molar ratio of 1502 to gold nanoparticle. The gold nanoparticle concentration was kept constant at 1 nM, and the aptamer concentrations ranged from 2 nM to 1000 nM, respectively.

#### **3.4.e. Determining the actual loading of aptamer to gold nanoparticle**

The molar ratios of aptamer to gold nanoparticle were determined by the input of aptamer 1502 used for immobilization. To determine the actual loading of 1502 onto the gold nanoparticle, free 1502 was removed from the supernatant by centrifugation at 13,500× rpm. NanoDrop was used to read the absorbance at 260 nm to determine the free aptamer concentration in the supernatant at each of the five ratios, comparing the aptamer concentrations to a standard curve that plotted free aptamer concentrations respective to the aptamer:gold nanoparticle ratios (1000, 400, 200, 20, 2, and 0 nM). Each ratio was prepared and analyzed three times.

#### **3.4.f. Targeted hyperthermia**

A series of AuNP-PEG and aptamer conjugated AuNP-PEG samples were prepared, first at varying ratios of aptamer to gold nanoparticle, and subsequently at optimized ratios. The AuNP-PEG concentration ranged between 400 and 600 pM in 200  $\mu$ L of aptamer binding buffer (1x PBS with 5 mM  $\text{Ca}^{2+}$  and 1 mM  $\text{Mg}^{2+}$ ). Plated cells were incubated with AuNP samples for 2 h at 37°C. Samples were removed and washed with 1X PBS once. Media was added and the cells

were treated with an 800 nm IR laser for 5 min to induce hyperthermia of the gold nanoparticles. The cells were then washed once with 1X PBS, and treated with 200  $\mu$ L of 1  $\mu$ M calcein AM: 2  $\mu$ M ethidium bromide from a Live/Dead Cell Assay Kit (Life Technologies). The dye was incubated at room temperature for 30 min, removed, and washed once with 1X PBS. The cells were fixed with 1.5% PFA for 15 min and transferred to slides for imaging using the Zeiss LSM 700 confocal microscope.

## CHAPTER IV

### APPLICATION OF APTAMER 1502 FUNCTIONALIZED HYBRID LIPID-PLGA NANOPARTICLES FOR SELECTIVE CELL KILLING

#### 4.1 Introduction

When determining a translational, targetable drug delivery platform that could take advantage of aptamer's high specificity and strong affinity for pancreatic ductal adenocarcinoma, it was important to utilize a drug delivery platform that was biocompatible, with hydrophilic properties, but also able to carry small molecule therapeutics, often hydrophobic in nature. This platform had to be able to be directed to PDAC by aptamer 1502, and have stability if translated into *in vivo* studies in the future. The platform also needed to be tunable and versatile, so that it could be further optimized to work with a series of detectable dyes or desired therapeutic drugs, and also able to be functionalized by other selected 15<sup>th</sup> round aptamers (if necessary). Despite this growing list of requirements, we found a proven nanoparticle drug delivery platform that would allow for these needs, including a facile synthesis and self-assembled functionalization with aptamer 1502.

We chose to develop hybrid lipid-poly(lactic-co-glycolic acid) (PLGA) nanoparticles that can be functionalized with aptamer 1502 for targeted therapeutic delivery. These nanoparticles combine the properties of traditional PLGA nanoparticles with the characteristics of lipid based nanoparticles, combining the advantages that each nanoparticle system has individually. Both liposome nanoparticles and PLGA nanoparticles exhibit properties such as high drug loading



capabilities, biocompatibility, the potential for a long half-life, and flexibility in size.

Individually, lipid based and PLGA based nanoparticles have their own advantages and disadvantages as well <sup>39-43</sup>.

PLGA nanoparticles do have some control over the degradation rate of the nanoparticle, as the ratio of lactic acid to glycolic acid is easily tunable, and often commercially sold in varying ratios (we chose 50:50 in our studies). Another advantage of PLGA is that many different compounds can be incorporated into the polymer, allowing the nanoparticle to be very versatile in what it can deliver to the diseased cells or tissue. Unfortunately, PLGA nanoparticles don't always last in *in vivo* studies because it has a short half-life in serum. Also, for our purposes of targeting the nanoparticle to PDAC, PLGA would not be useful because the surface chemistry is difficult to modify.

The surface of lipid or liposome nanoparticles can alternatively easily be modified with targeting ligands. There are lipids that have reactive chemical groups that can be incorporated so that surface modifications and the conjugation of targeting ligands are possible. Lipids typically are composed of both hydrophobic tails and hydrophilic heads and therefore can incorporate different types of molecules for carrying or functionalizing purposes. Unfortunately, synthesizing lipid nanoparticles can be very difficult and hard to reproduce with consistent size and properties, and they often do not store very well for long periods of time.

We aimed to take advantage of the desirable properties of both types of nanoparticles by formulating a hybrid lipid-PLGA nanoparticle. These nanoparticles have been used with great promise to deliver various chemotherapies, markers, as well as dyes for *in vivo* application. In our case, we aim to encapsulate both dyes and small molecule drugs (at separate times) to observe the targeting effect of a 1502 functionalized nanoparticle, and subsequently deliver a

cytotoxic drug to PDAC, resulting in selective cell death. The PLGA core can encapsulate these dyes or drugs, and a single layer lipid outer layer can facilitate the functionalization with aptamer 1502. This type of encapsulation will allow for a stepwise release of the dye or drug, which could aid in reduced toxicity and improved therapeutic properties. This type of hybrid lipid-PLGA nanoparticle has been utilized in delivering chemotherapies, vaccines, and other types of therapies in previous studies<sup>44-47</sup>.

To functionalize the outer lipid layer of the lipid-PLGA nanoparticle, the previously synthesized 1502 aptamer with a 5' stearyl modification can be used. This stearyl group mimics a lipid tail, and does not interact with the functional arms of the aptamer. Once folded into its functional secondary structure, aptamer 1502 can be mixed with the formulated nanoparticles and self-insert into the outer lipid layer without the need for a chemical reaction. The stearyl group can interact with the lipid tails of the two lipids that we used, DSPE-PEG and lecithin, with the functional aptamer outside of the nanoparticle. Aptamer 1502 can then direct the lipid-PLGA nanoparticle to PDAC cells, internalize through receptor mediated endocytosis, and deliver small molecule dyes or therapeutic drugs selectively to PDAC.

Initially we planned on testing this functionalization with Nile red dye, a fluorescent dye that emits at 555 nm, allowing visualization on the confocal microscope. For subsequent *in vivo* studies, we chose to use NIR dye cardiogreen (ICG), which excites around 790 nm (see Chapter 5 for details). For a targeted drug delivery and cell killing effect against PDAC, which was the overall goal of this aim, we chose to use cytotoxic small molecule SN-38. SN-38 is an active metabolite of irinotecan that is actually 1000 times more toxic than irinotecan. It targets the topoisomerase I and acts as an inhibitor, killing cells through its cytotoxicity<sup>48</sup>. Because we can observe the cell-killing effects of this 1502 targeted lipid-PLGA nanoparticle platform through the

cytotoxicity of SN-38, we decided that this was an appropriate formulation to test our hypothesis. Future studies may incorporate other chemotherapeutic drugs or NIR dyes to further apply this targeted therapeutic tool against PDAC.

## **4.2 Results and Discussion**

### **4.2.a. Construction, characterization, and functionalization of the lipid-PLGA nanoparticle**

The hybrid lipid-PLGA nanoparticles have shown great biocompatibility and function *in vivo* in previous studies<sup>49-51</sup>. The outer lipid layer consists of both DPSE-PEG (Avanti Polar Liquids) and lecithin from soy (Sigma) and the inner polymer consists of PLGA (Sigma). The DSPE-PEG has shown to provide an increased stability and circulation time *in vivo* while the lecithin can provide structural stability to the nanoparticle. The polymer based PLGA can carry organic small molecules and will interact with the lipid tails of the DPSP-PEG and lecithin to self-assemble into nanoparticles.

The construction of the hybrid lipid-PLGA nanoparticles underwent several rounds of optimization before finding a protocol that allowed for a low and consistent PDI of the size, ranging from 70-90 nm<sup>52</sup>. Several conditions were tested for synthesis and characterization (data not shown). Initially, the concentrations and ratios of DPSE-PEG to lecithin were tailored to balance the benefit of PEG with the stability provided by lecithin. Each variation synthesized was characterized by size, zeta potential, and PDI to determine the best conditions for a consistent and desired nanoparticle synthesis. These conditions included an 8.5:1 molar ratio of lecithin to DSPE-PEG and a 1:10 organic (PLGA) to aqueous (DSPE-PEG and lecithin) molar ratio.

After purification with a 10K column to removed free reagents and washed with 1X PBS three times, the nanoparticles were functionalized with the 5' stearyl modified 1502 aptamer, as well as the 5' stearyl modified 1502 scrambled aptamer (control). A series of nanoparticles were prepared without an aptamer for an additional control. The pre-folded aptamer with the 5' "lipid-like" tail should self-assemble and insert into the outer lipid layer of the formulated lipid-PLGA nanoparticle to functionalize the nanoparticle and allow for specific targeting to PDAC cells. To confirm this proof-of-concept, Nile red dye added to the PLGA polymer. This dye allowed for visualization of the nanoparticle after targeted delivery to PDAC cells, demonstrating that the 1502-stearyl aptamer successfully inserted into the nanoparticle and is functional. Once determined successful, cytotoxic small molecule SN-38 was added to the PLGA polymer, with the aim of specifically delivering this nanoparticle to PDAC cells, resulting in a selective cell killing effect. A schematic representing this process can be seen in Figure 4.1.

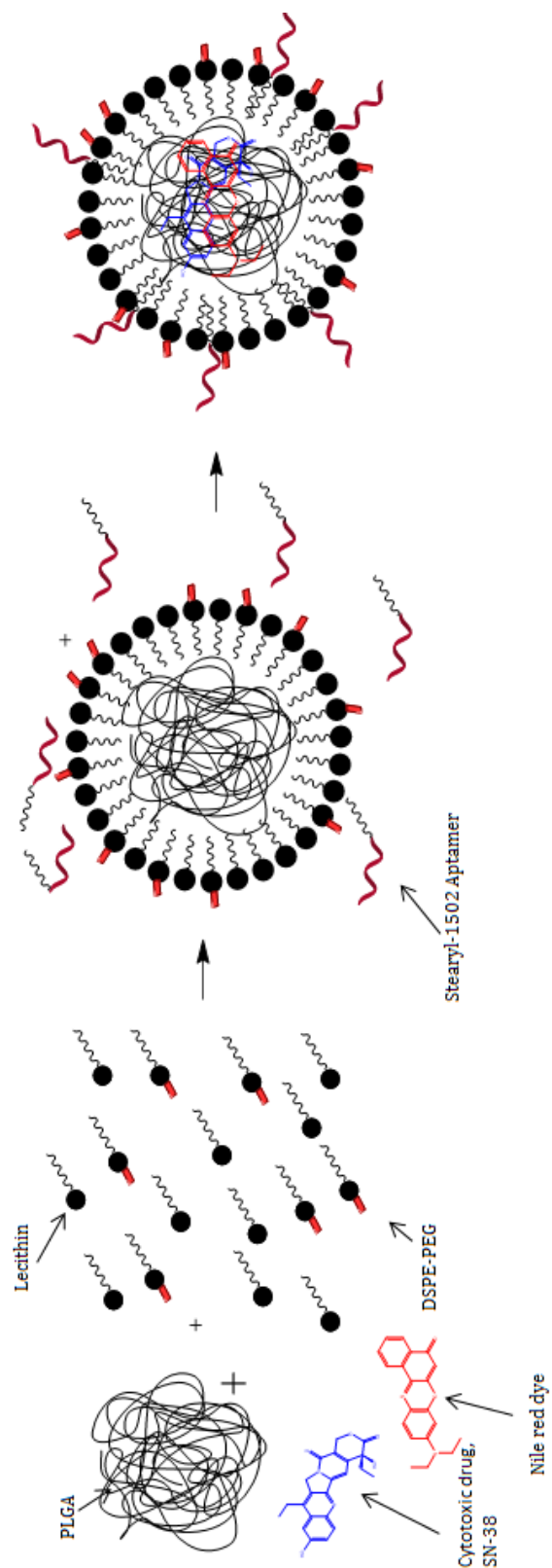
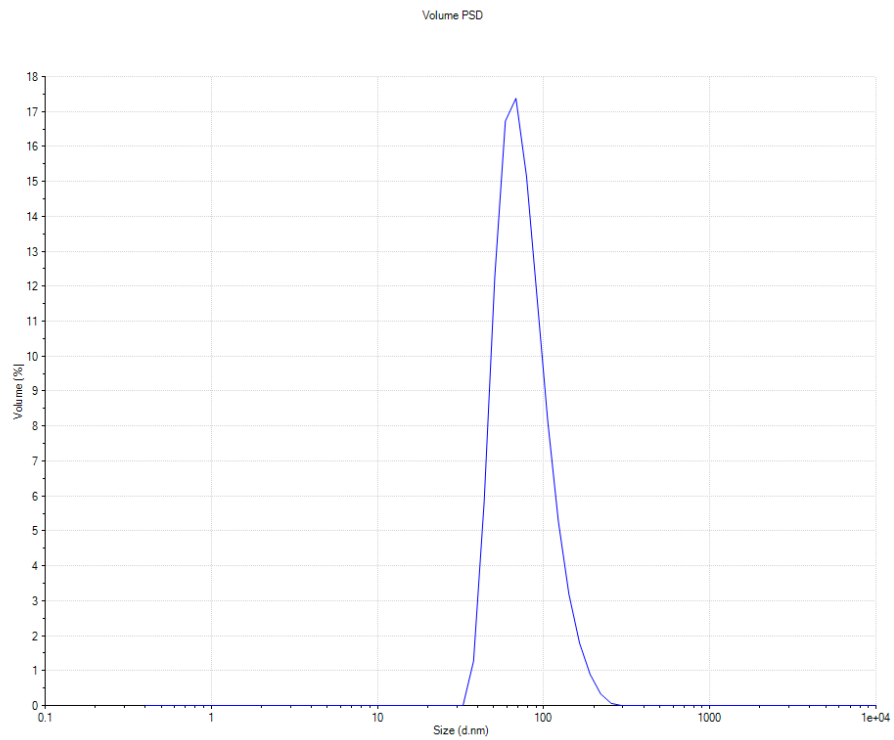


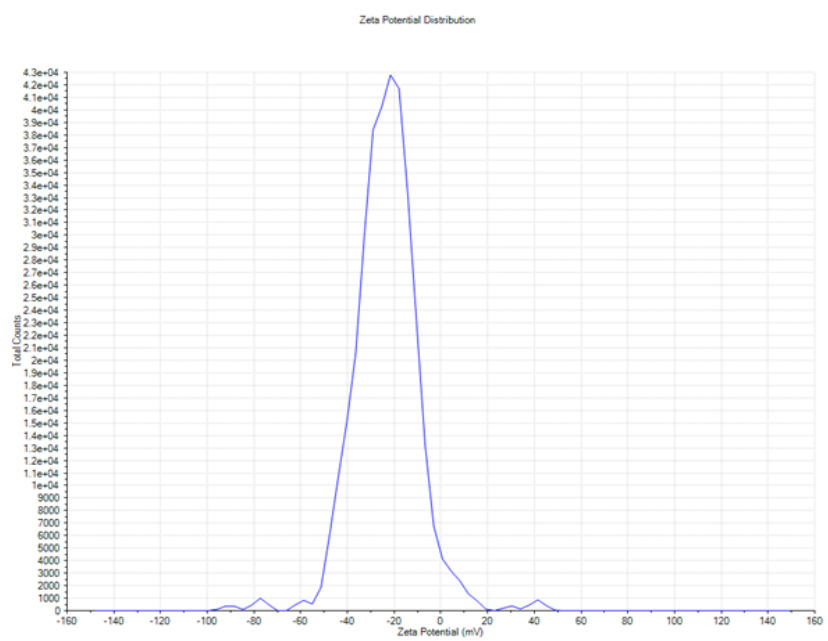
**Figure 4.1** Schematic of the synthesis and functionalization of 1502 lipid-PLGA nanoparticles, containing either Nile red dye or cytotoxic small molecule drug, SN-38.

The nanoparticles were characterized with a Malvern Zeta Sizer. Measurements were taken for three samples, 3X and averaged with a standard deviation. The results for size, PDI, and zeta potential for the lipid-PLGA nanoparticles and aptamer 1502 functionalized lipid-PLGA nanoparticle can be seen in Figure 4.2. The lipid-PLGA nanoparticles were measured and resulted in an average size of  $78.65 \text{ nm} \pm 11.7 \text{ nm}$  and a PDI of 0.124. The 1502 functionalized lipid-PLGA nanoparticle measured an average size of  $89.1 \text{ nm} \pm 15.6 \text{ nm}$  and a PDI at 0.187. With an 8 nm length for the 1502 aptamer, this increase in size is within the range of what we would expect. This increase in size also indicates that the aptamer successfully self-assembled into the lipid outer layer of the nanoparticles. The zeta potential measurements were taken of the same group of samples, and measured to be  $-23.2 \text{ mV} \pm 14.1 \text{ mV}$  for the lipid-PLGA nanoparticle and  $-27.0 \text{ mV} \pm 13.8 \text{ mV}$  for the 1502-lipid-PLGA nanoparticle. With a negative charge on the 1502 aptamer, it was expected that the zeta potential would be more negative for the nanoparticle functionalized by the RNA aptamer. This characterization was repeated for every synthesized, purified, and functionalized lipid-PLGA nanoparticle that was assembled throughout the necessary studies.

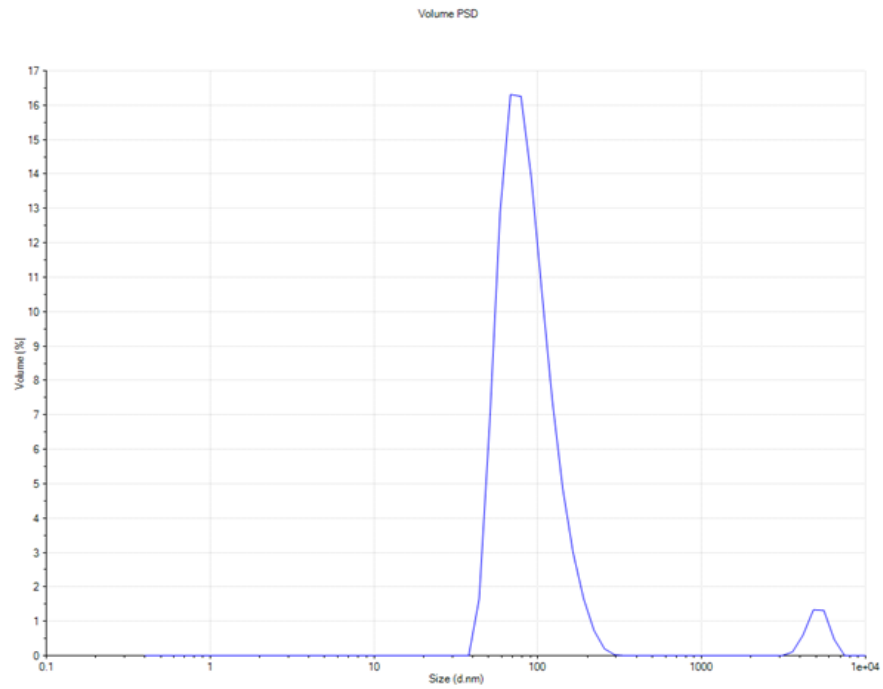
A)



B)



C)



D)

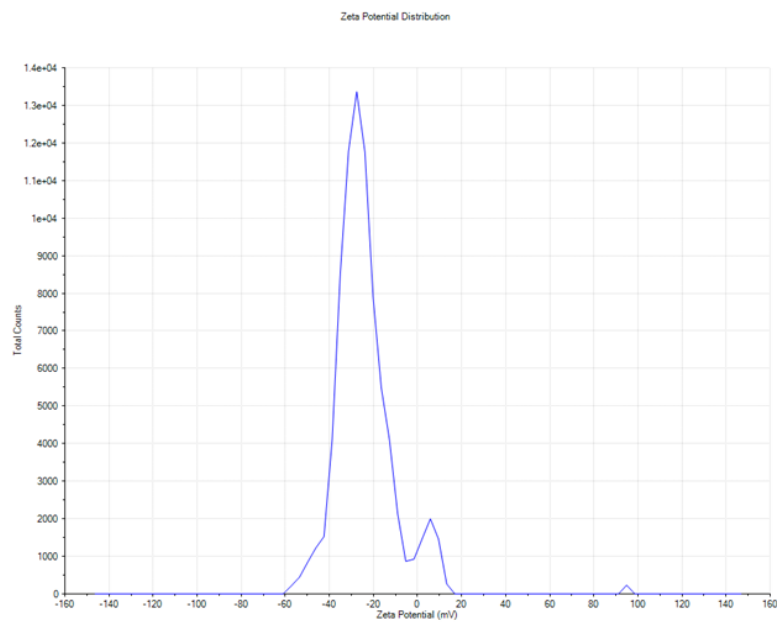


**Figure 4.2** Zeta Sizer measurements for A) Size (78.6 nm) and PDI (.135) of lipid-PLGA nanoparticles, B) Zeta Potential of lipid-PLGA nanoparticles (-23.3 mV), C) Size (89.1 nm) and PDI (.187) of 1502-lipid-PLGA nanoparticles, and D) Zeta Potential of 1502-lipid-PLGA nanoparticles (-27.0 mV).

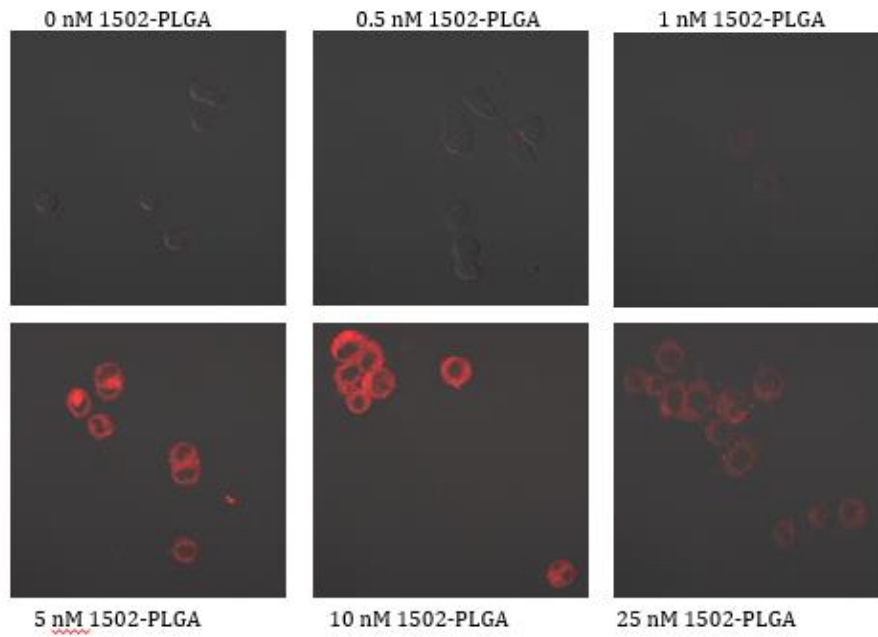


#### **4.2.b. Confocal microscopy demonstrates successful targeting of 1502-lipid-PLGA nanoparticles with an effective 1502 aptamer concentration**

When functionalizing the aptamer, the idea concentration of the aptamer loaded into the nanoparticle was a consideration. As seen in Chapter 3 with the functionalization of the gold nanoparticle, a higher concentration of aptamer does not always mean a more effective targeting of PDAC cells. With higher concentrations, there is the potential issue of steric and electrostatic interactions among the aptamers. With lower concentrations, the concentration of the aptamer could be too low to have a selective and effective targeting effect against PDAC cell lines. To determine the optimal concentration of aptamer 1502, lipid-PLGA nanoparticles containing Nile red dye were functionalized with titrated concentrations of aptamer 1502. It was advantageous to find a concentration where the aptamer input equaled the aptamer inserted into the nanoparticle, a concentration that has a 100% loading efficiency. This avoided the need to remove free, un-inserted 1502. Second, the aptamer concentration should be effective in targeting and delivering the lipid-PLGA nanoparticles to PDAC cell lines.

Initially, higher concentrations of aptamer 1502 were tried, including 1000 nM and 300 nM, however these concentrations were too high to yield 100% loading efficiency (data not shown). Lower concentrations of aptamer loading, including 0, 0.5, 1, 10, and 25, and 50 nM of aptamer 1502 testing during the functionalization of the lipid-PLGA nanoparticles containing Nile red. These nanoparticles were then incubated with AsPC-1 and HPNE cell lines to observe their subsequent targeting and internalization capability. Figure 4.3 illustrates this varying targeting effect of the titrated samples, also demonstrating that the self-assembly of 1502-stearyl was successful.

A.



B.

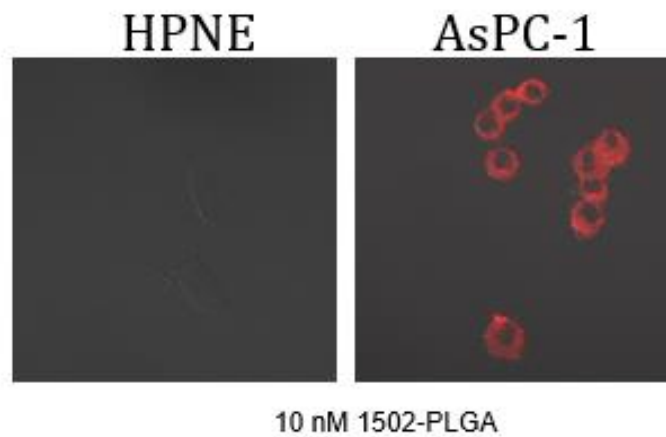


**Figure 4.3** A. Titrated concentrations of aptamer 1502 inserted into lipid-PLGA nanoparticles illustrate that 10 nM 1502 is most effective to target AsPC-1 cells, and B. when tested on HPNE, there is no such targeting and internalization effect.

To confirm that the loading of the aptamer at these varying concentrations is efficient, and not leaving free unreacted 1502, a PAGE denaturing gel was run of the input concentration of aptamer 1502, the aptamer inserted into the lipid-PLGA nanoparticle at corresponding concentrations, and the lipid-PLGA nanoparticle without 1502 as a control. Figure 4.4 demonstrates this analysis, showing that at input aptamer concentrations of 1, 10, and 25 nM, there is no free aptamer observed in the gel after functionalization with lipid-PLGA nanoparticles. The lipid-PLGA nanoparticle alone was run as a control and did not show any observable bands on this denaturing gel.

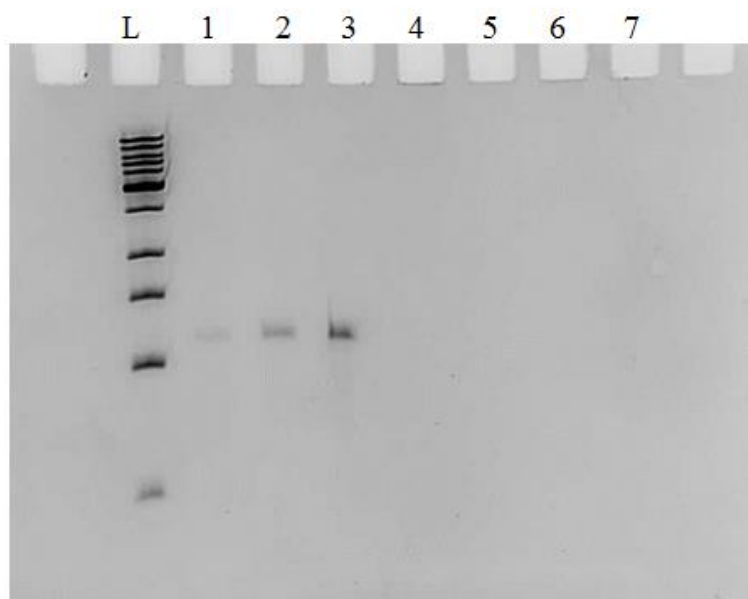
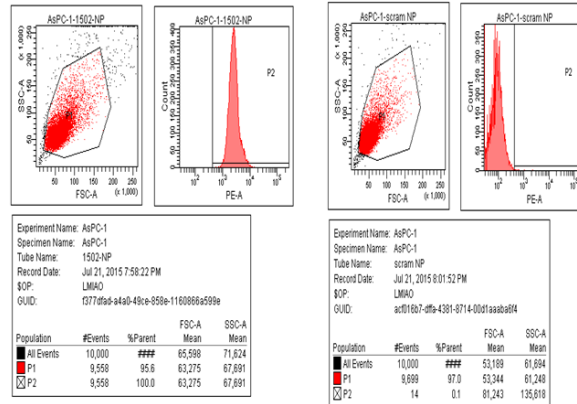
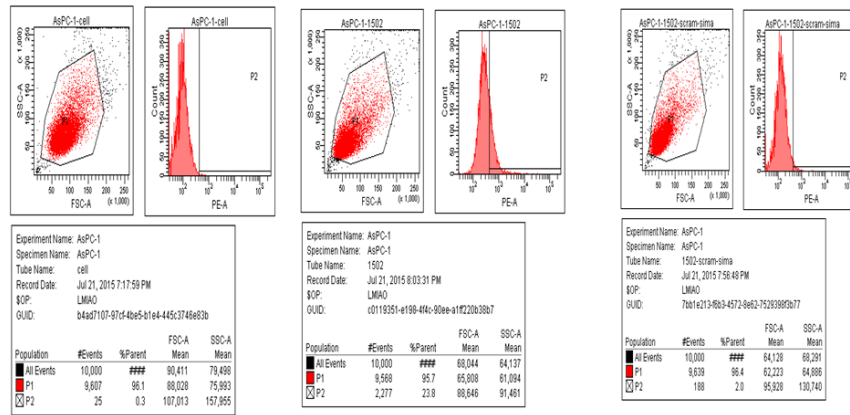


**Figure 4.4** PAGE denaturing gel of L – ladder, 1 – 1 nM 1502, 2 – 10 nM 1502, 3 – 25 nM 1502, 4 – lipid-PLGA nanoparticle (NP) only, 5 – 1 nM 1502-lipid-PLGA NP, 6 – 10 nM 1502-lipid-PLGA NP, and 7 – 25 nM 1502-lipid-PLGA NP demonstrates that there is no observed free aptamer 1502 after functionalization with the nanoparticles at any of the input concentrations.

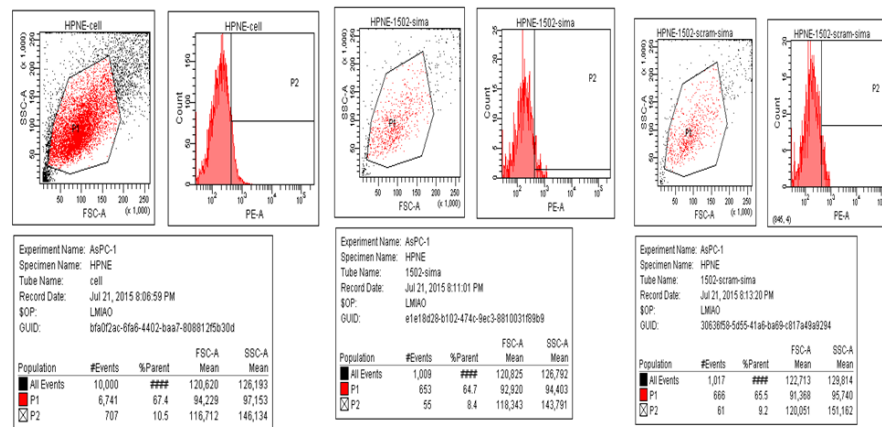
With these results, we felt confident in the proof of concept of utilizing 1502 with a 5' stearyl to functionalize the outer layer of the lipid-PLGA nanoparticles. We could now forward in developing a 1502 functionalized hybrid lipid-PLGA nanoparticle that could be used for PDAC specific cytotoxic cell killing.

#### **4.2.c. Flow cytometry illustrates quantitative binding of 1502-lipid-PLGA nanoparticles to AsPC-1 but not HPNE cells**

In an effort to determine the quantitative cell binding of the lipid-PLGA nanoparticles functionalized with aptamer 1502, flow cytometry was done. A lipid-PLGA nanoparticle was loaded with Nile red dye, as prepared previously, and functionalized with RNA aptamer 1502-original-stearyl or a non-functional RNA aptamer, 1502-scrambled-stearyl. These formulations were incubated with AsPC-1 or HPNE cell lines at 37°C for 2 h, and transferred to FACS tubes with FACS solution to be read for flow cytometry. As seen in Figure 4.5, there is a shift in the binding of both Sima-labeled 1502 (positive control), and of the 1502-lipid-PLGA nanoparticle loaded with Nile red dye. The shift of the latter is significantly more than 1502 only, likely due to a multivalent effect. When the aptamers were tested on HPNE cells, there was no shift in cell population, as seen with the scrambled aptamer and the scrambled aptamer on the nanoparticle. This confirms the specificity and binding of not only the aptamer, but of the aptamer conjugated to the lipid-PLGA nanoparticle.



A)



B)

**Figure 4.5** Flow cytometry of A) AsPC-1 cells treated with PBS, Sima-1502, Sima-scrambled-1502, 1502-lipid-PLGA nanoparticle with Nile red, and 1502-scrambled-lipid-PLGA nanoparticle showed binding of 1502 and 1502 nanoparticle but not the scrambled 1502 sequence. B) HPNE (control) cells were treated with PBS, Sima-1502, and Sima-scrambled-1502 and illustrated no significant binding shift.

#### **4.2.d. Targeted cell killing of hybrid lipid-PLGA nanoparticle loaded with SN-38**

To elicit a targeted cell-killing effect against PDAC, the hybrid lipid-PLGA nanoparticles were encapsulated with a small molecule, cytotoxic drug, SN-38. The nanoparticles were synthesized with varying titrated concentrations of SN-38, and purified, and functionalized as done for the nanoparticles containing Nile red dye. The actual concentration of SN-38 in the stock nanoparticles, after purification and before functionalization, was measured by breaking the nanoparticles open with acetonitrile and using UV-vis to measure the absorbance of SN-38 at 380 nm. This was done to determine the loading efficiency of SN-38, after removing free SN-38 and accounting for leakage of the small molecule from the PLGA core. The final concentrations that are reported for the nanoparticle are the actual encapsulated drug concentrations, taking these factors into consideration and adjusted accordingly. The functional and non-functional nanoparticles had 0, 0.25, 2.5, 25, and 2500 nM SN-38 encapsulated. These formulations were tested on AsPC-1 and HPNE cells with varying incubation times, followed by a live/dead cell assay (Life Technologies) to determine if the cells were living or dying (the green color of the calcein AM indicates living cells, and the red color indicates dying cells). Figure 4.6 illustrates this assay's results after 2, 4, and 6 h of incubation with the functionalized 1502 lipid-PLGA nanoparticle with only 2.5 nM of SN-38. Other SN-38 concentrations, HPNE control cell line, as well as non-functional nanoparticles were also tested at varying time points; however the data is not shown here. These results indicate that even after only 2 h of incubation, the functionalized nanoparticle can target, internalize, deliver SN-38 to the nucleus, and begin to have a cell-killing

effect. After 6 h, the AsPC-1 cells are dead, as indicated by the red color of the live/dead cell assay dye.

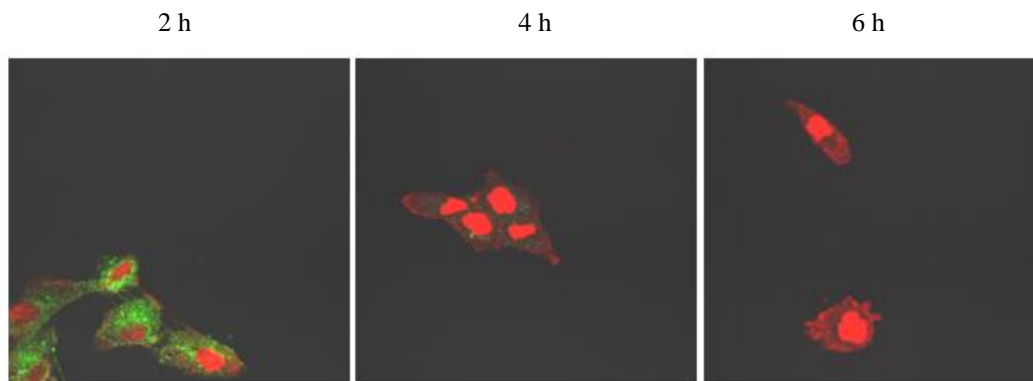


**Figure 4.6** Confocal microscopy images of AsPC-1 cells that were first treated with 1502 lipid-PLGA nanoparticles containing 2.5 nM SN-38 for 2, 4, or 6 h at 37°C. Live/dead cell assay dye was added to indicate if the cells were living (green) or dying (red).

It was determined that 2 h was enough incubation time to have a noticeable effect, however 4-6 h was enough time for internalization and toxicity to the cell. It is with these results that we performed a more comprehensive study of this live/dead cell assay, testing control samples (PBS and free SN-38 at 2.5 nM), 1502 lipid-PLGA nanoparticle with 0, 0.25, 2.5, 25, and 2500 nM SN-38, and an untargeted lipid-PLGA nanoparticle with 2.5 nM SN-38 encapsulated on both AsPC-1 and HPNE cells. Figure 4.7 demonstrates the results (not all results shown) from this study. It is evident that there is a cell killing effect from 1502 lipid-PLGA nanoparticles at 2.5 nM and 25 nM concentrations of SN-38 with no such effect for the untargeted nanoparticle or the targeted nanoparticle with 0 nM SN-38. For HPNE, the higher SN-38 concentration (25 nM) encapsulated in the 1502 lipid-PLGA nanoparticle that had a cell killing effect (as seen in the figure), is shown to have no cell killing effect here. This suggests that this platform is selectively targeting AsPC-1 cells over HPNE and that the targeting is

dependent upon aptamer 1502. Effective cell killing can be seen with SN-38 concentrations as low as 2.5 nM. These results were useful when planning the quantitative MTS assay studies.

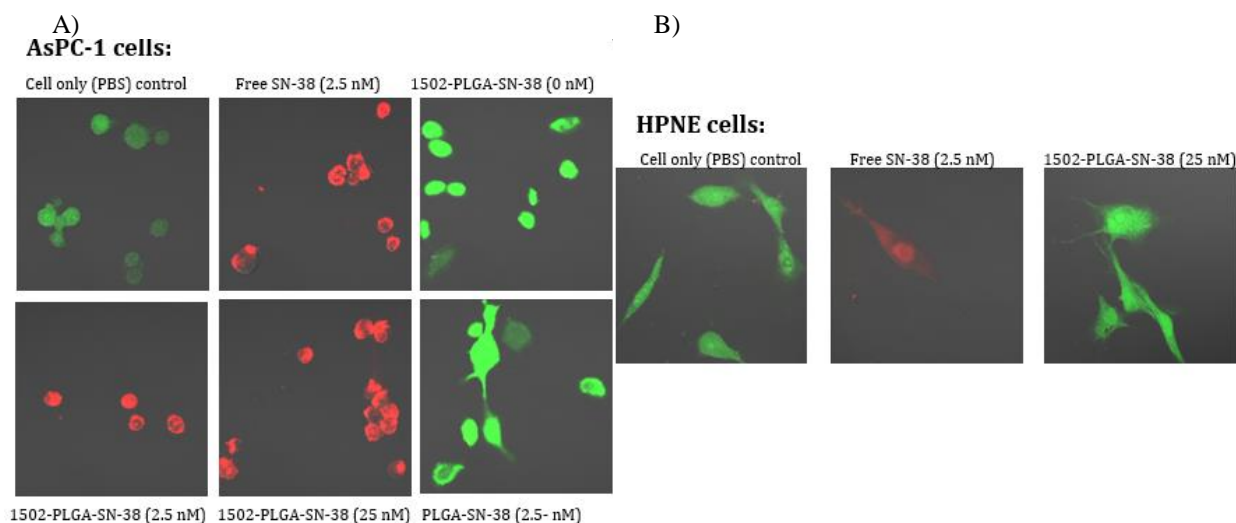


**Figure 4.7** A) AsPC-1 cells were treated with PBS, free SN-38 at 2.5 nM, 1502 lipid-PLGA nanoparticles with varying concentrations of SN-38, and lipid-PLGA nanoparticles with 2.5 nM SN-38 for 6 h at 37°C, followed by live/dead cell assay dyes. B) HPNE cells were treated under the same conditions (with controls and 1502 lipid-PLGA nanoparticles with SN-38 shown).

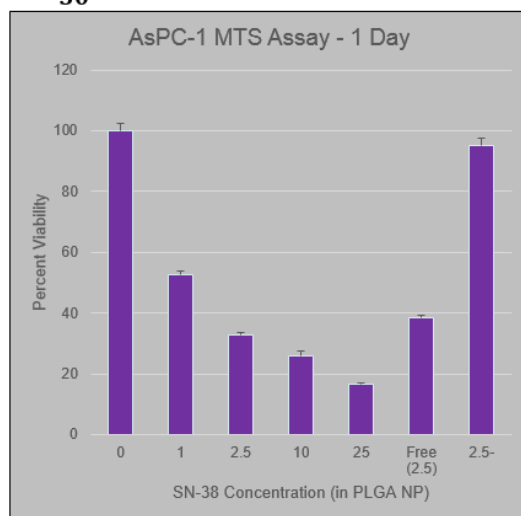
To quantify this cell killing effect, a MTS assay was done on both AsPC-1 and HPNE cells. The same titrated preparations of 1502 lipid-PLGA encapsulated with SN-38 were used (0, 0.25, 2.5, 25, 2500 nM). The goal was to quantify the cell killing specificity of the targeted lipid-PLGA nanoparticle carrying SN-38 by determine an  $IC_{50}$  for the nanoparticle for AsPC-1 and HPNE cells. Samples were treated onto HPNE or AsPC-1 cells, plated in 96-well plates, for 6 h at 37°C to allow for maximum internalization. Samples were removed and media was added to allow for cell growth over 1 day. The MTS assay was performed by first adding CellTiter 96 AQueous to the cells, which is composed of MTS (3-(4,5-dimethylthiazol-2-yl)-5-(3-carboxymethoxyphenyl)-2-(4-sulfophenyl)-2H-tetrazolium). When MTS is in PBS, and interacts with mitochondrial reductase, which is formed when a cell is dying, it produces a formazan product that has an absorbance at 490 nm<sup>53</sup>.



Initially, several conditions were tested to determine the best conditions for this assay. This included cell confluence when plated, time of sample incubation, time of cell incubation after media was added, and MTS incubation time. The optimal conditions of this MTS assay that were determined were 10% cell confluence when plated, 1 day sample incubation after the addition of media, and 3 h MTS incubation. Figure 4.8 shows the percent viability of AsPC-1 or HPNE cells when treated with the 1502 targeted nanoparticles with varying concentrations of SN-38 as well as free SN-38 (2.5 nM) and untargeted lipid-PLGA nanoparticles (with 2.5 nM SN-38), marked as 2.5-. The samples were done in triplicate with triplicate absorbance readings of each. Sample absorbances were normalized based on controls and adjusted to 100% viability. Results yielded an  $IC_{50}$  of  $14 \pm .5$  nM for AsPC-1 cells and an unmeasurable  $IC_{50}$  for HPNE, as the cell viability never reached below 50% for these studies. Free SN-38 is expected to have cytotoxicity with both AsPC-1 and HPNE, which is seen in Figure 4.8. However, when encapsulated in the nanoparticle, SN-38 did not affect HPNE cells. While there was some decrease in cell viability for the free SN-38 drug and the untargeted nanoparticle for AsPC-1 cells, these samples did not have as much of an effect as the corresponding 1502 lipid-PLGA nanoparticle containing 2.5 nM SN-38.

A)

**IC<sub>50</sub>: 14 ± .5 nM**



B)

**IC<sub>50</sub>: not measurable**

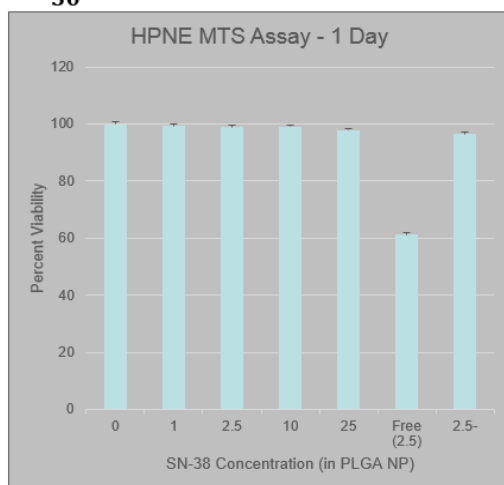


**Figure 4.8** A) The viability of AsPC-1 cells treated with 1502 lipid-PLGA nanoparticles with SN-38 at varying concentrations, free SN-38 at 2.5 nM, and lipid-PLGA nanoparticles at 2.5 nM SN-38 gives an IC<sub>50</sub> of 14 ± .5 nM. B) The viability of HPNE cells is close to 100% for all targeted and untargeted nanoparticle samples, yielding a non-measurable IC<sub>50</sub>.

#### 4.2.e. Encapsulation efficiency of lipid-PLGA nanoparticles with Nile red dye or SN-38

To determine the encapsulation efficiency of the lipid-PLGA nanoparticles, loaded with either Nile red or SN-38, a serum stability assay was done with 50% serum over several time points including 0 min, 5 min, 2 h, 4 h, 8 h, 12 h, and 24 h. Nanoparticles were prepared in PBS, and ultracentrifuged at 18,000 rpm for 1 h at 4°C. The nanoparticle pellet and supernatant were both measured for absorbance at 555 nm, for Nile red, and 380 nm, for SN-38 using our NanoDrop. Similar to other studies found in the literature<sup>54-58</sup>, there was an initial burst release of both Nile red and SN-38 after approximately 4 h, followed by a slow release over the remaining time points.

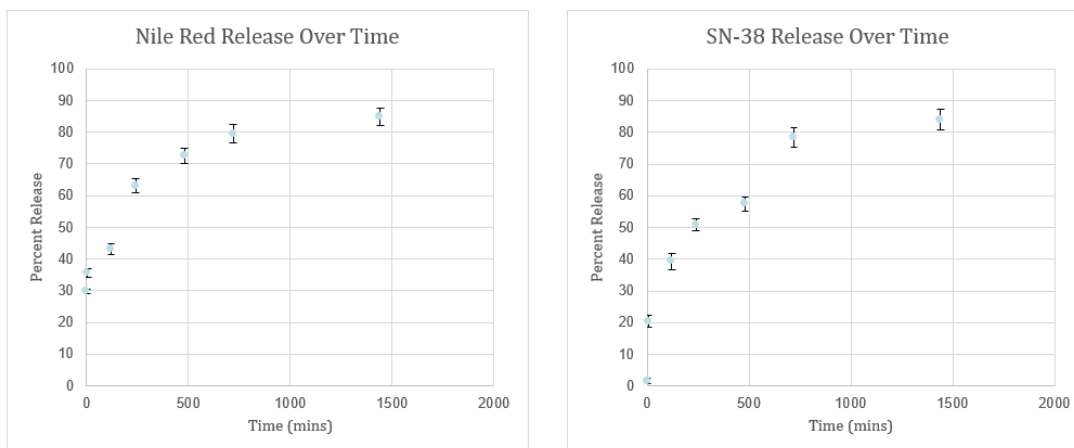


**Figure 4.9** The Nile red and SN-38 release from the lipid-PLGA nanoparticle when treated with 50% serum for up to 24 h.

#### 4.2.f. Determining the functional stability of 1502-lipid-PLGA nanoparticle with a serum stability assay

To translate this targeted delivery platform to *in vivo* studies, it was important to first determine if the functionalized lipid-PLGA nanoparticle can continue to target the AsPC-1 tumor

after circulation in the blood. A serum stability assay was done using the 1502 lipid-PLGA nanoparticle that encapsulated either Nile red or SN-38 (at 2.5 nM). The nanoparticles were treated with 50% mouse serum in PBS for 0, 5 min, 2, 4, 8, 12, and 24 h. The size of the nanoparticles, loaded with either Nile red dye or SN-38 was measured by a Zeta Sizer to determine if longer treatment with serum disrupted the size of the nanoparticles. Results seen in Figure 4.10, demonstrates a relatively stable size of the both nanoparticle formulations after being treated with serum for up to 24 h.

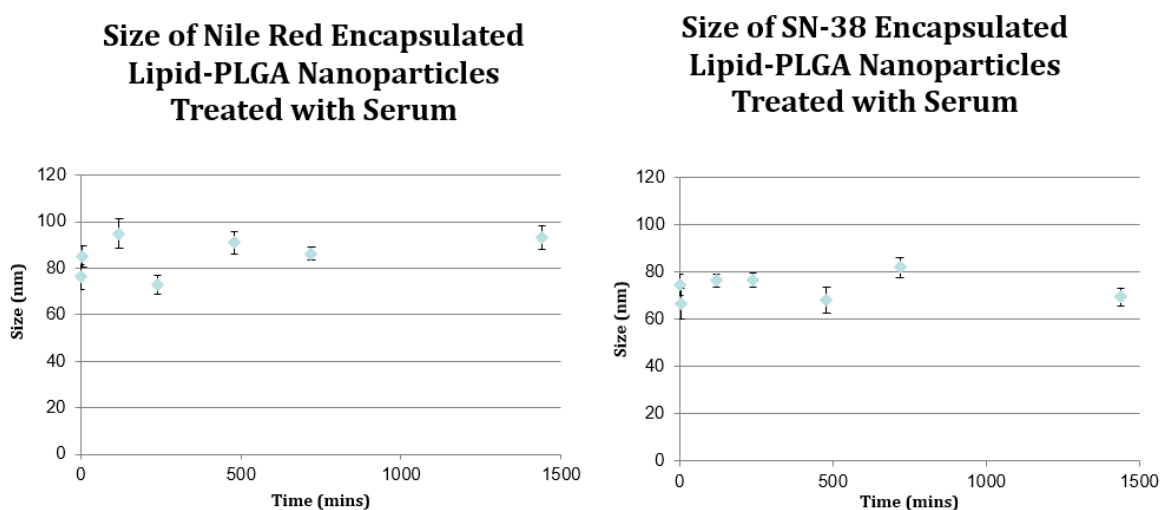


**Figure 4.10** Size of Nile red encapsulated and SN-38 lipid-PLGA nanoparticles treated with 50% serum over 24 h.

Confocal microscopy was used to visualize the targeting of the Nile red encapsulated nanoparticles to AsPC-1 vs. HPNE cells after being treated with 10% mouse serum at the previously mentioned time points (5 min not shown). This was done with the targeted 1502 lipid-PLGA nanoparticles, the untargeted lipid-PLGA nanoparticles, and lipid-PLGA nanoparticles functionalized with scrambled 1502. Results from these tests are shown in Figure 4.11.a.-f.

**AsPC-1 1502 lipid-PLGA nanoparticle with Nile red dye**

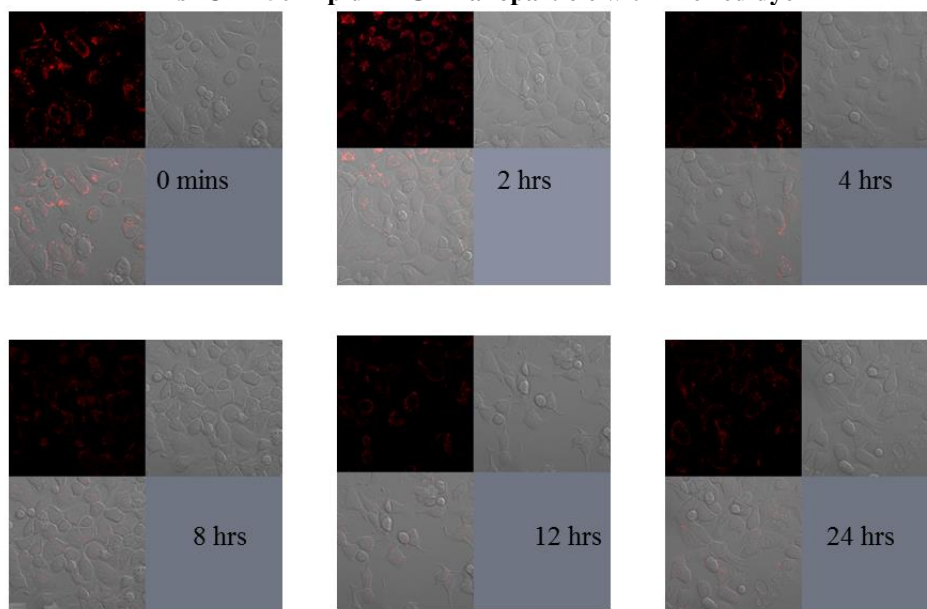


**Figure 4.11.a.** 1502 lipid PLGA nanoparticles encapsulating Nile red dye were treated with 0, 2, 4, 8, 12, and 24 h of mouse serum and then incubated with AsPC-1 cells for 2 h at 37°C and read on confocal microscopy.

**AsPC-1 1502 scrambled lipid-PLGA nanoparticle with Nile red dye**

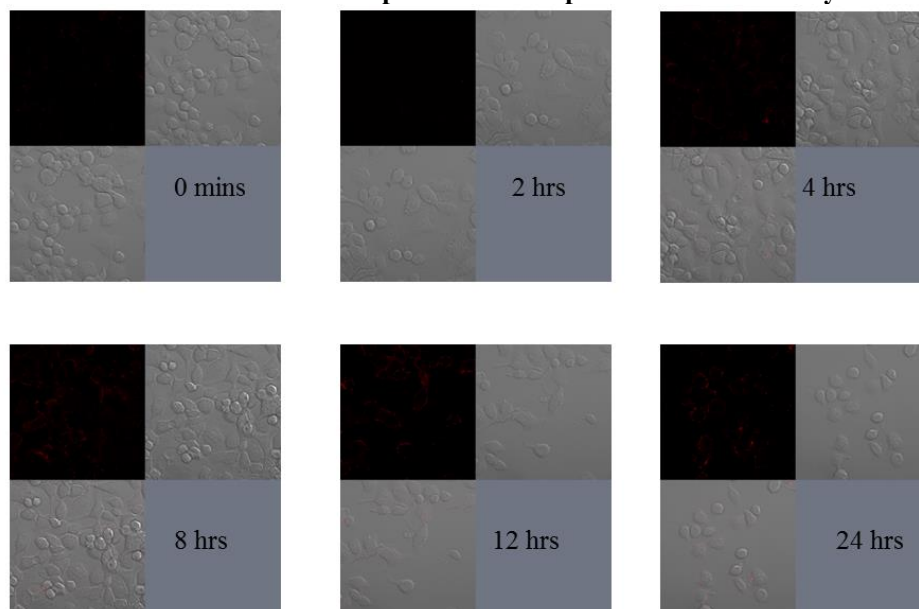


**Figure 4.11.b.** 1502 scrambled lipid PLGA nanoparticles encapsulating Nile red dye were treated with 0, 2, 4, 8, 12, and 24 h of mouse serum and then incubated with AsPC-1 cells for 2 h at 37°C and read on confocal microscopy.

**AsPC-1 lipid-PLGA nanoparticle with nile red dye**

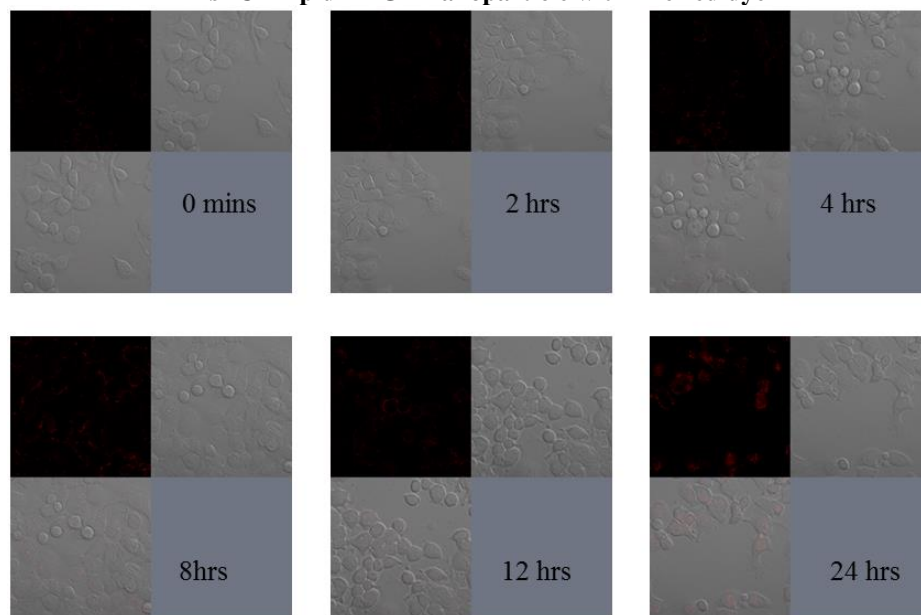


**Figure 4.11.c.** Lipid PLGA nanoparticles encapsulating Nile red dye were treated with 0, 2, 4, 8, 12, and 24 h of mouse serum and then incubated with AsPC-1 cells for 2 h at 37°C and read on confocal microscopy.

**HPNE 1502 lipid-PLGA nanoparticle with Nile red dye**

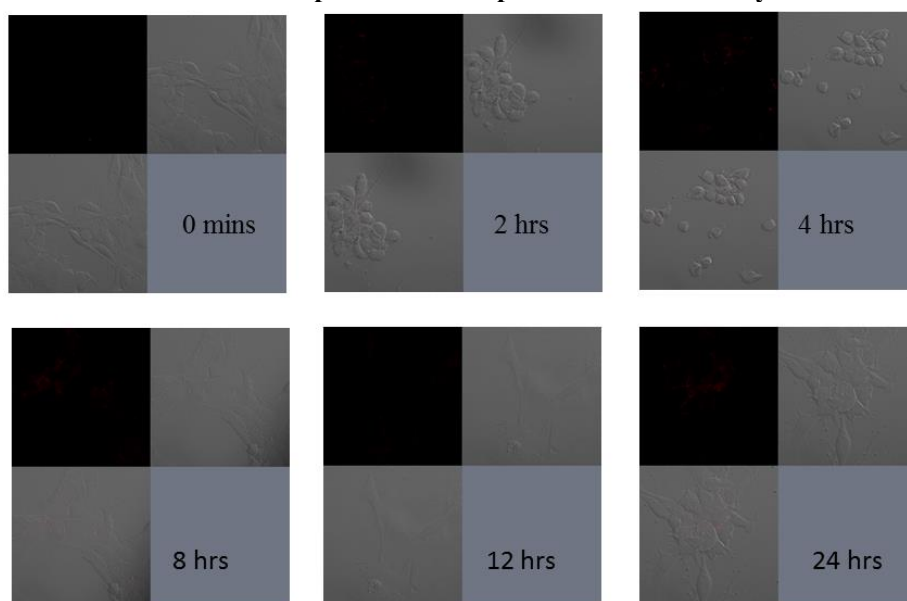


**Figure 4.11.d.** 1502 lipid PLGA nanoparticles encapsulating Nile red dye were treated with 0, 2, 4, 8, 12, and 24 h of mouse serum and then incubated with HPNE cells for 2 h at 37°C and read on confocal microscopy.

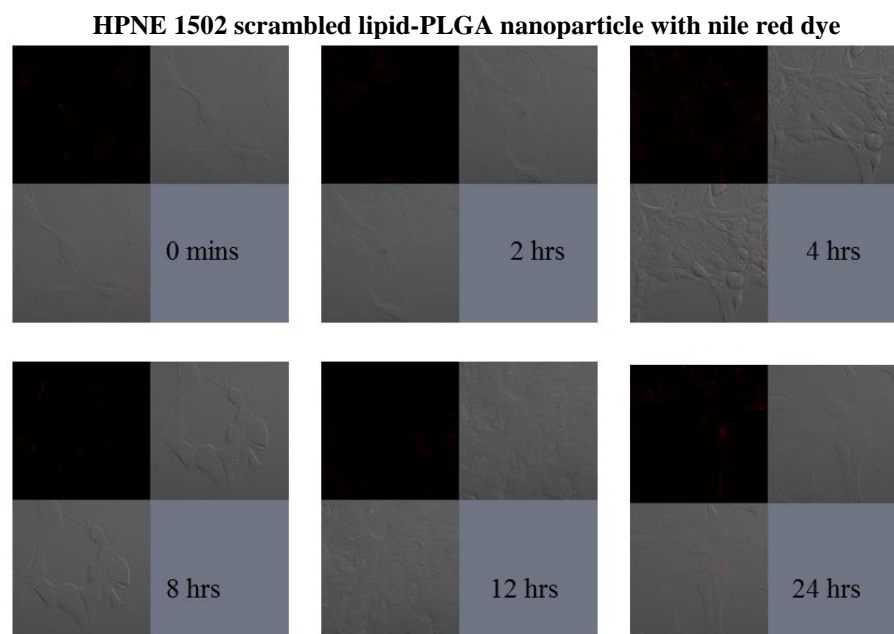


**Figure 4.11.e.** 1502 scrambled lipid PLGA nanoparticles encapsulating Nile red dye were treated with 0, 2, 4, 8, 12, and 24 h of mouse serum and then incubated with HPNE cells for 2 h at 37°C and read on confocal microscopy.

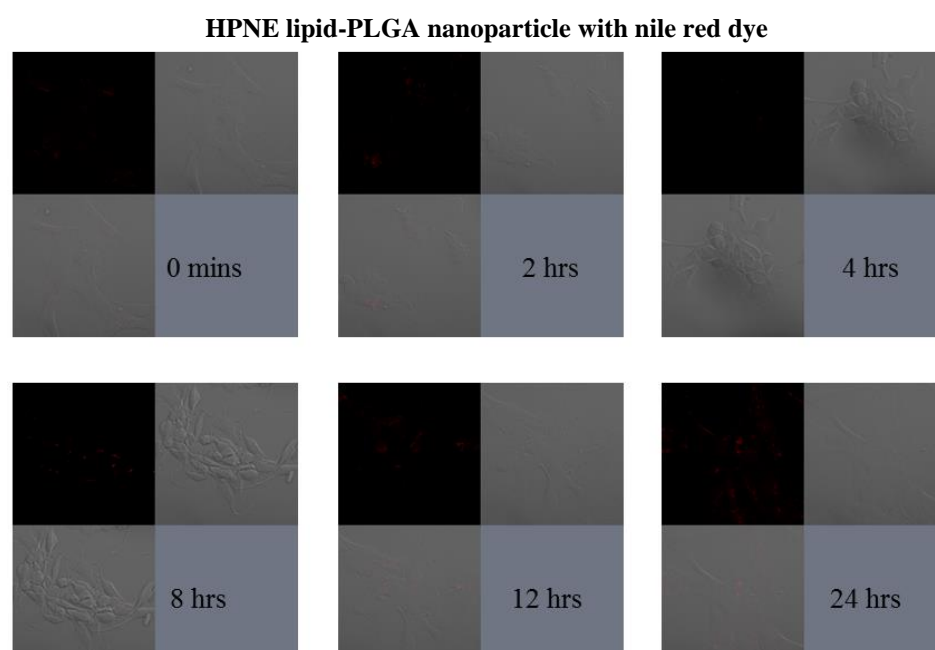


**Figure 4.11.f** Lipid PLGA nanoparticles encapsulating Nile red dye were treated with 0, 2, 4, 8, 12, and 24 h of mouse serum and then incubated with HPNE cells for 2 h at 37°C and read on confocal microscopy.

For AsPC-1 cells, it does appear that there is a strong targeting effect of the 1502 lipid-PLGA nanoparticle at 0, 2, and 4 h. After 8 h, there is some decrease in signal from Nile red, however there is a clear cell-surface targeting effect up to 24 h. With the scrambled 1502 lipid-PLGA nanoparticle and the untargeted nanoparticle, there is signal after 8 h, however the signal appears weaker than it does at the same time points for the 1502 lipid-PLGA nanoparticle. This suggests that there may be some non-specific delivery of the nanoparticle to AsPC-1 cells if the nanoparticle was treated with mouse serum for 8+ h. This non-specificity can be addressed easily by tuning the nanoparticle's composition and improving upon the circulation properties (as suggested in the next section).

From these results, there doesn't seem to be much of an effect of the targeted 1502 and 1502 scrambled nanoparticles on HPNE cells. There is some non-specific signal for the lipid-PLGA nanoparticle treated with serum for 24 h. The stability of the nanoparticle itself may have to be further analyzed and improved upon *in vivo*, however non-specific uptake has been an addressable problem in the past<sup>59,60</sup>. Even adjusting the DSPE-PEG concentration can allow for increased circulation time and decreased specificity issues.

#### **4.3. Concluding Remarks**

While the targeted hyperthermia assay in Chapter 3 resulted in specific cell killing of PDAC, it is debatable if targeted hyperthermia is clinically translatable for the treatment of pancreatic cancer. While a NIR laser can penetrate through human skin, the targeted hyperthermia application may be more useful for a cancer that is closer to the skin's surface, such as a head and neck cancer. The pancreas is tucked behind the stomach and would be difficult to access with a laser. There have been discussions around using orthoscopic methods to deliver



a laser to the pancreas, however this idea is preliminary. We needed a targeted delivery platform that could reach the pancreas and more specifically, the pancreatic tumor, through the bloodstream. Moreover, it would be useful if this platform was biocompatible, tunable, and allowed for the delivery of various chemotherapeutic drugs to PDAC tumors.

The hybrid lipid-PLGA nanoparticle was a great model for the delivery platform that we were looking to develop. It had already been proven to be biocompatible with low toxicity and an adjustable circulation half-life. Our goal was to synthesize both the nanoparticle and aptamer 1502 so that the nanoparticle could be directed to PDAC tumors by aptamer 1502. We wanted a process that was easy and simple, with very little chemistry. We conceptualized utilizing aptamer 1502 that had a 5' stearyl group to functionalize this lipid outer layer of the hybrid nanoparticle. The stearyl group mimics a lipid tail, and interacted with the DSPE-PEG and lecithin lipids similar to the lipids themselves. With the 5' stearyl insertion into the nanoparticle, functional aptamer 1502 remained on the outermost layer of the nanoparticle to direct the targeting to PDAC cells. We were able to prove this concept by loading the polymer core of the nanoparticle with Nile red dye. The encapsulated Nile red dye nanoparticles were functionalized with aptamer 1502 and delivered selectively to AsPC-1 and not HPNE cells. It was with this data that we felt comfortable moving forward to a targeted cell-killing assay.

The hybrid lipid-PLGA nanoparticles were loaded with SN-38, a cytotoxic small molecule drug that is known to have a cell killing effect. With the hydrophobicity of the PLGA, the functionalized lipid-PLGA nanoparticle could easily encapsulate a different chemotherapeutic if that were desired for a specific therapeutic regimen. Once functionalized with aptamer 1502, the nanoparticle platform was delivered to AsPC-1 vs. HPNE cells to determine an  $IC_{50}$  and specificity of this targeted therapeutic. An MTS assay demonstrated that the 1502

functionalized nanoparticle could selectively target AsPC-1 cells, internalize, and result in a cell killing once the SN-38 was released. This effect was not observed in HPNE cells, proving the specificity of the targeted therapeutic to AsPC-1. Serum stability tests for this nanoparticle indicated that the aptamer's function was maintained up to 24 h in 10% serum and the specificity was maintained up to 8 h in 10% serum. These results indicate that the 1502 lipid-PLGA nanoparticle has potential as a translational targeted delivery tool against PDAC tumors *in vivo*.

#### **4.4 Materials and Methods**

##### **4.4.a. Construction, functionalization, and characterization of hybrid lipid-PLGA nanoparticles**

Hybrid lipid-PLGA nanoparticles were prepared following a protocol in the literature (reference). Stock solutions of lecithin (1 mg/mL in 4% ethanol), DSPE-PEG (1 mg/mL in 4% ethanol), and PLGA (2 mg/mL) in acetonitrile were prepared. An 8.5:1 molar ratio of lecithin to DSPE-PEG was mixed at 65°C until the solution was homogeneous. The solution was cooled to room temperature, and PLGA was added drop wise at a 1:10 organic:aqueous molar ratio. The solution was vortexed for three min, followed by slow stirring at room temperature for 2 h to allow for self-assembly.

Nanoparticles were purified by a Millipore 10K centrifuge column by centrifugation at 4000× rpm for 15 min at 4°C. Nanoparticles were washed three times with 1X PBS. Resulting 'stock' nanoparticles were considered to be at a 50X concentration at 300 µL.

Functionalization of the hybrid lipid-PLGA nanoparticles with aptamer 1502 was done through self-assembly by adding the 1502 aptamer containing a 5' stearyl modification to the purified nanoparticle (final concentration = 1X). The aptamer with the nanoparticle was slowly rotated at room temperature overnight to allow for self-assembly.

The non-functional and functional nanoparticles were characterized by the Malvern Zeta Sizer for size, PDI, and zeta potential. Size and PDI were calculated three times using a disposable cuvette, where zeta potential was measured three times in a DTS1060 cuvette.

#### **4.4.b. Confocal microscopy of 1502 lipid-PLGA nanoparticles encapsulated with Nile red**

During construction, the lipid-PLGA nanoparticles were encapsulated with Nile red dye (Sigma) at a 1:10 ratio by volume to the PLGA (stock was 1 mg/mL in acetonitrile). The concentration of Nile red dye was optimized to have visible signal at 555 nm on the confocal microscopy as well as encapsulation efficiency. Purified nanoparticles were functionalized with aptamer 1502-stearyl or aptamer 1502-scrambled that contained a 5'-stearyl. To test the targeting and internalization of functionalized vs. non-functional nanoparticles against AsPC-1 cells, cells (AsPC-1 and HPNE) were plated. Lipid-PLGA nanoparticles containing Nile red dye, 200  $\mu$ L, were added to the plated cells for 6 h at 37°C. Samples included 1502-lipid-PLGA nanoparticles, lipid-PLGA nanoparticles (control), and 1502-scrambled-lipid-PLGA nanoparticles (aptamer control). After incubation, samples were removed and cells were washed with 1X PBS once. Cover slips were transferred to slides with cell-adhesion solution and samples were read at 555 nm wavelength with a Zeiss 700 confocal microscope at a 40 $\times$  oil objective lens.

#### **4.4.c. Optimization of aptamer loading**

To ensure efficient delivery and internalization of the lipid-PLGA nanoparticles, varying concentrations of aptamer 1502 were added during the functionalization of the nanoparticles. Concentrations tested included 0, 0.5, 1, 5, 10, and 25 nM of aptamer 1502. These functional nanoparticles were tested with confocal microscopy, as seen in section 1.4.b, to determine the

optimal concentration of aptamer 1502. Subsequently, the aptamer's actual loading efficiency was tested by centrifuging the nanoparticle, removing the supernatant containing free 1502, and running a PAGE denaturing gel to quantify the free aptamer.

#### **4.4.d. MTS assay of lipid-PLGA SN-38 for AsPC-1 and HPNE**

In a new formulation, lipid-PLGA nanoparticles were constructed by adding a 1:10 ratio of cytotoxic small molecule SN-38 (made by a collaborator) to the PLGA polymer. The final concentrations of SN-38, post purification and functionalization, included 0, .25, 2.5, 25, 250, and 2500 nM. These concentrations were confirmed by breaking open the functionalized nanoparticle with acetonitrile and measuring the encapsulated SN-38 by UV-vis at 380 nm.

AsPC-1 or HPNE cells were plated in a 96-well plate at approximately 40% confluence. Lipid-PLGA nanoparticles containing SN-38 (100  $\mu$ L) were incubated with AsPC-1 or HPNE cells for up to 6h at 37°C to allow for targeted delivery, internalization, and effective cytotoxicity. In addition to the non-functional nanoparticles carrying SN-38, 1502-lipid-PLGA nanoparticles with SN-38 were tested, along with free SN-38 at 2.5 nM. All samples and controls were done in triplicate. Post-incubation, samples were removed and 100  $\mu$ L of the corresponding media was added. Cells were returned to 37°C for 24 h.

For the MTS assay, cells were treated with 20  $\mu$ L of the CellTiter 96® Aqueous One Solution Reagent (Promega) for 1 to 4 h at 37°C. The samples were read with a BioTek Fluorescence plate reader at an absorbance of 490 nm to determine the relative viability of the cells. Raw data was normalized with the controls and triplicate samples were averaged and standard error was determined.

#### **4.4.e. Testing the functional stability of aptamer 1502-stearyl with a serum stability assay**

Six lipid-PLGA nanoparticle constructions were tested for the functional stability of the aptamer. This included lipid-PLGA nanoparticle (nile red), 1502-lipid-PLGA nanoparticle (nile red), 1502-scrambled-lipid-PLGA nanoparticle (nile red), lipid-PLGA nanoparticle (SN-38, 2.5 nM), 1502-lipid-PLGA nanoparticle (SN-38, 2.5 nM), and 1502-scrambled-lipid-PLGA nanoparticle (SN-38, 2.5 nM). All nanoparticle samples were incubated in either 10% or 50% mouse serum (Gibco) at 37°C for varying lengths of time (0, 5 min, 2, 4, 8, 12, and 24 h). Each of the nanoparticles containing SN-38 were done in triplicate to allow for standard error.

#### **4.4.e.i. Nanoparticle characterization with Zeta Sizer**

In order to determine the effect that mouse serum has on the formulated nanoparticles, the nanoparticles and the aptamer functionalized-nanoparticles were characterized. The serum-treated nanoparticles were characterized by the Malvern Zeta Sizer for size, PDI, and zeta potential. Size and PDI were calculated three times using a disposable cuvette, where zeta potential was measured three times in a DTS1060 cuvette.

#### **4.4.e.ii. Confocal microscopy**

AsPC-1 and HPNE (control) cells were plated. Serum-treated lipid-PLGA nanoparticles containing Nile red dye, 200  $\mu$ L, were added to the plated cells for 6 h at 37°C. Samples included 1502-lipid-PLGA nanoparticles, lipid-PLGA nanoparticles (control), and 1502-scrambled-lipid-PLGA nanoparticles (aptamer control) at each of the respective time points and serum conditions. After incubation, samples were removed and cells were washed with 1X PBS once. Cover slips were transferred to slides with cell-adhesion solution. Samples were read at 555 nm

wavelength with a Zeiss 700 confocal microscope at a 40× oil objective lens to determine the targeted functionality of aptamer 1502.

#### **4.4.e.iii. Encapsulation efficiency of lipid-PLGA nanoparticles with nile red or SN-38**

The effect of serum on the encapsulation of nile red from the nanoparticle was also tested. Both lipid-PLGA nanoparticles containing nile red or SN-38 and 1502-lipid-PLGA nanoparticles containing nile red or SN-38 that were treated with 10% serum were ultracentrifuged at 18,000 rpm for 1 h at 4°C. The nanoparticles containing nile red dye or SN-38, treated with serum for varying lengths of time, were pelleted, leaving the supernatant with dye that was no longer encapsulated. The UV-Vis of nile red dye remaining in the supernatant was measured using the NanoDrop at an absorbance of 555 nm and the UV-Vis of SN-38 was measured at 380 nM. The concentrations were calculated and compared to the starting concentration of the nanoparticle not treated with serum to determine the effect that the mouse serum had on the encapsulation of nile red dye or SN-38.

#### **4.4.e.iv. MTS assay**

AsPC-1 or HPNE cells were plated in a 96-well plate at approximately 40% confluence. Serum treated lipid-PLGA nanoparticles containing SN-38 (100 µL) were incubated with AsPC-1 or HPNE cells for 6 h at 37°C to allow for targeted delivery, internalization, and effective cytotoxicity. In addition to the non-functional nanoparticles carrying SN-38, 1502-lipid-PLGA nanoparticles with SN-38 were tested, along with free SN-38 at 2.5 nM. All samples and controls were done in triplicate. Post-incubation, samples were removed and 100 µL of the corresponding media was added. Cells were returned to 37°C for 24 h.

For the MTS assay, cells were treated with 20  $\mu$ L of the CellTiter 96® Aqueous One Solution Reagent (Promega) for 1 to 4 h at 37°C. The samples were read with a BioTek plate reader at an absorbance of 490 nm to determine the relative viability of the cells. Raw data was normalized with the controls, triplicate samples were averaged, standard error was determined.

#### **4.4.e.v. Flow cytometry of lipid-PLGA nanoparticles**

To monitor the targeting of 1502-lipid-PLGA nanoparticles to AsPC-1 vs HPNE cells, lipid-PLGA nanoparticles were prepared with Nile red dye, as done previously, and functionalized with either RNA aptamers 1502-original-stearyl or non-functional 1502-scrambled-stearyl. The nanoparticles, and aptamers only were incubated with  $1 \times 10^6$  cells in 400  $\mu$ L binding buffer at 4°C for 30 min. Cells were washed twice after incubation and analyzed by flow cytometry. Flow cytometry was performed on a FACScan cytometer with CellQuest software (Becton Dickinson).

## CHAPTER V

### COLLABORATIONS AND FUTURE DIRECTIONS

#### 5.1 Introduction

To progress aptamer 1502 towards the clinic, there are two major studies that need to be done. One of the two directions is the identification of the aptamer's target. The second major study is the delivery of aptamer 1502 *in vivo*. During my dissertation research, I began experiments towards both, and through collaborators, we are able to continue these studies post-defense.

We know that this target is present on the cell surface of several tested PDAC cells, but not many of the non-pancreatic cancer cell lines tested. Identifying this target could make significant advancements towards the diagnostic and therapeutic development that is specific for pancreatic ductal adenocarcinoma. A visiting scholar, Lu Zhang, along with collaborator Dr. Kevin Xiao, is working towards this goal.

As for the *in vivo* studies, the tumor targeting effect of aptamer 1502 is being tested using two platforms. The first is aptamer 1502 that has been labeled Cu<sup>64</sup> labeled through aptamer modification with DOTA. This can then be traced through PET imaging. The second targeted delivery platform is the 1502-functionalized hybrid lipid-PLGA nanoparticle that was developed in Aim 3. Both delivery methods have promising preliminary data against PDAC tumors that



were inoculated into nude mice and will continue to be tested by our collaborator, Dr. Zibo Li, including research associate professor Dr. Hui Wang, and graduate student, Mengzhe Wang.

## **5.2 Biomarker identification**

So far, only a few biomarkers (such as the 85-90 kDa palladin isoform, plectin-1, ALPPL-2, and cyclophilin B) have been implicated in PDAC. The identification of a potentially novel biomarker might allow the discovery of a novel targetable PDAC receptor that can be used for both targeted diagnosis and therapy<sup>61,62</sup>.

Currently, there is an urgent need for the identification of PDAC-specific cell surface biomarkers that are of great importance in the targeted diagnosis and therapy of PDAC. Aptamer 1502 has been able to bind to all 11 pancreatic cancer cell lines available to us, as well as 2 liver cancer cell lines, a type of cancer that has shown to share overexpressed biomarkers with PDAC. There has been no binding to normal pancreatic cells as well as other several other non-pancreatic cancer cells. Our results clearly indicate that the selected aptamers bind to a highly valuable cell-surface receptor that is universally present on most PDAC cells but not on normal pancreas cells or non-pancreatic cells.

### **5.2.a. Plan for biomarker identification**

The identification of this novel biomarker might allow for the discovery of a novel targetable PDAC receptor that can be used for both targeted diagnosis and therapy. The high binding affinity and specificity of this aptamer greatly facilitate the identification of its binding target. To identify this unknown PDAC cell-surface biomarker, there are several synthesized aptamers that can be utilized. I have already synthesized and purified the previously optimized

1502 aptamer with a biotin at the 3' end. This aptamer has been and will continue to be used to capture the biomarker from the membrane-bound fraction of different PDAC cell lysates, whereas the lysates from normal pancreas cells (HPNE cells) are being used as negative controls. The aptamer/biomarker complexes will be isolated using streptavidin agarose beads (Figure 5.1), as we have extensively used in other projects <sup>63-65</sup>.

The identity of the biomarker will be determined by mass spectrometry as we have reported for the identification of other drug-binding protein targets from mouse brain lysate <sup>66</sup>. One concern is that the extremely strong interaction between the biotin and streptavidin requires harsh elution conditions that could result in the release of many background proteins from the solid support. To address this problem, an excess concentration of the antisense of the aptamer can be incubated with the complexes to disrupt the interaction between the immobilized aptamer and the captured protein target (Figure 5.1). We have confirmed that this antisense sequence does bind to aptamer 1502 and should compete with the target protein's interaction with 1502 to elute the target.

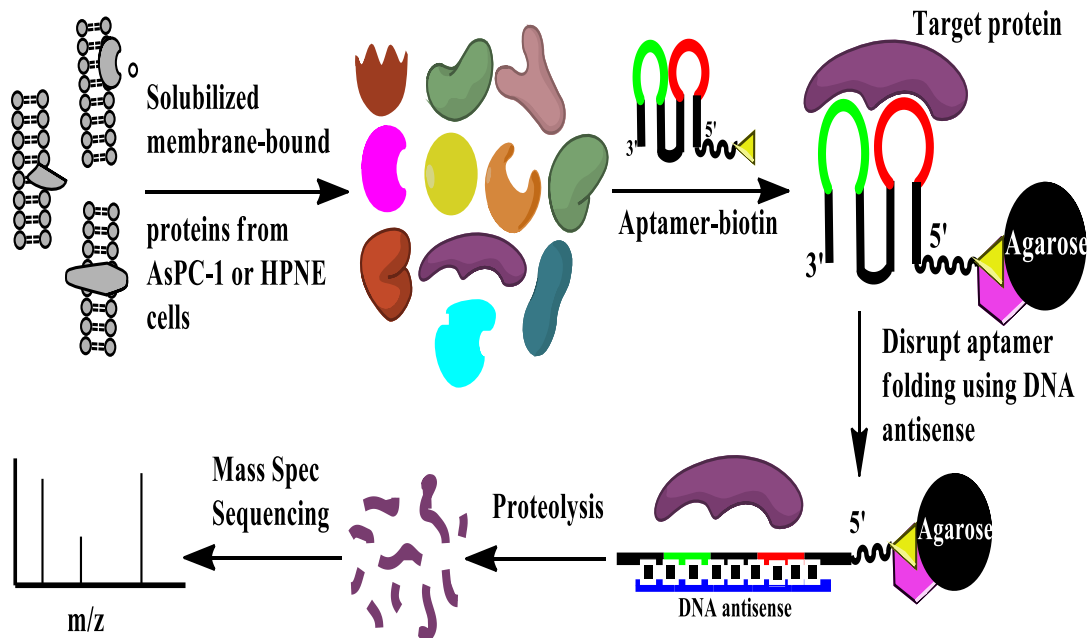


**Figure 5.1** General strategy for isolation, identification and detection of aptamer-binding target protein using an antisense elution approach.

Due to varying expression levels of membrane bound proteins, there may be an issue with a low concentration of the target protein, making it difficult to extract enough of the protein target for mass spectrometry. An alternative approach to using the biotinylated aptamer to extract the target protein, is to utilize a platform that we have already demonstrated to be successful in binding our aptamer's target. Aptamer 1502, conjugated to gold nanoparticles (AuNPs), allows for an avidity effect with the optimized 20:1 molar ratio of aptamer to gold nanoparticle. This platform should allow for an increase in binding affinity of the aptamer to its target protein. The gold nanoparticle conjugated to 1502 can be incubated with the AsPC-1 membrane-bound proteins and compared to the gold nanoparticle alone as well as HPNE cell lysates (controls). Through centrifugation, 1502-AuNP will be pelleted, with the target protein bound to the aptamers attached to the nanoparticle. By removing the non-specific membrane bound proteins

in the supernatant, the target protein can be isolated. The visualization and identification of the target will be done as described for the biotinylated aptamer.

Finally, there may be issues with removing the non-specific proteins that bind to the streptavidin beads and contaminate the isolated target protein(s). If this appears to be the case, we will use a biotin molecule containing an acylhydrazone cleavable linker as the Liu and Kohn labs have published, which allows for gentle release of the bound target(s) under very mild, slightly acidic conditions (Figure 5.2)<sup>67</sup>. Mass spectroscopy will be used to identify the unknown biomarker.

For any of these biomarker identification approaches, further confirmation studies will be performed with various biochemical and cellular assays, including cell binding and sorting, IP and pull-down using antibodies or aptamers, and siRNA. The availability of such information will allow us to provide both a novel biomarker and the corresponding targeting ligand to the PDAC research community.



solubilization while keeping aptamer 1502 functional. Initially, when the eluted fractions were run on a SDS-PAGE gel and silver stained, the target protein fraction yielded too many non-specific proteins, ones that most likely bound to the streptavidin beads even though they were pre-blocked. A glycine buffer, pH 2.5 was added to the eluting protocol to add stringency to the target isolation elution. This additional step did allow for an increased stringency, however, the conditions were too harsh, and there were no longer an isolated protein in the eluted fraction that was concentrated enough for mass spec. A summary of the isolated proteins that were pulled down with these conditions can be seen in Figure 5.3. We determined the elution conditions needed to change in future studies to allow for more specific protein isolation. Additionally, we needed to increase the concentration of the target protein to yield a band that could be analyzed by mass spec. A visiting scholar, Lu Zhang, has utilized the information gained from these experiments to improve conditions of the target protein's isolation and elution.

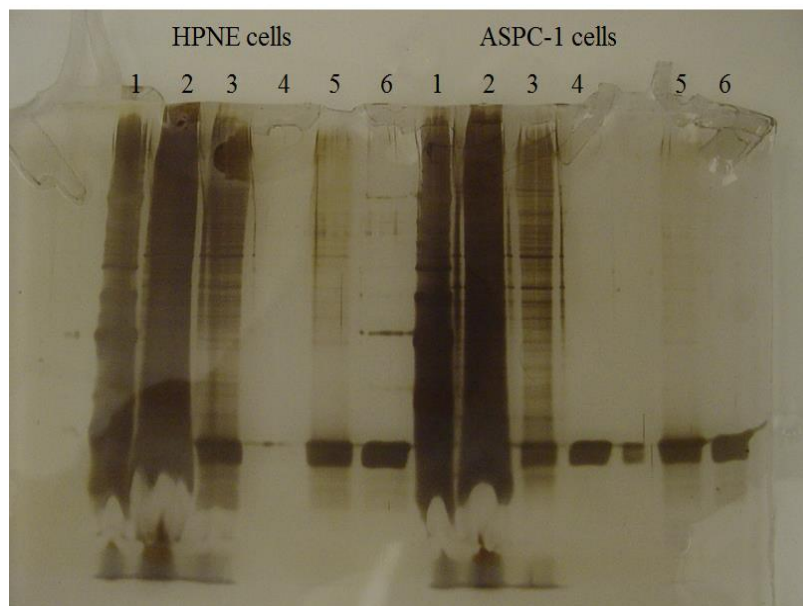


**Figure 5.3** SDS-PAGE silver stained gel loaded with: 1 – ladder, 2 – membrane protein supernatant + SA beads, 3 – membrane protein supernatant + B-1502, 4 – membrane protein supernatant (no aptamer), 5 – membrane protein supernatant + B-1502 + glycine buffer, and 6 – membrane protein supernatant + glycine buffer (no aptamer).

### **5.2.b.ii. Isolation of aptamer 1502's target protein using AuNPs**

After the development of the aptamer-gold nanoparticle (Chapter 3), it was thought that this platform could be useful in the aptamer's target identification. The theory behind this approach is that the 1502-AuNP-PEG provides a multi-valiancy effect with several aptamers conjugated to the gold nanoparticles. This would help to increase the concentration of the aptamer bound target protein(s) during the elution steps. Additionally, through centrifugation, these functionalized nanoparticles and their target(s) could be isolated, aiding in 1502's target identification. This approach was performed similarly to the biotinylated 1502, however when the proteins were eluted, there were three specific methods used for elution. The first elution utilized the synthesized 1502 antisense DNA aptamer that could bind to RNA aptamer 1502 to disrupt the binding and release its target protein. The second elution method involved RNase A, an enzyme that digested the RNA, allowing for the release of its bound target protein. The third elution fraction involved heating the gold nanoparticles to 95°C for 5 min to remove any remaining specific or non-specific proteins bound to the aptamer or gold nanoparticles. Unfortunately, there weren't distinct bands from this study to move forward with these conditions using this approach (data not shown). However we have incorporated some of the elution conditions when moving forward.

### **5.2.c. Ongoing target identification with collaborator – preliminary data**

Lu Zhang has begun her efforts to identify the potentially novel biomarker of aptamer 1502, with an optimized protocol seen in the proposed methods section. She has initially tested AsPC-1 cells and has compared biotinylated 1502 plus streptavidin beads (test sample) to streptavidin beads alone (control). After running a SDS-PAGE gel and doing a silver stain, seen in Figure 5.4, there were noticeable additional protein bands present in the test sample. Both the

test sample and the control were submitted to collaborator Dr. Kevin Xiao for mass spec analysis (not shown). The initial mass spec data did isolate proteins that were present in the test sample and not in the control, however there were still too many proteins to do further binding analysis.

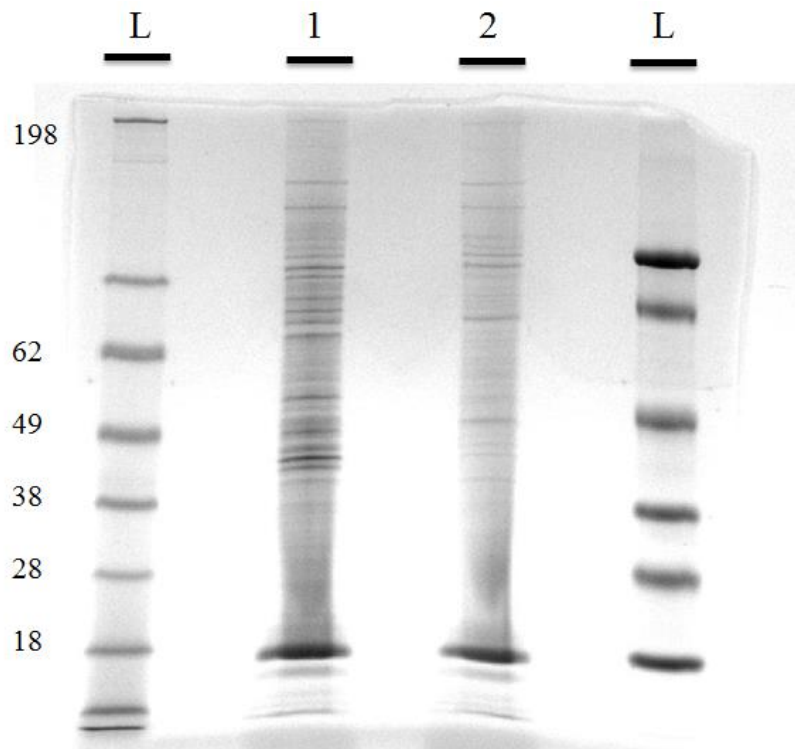


**Figure 5.4** SDS-PAGE silver stained gel loaded with: L – ladder, 1 – Biotin-1502 and SA beads, 2 – SA beads only.

Additional controls were added, such as HPNE cells and additional elution steps, as seen with the gold nanoparticle approach, to further isolate the protein target of interest. Figure 5.5 illustrates the promising preliminary results, with a noticeable band around 150 KD that is present in the AsPC-1 sample but not in the HPNE. These proteins were sent to Dr. Xiao for mass spec analysis.



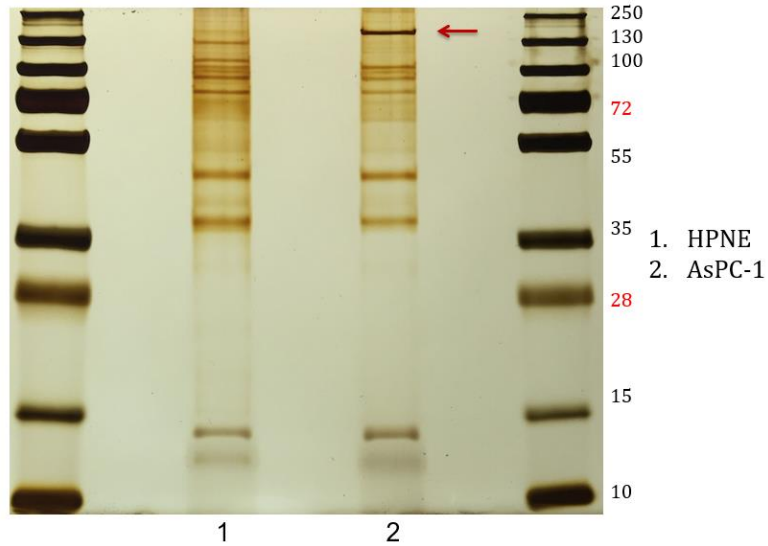


**Figure 5.5** Silver stained gel demonstrates proteins eluted with a 2X concentration of 1502's antisense oligo. This was done for both HPNE cells (lane 1) and AsPC-1 cells (lane 2).

#### 5.2.d. Proposed materials and methods

There are two approaches that we have taken in aims of isolating and identifying the cell-membrane target of aptamer 1502. The first approach, represented in Figure 5.1, used a biotinylated aptamer and streptavidin agarose beads to isolate the target protein. The second approach took advantage of the aptamer:gold nanoparticle that we developed in Aim 2. While there were similar methods utilized in this approach, the density of the gold nanoparticle was advantageous to isolate the target that was bound by several aptamers on the surface of the gold nanoparticles. For the target elution, several elution approaches were used, including but not limited to elution with 1502's DNA antisense, RNase I, and boiling. Both methods were performed during my dissertation research and will be considered and improved upon for current and future studies.

#### **5.2.d.i. Isolation of aptamer 1502's target protein using a biotinylated aptamer**

Permeabilization buffer (Thermo), 1 mL was added to the cell pellet ( $1 \times 10^7$  ASPC-1 cells/tube). The buffer was vortexed briefly to obtain a homogeneous cell suspension and incubated for 10 min at 4°C with constant mixing. Permeabilized cells were transferred to a new Eppendorf tube and centrifuged for 15 min at 16,000×g. The supernatant, containing cytosolic proteins, was carefully removed and transferred to a new tube. 30 µL of cytosolic proteins were mixed with 10 µL of 4X loading buffer to check the protein level in the gel. 0.5mL of solubilization buffer (Thermo) or binding buffer: PBS with 0.1% SDS, 1% NP-40, RNase inhibitor, protease inhibitor (EDTA-) was added to the pellet and resuspended. Alternative detergents, such as 1% DDM and Triton-X-100 were also tried in the solubilization buffer. Samples were incubated at 4°C for 30 min with constant mixing. Tubes were centrifuged at 16,000×g for 15 min at 4°C followed by the transfer of the supernatant containing solubilized membrane and membrane-associated proteins to a new tube. 30 µL of the supernatant was removed and mixed with 10 µL of 4X loading buffer to check the membrane protein level in a PAGE gel.

The supernatant was diluted 10x with the aptamer-binding buffer. Pre-folded (80°C for 3 min and cooled slowly to room temperature) 400 nM biotin-aptamer 1502 was added to the buffer and supernatant containing membrane proteins. The sample was rotated for 2 h at 4°C, followed by the addition of streptavidin (SA) beads (GE Healthcare). The sample was rotated for 30 min at 4°C followed by centrifugation for 2 min at 2000 rpm. The supernatant was removed and the sample washed three times with 1 mL of aptamer binding buffer. 40 µL of 2X loading buffer was added to the sample and run a on a SDS-PAGE gel treated with silver staining.

With this approach, it is possible that non-specific proteins may bind to the streptavidin agarose beads, contaminating the eluted sample. If this is the case, there are additional elution steps that can aid in removing the streptavidin agarose (SA) beads that is tightly bound to the biotinylated aptamer, and any of the non-specific proteins that are bound to the SA as well. A few of these elution methods were tried in the preliminary experiments, and may be continued in future approaches. One elution step involves adding an antisense of the 1502 RNA aptamer (25X molar excess of 1502) to elute the target protein. Second, RNase A (0.5  $\mu$ L/2.5U/minimal) could be added for 30 min at 37°C. Finally, the pellet can be boiled at 95°C to disrupt and elute any proteins that were still bound to the SA beads. These methods have been utilized in an alternative 1502-AuNP-PEG approach, and can be used here as well. Finally, the SA:biotin interaction can be disrupted to release and elute the aptamer with the bound protein by heating the sample to 65°C for 2 min in 10 mM EDTA, pH 8.2, and 95% formamide (Life Technologies).

#### **5.2.d.ii. Isolation of aptamer 1502's target protein using AuNPs**

AsPC-1 or HPNE (control) cells ( $2-3 \times 10^7$ ) were lysed with lysis buffer 1. Cells were placed in -80°C for 10 min, and then thawed to room temperature, three times. Cells were transferred to a glass tube and “crushed” to further lyse the cells. Lysis buffer 2 was added to cells and they were distributed to Eppendorf tubes (2 mL each) and spun down at 4000 rpm at 4°C for 30 min. The supernatant (S1), containing all of the soluble proteins, was removed and saved for the total protein gel. Solubilizing buffer was added, cells were vortexed, and spun at 3000 rpm for 30 min at 4°C. The supernatant (S2), containing the membrane bound proteins, was removed for incubation with aptamer.

The optimized molar ratio of aptamer 1502 to gold nanoparticles was synthesized, with 5 nM of AuNPs, for incubation with the membrane bound proteins. For AsPC-1, this ratio was

20:1. A 20:1 molar ratio of 1502 DNA oligo conjugated to the gold nanoparticles was used as a negative control. 1502-AuNP and 1502(DNA)-AuNP were incubated at room temperature for 2 h. The samples were centrifuged at 4000 rpm for 15 min to form a pellet of the AuNP-1502 bound to the target protein. The supernatant was removed and washed three times solubilizing buffer. With this protocol, there was a three step extraction to further isolate the target protein. First, an antisense of the 1502 RNA aptamer was added (25X molar excess of 1502). Second, RNase A (0.5  $\mu$ L/2.5U/minimal) was added for 30 min at 37°C. Finally, the pellet was boiled at 95°C to disrupt and elute any proteins that were still bound to the gold nanoparticle.

#### **5.2.e. Potential impact**

Given the absence of clinically useful biomarkers for pancreatic ductal adenocarcinoma, the identification of a novel biomarker is critical for the advancement of targeted therapeutics and diagnostic probes. We know that RNA aptamer 1502 specifically targets a cell surface protein present in PDAC cells and PDX tissue samples. This aptamer does not target many of the non-pancreatic cancer cell lines tested, including normal pancreas. If 1502's target is a putative biomarker and this biomarker is identified, it could become an extremely useful tool for diagnostics. Additionally, because 1502 already is known to have a specific and strong affinity for this biomarker, it can be further developed, as we have done in Chapter 3, as a targeted drug delivery tool against pancreatic ductal adenocarcinoma.

#### **5.3 *In vivo* delivery of 1502 and 1502 functionalized lipid-PLGA nanoparticle**

To demonstrate the applied translational capabilities of this project, we have performed initially preliminary studies to test aptamer 1502, which was characterized and optimized in Aim

1, in orthotopic PDAC mouse models. This continuation of my dissertation research is not actively being continued at this time; however it is a future direction that is significant and potentially impactful to the comprehensive understanding of how aptamer 1502 can translate its targeting effect against pancreatic ductal adenocarcinoma.

Immunohistochemistry studies in Aim 1 illustrated the binding of the optimized 1502 aptamer to three Patient-derived Xenograft (PDX) tissue samples, using a positive control (AsPC-1 cells) and negative controls (A375 xenograft tissue) as comparison, showing that the PDAC biomarker is present in patient tissue as well. This preliminary data suggests that the aptamer may be able to be translated beyond *in vitro* cellular targets and assays.

Additionally, the stability of both aptamer 1502 against nuclease degradation and the functional stability of 1502 that is inserted into the outer layer of the hybrid lipid-PLGA nanoparticles was tested with serum stability assays (Chapters 2 and 4 respectively). Aptamer 1502 that was synthesized with a 5' amino had an increased stability against nuclease degradation when compared with a phosphoryl labeled 1502 aptamer. Both were partially modified with 2'-F C/U, with differing 5' moieties. It appeared that the 5' amino added additional protection of the aptamer against the nucleases found in the serum, which is promising moving forward to *in vivo* studies. The functional stability of aptamer 1502 with the 5' stearyl moiety was also tested in serum after being inserted in to the lipid-PLGA nanoparticles. These results indicated that there was functional specific targeting of 1502 up to 8 h of incubation in serum, with non-specific internalization for the nanoparticles, functional and non-functional, at 12 and 24 h in serum. This is expected for this type of lipid-PLGA nanoparticles, as they are utilized in *in vivo* drug delivery, even without a targeting ligand. Given the serum stability

results, we decided to test both RNA aptamer 1502 alone and the 1502 functionalized hybrid lipid-PLGA nanoparticles *in vivo* to determine the tumor targeting potential of aptamer 1502.

### 5.3.a. Plan for future *in vivo* studies

The studies delivering aptamer 1502-functionalized lipid-PLGA nanoparticles will be performed by *in vivo* fluorescence imaging with a Xenogen IVIS™ system using an orthotopic pancreatic cancer model. We have successfully demonstrated this technique in a previous study (Figure 5.5), by injecting with an IRDye-BiEGFR targeting ligand, a novel targeting ligand developed in the Liu lab.

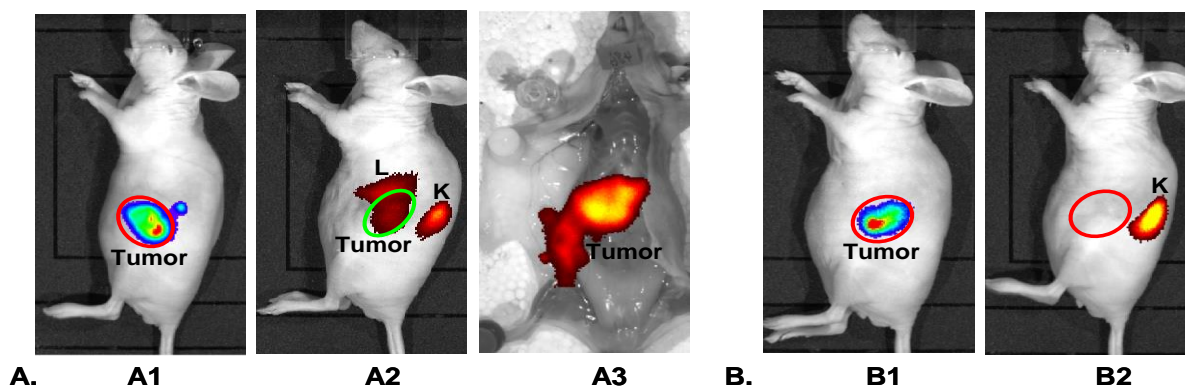


**Figure 5.5** Xenogen imaging of targeting two orthotopic AsPC-1 pancreatic cancer mice using 0.5 nmol IRDye-BiEGFR by i.v. injection. In mouse B, the IRDye-BiEGFR ligand was proteolytically cleaved prior to injection. A1 and B1: whole body Luc signal; A2 and B2: whole body NIR signal; A3: *Ex vivo* NIR signal after sacrificing mouse A. L: liver; K: kidney.

Our plan for utilizing the 1502-amino labeled aptamer would be to first characterize the PDAC cell-binding affinity and specificity of the synthesized aptamer by reacting the synthesized aptamer with FITC (together with a control aptamer). Once shown to be successfully reacted and functional, we would react the 1502-amino with NHS-DOTA under alkaline

conditions for copper 64 labeling *in vivo*. For these studies, we would be using the orthotopic PDAC animal model that the Liu lab has been using for the targeted imaging studies.  $2 \times 10^6$  AsPC-1 cells would be inoculated into each nude mouse, and the tumor was allowed to reach an appropriate size for 4-5 weeks. Once this would occur, both aptamer 1502-DOTA and a negative control aptamer 1502-scrambled-DOTA probe, will be labeled with copper 64, and be intravenously injected. The relative concentration of copper 64 in the AsPC-1 tumor will be traced and visualized with PET imaging, at time points up to 24 h. This will be done with both RNA aptamer 1502 and the scrambled RNA aptamer 1502 control.

In addition to delivering aptamer 1502, we plan on delivering hybrid lipid-PLGA nanoparticles that are targeted with 1502, development can be seen in Chapter 4. This nanoparticle formulation has shown to be very efficacious in the literature *in vivo* with low toxicity and high biocompatibility (references). We would initially deliver the 1502 functionalized lipid-PLGA nanoparticle that carries cardiogreen, also known as ICG (Sigma) and Nile red dye, which was previously used to monitor the internalization of these nanoparticles into cells. The Nile red dye could be utilized in *ex vivo* studies with confocal microscopy at an excitation of 555 nm and the ICG delivery observed under fluorescent imaging at an excitation around 780 nm. Recently, *in vivo* imaging using near-infrared (NIR, 700 nm - 900 nm) fluorescent light has received considerable interest. NIR fluorescent light has a high transmission through living tissue and is able to penetrate into the tissue to depths of several centimeters with robust safety.

For continuing experiments using local application of the 1502-lipid-PLGA nanoparticles carrying ICG and Nile red, mice will be anaesthetized, laparotomy performed, prior to the local application to the pancreas of either positive or control scrambled aptamer nanoparticle platform.

The mice will be monitored at multiple time points using an IVIS Imaging System. For *ex vivo* imaging, mice will be sacrificed, pancreas with tumors explanted, and the tissues subjected to fluorescence imaging.

If determined successful, the long term plan for this targeted delivery platform is to deliver a small molecule drug, carried by the PLGA at the core of the nanoparticle, to aid in reducing the AsPC-1 tumor size. This therapeutic approach is extremely versatile and flexible, as it would allow for a PDAC targeted delivery of a hydrophobic therapeutic of choice, with optimizations incorporated into the composition of the synthesized nanoparticle.

### **5.3.b. Proposed materials and methods**

#### **5.3.b.i. Aptamer 1502**

The 1502 aptamer would be labeled with NHS-DOTA for further interaction with copper<sup>64</sup>. Immediately after the NHS-DOTA is activated, the aptamer, folded and added to a borate buffer, pH 8.5, would be mixed at 4°C overnight. Free NHS-DOTA would be removed by a Nap 5 column (GE Life Sciences). If necessary, the aptamer would be ethanol precipitated to remove any unnecessary salts and further de-salt by a Nap 5 column. Copper<sup>64</sup> is reacted with the DOTA of the 1502-NHS-DOTA and free DOTA would be removed with a 5K or Nap5 column. Aptamer-NHS-DOTA was intravenously injected into AsPC-1 inoculated mice and monitored by PET imaging at various time points for the targeting of aptamer 1502 to the PDAC tumor.

#### **5.3.b.ii. Aptamer 1502 hybrid lipid-PLGA nanoparticle**

The lipid-PLGA nanoparticles would be prepared as done previously (Chapter 4), however 2 nmol of Nile red and 2 nmol of ICG dyes would be encapsulated with the PLGA (instead of Nile red alone). The proportions of the dyes has already been optimized so that



fluorescence was observed at 555 nm (for Nile red) and ~780 nm (for ICG), without a significant quenching effect. These absorbances could be quantified on a fluorometer as well as the IVIS system directly. Nanoparticles would be functionalized with 1502 and 1502-scrambled as done previously. Total volume for injection will be 200  $\mu$ L per mouse in 1X PBS. Injections would occur intravenously under anesthesia with 2-3% isoflurane.

Fluorescence imaging would be performed using the Xenogen *in vivo* Imaging System (IVIS Kinetics, Perkin Elmer). The system consists of a supersensitive cooled charge-coupled device (CCD) camera mounted inside a light-tight imaging chamber. The CCD chip is 2.7  $\text{cm}^2$  consisting of  $2,048 \times 2,048$  pixels at 13.5  $\mu\text{m}$  each. The camera is capable of detecting a minimum radiance of 100 photons per second per square centimeter per steradian ( $\text{p/s/cm}^2/\text{sr}$ ) and can achieve a minimal image pixel resolution of 50  $\mu\text{m}$ . The system does not allow for three-dimensional imaging, and hence spatial resolution is limited to a compressed, two-dimensional image for analysis. Images would be acquired at 10 min, 1 hour, 5 hours and 24 hours post 2 nmol tracer administrations via tail vein. The gray scale photographic images and fluorescence color images can be superimposed using the Living Image 4.1 software overlay (Perkin Elmer). For quantification, a region of interest (ROI) can be manually selected based on the signal intensity. The area of ROI would be kept constant and the intensity was recorded as average photons per second per square centimeter per steradian as described previously.

### **5.3.c. Potential Impact**

The ongoing and future *in vivo* studies with aptamer 1502 have significance for the future development of this aptamer as a potential tool for diagnosis and therapeutics. If the biodistribution of the aptamer *in vivo* confirms its specificity to PDAC and its effectiveness in

targeting PDAC over healthy tissue, this could be very useful as a diagnostic tool. Additionally, the hybrid lipid-PLGA nanoparticle delivery system could not only serve as a targeting tool against PDAC, but could also deliver a therapeutic drug that could aid in treating this horrible disease.

## REFERENCES

- [1] American Cancer Society. *Pancreatic Cancer*. Atlanta, GA. American Cancer Society; 2014.
- [2] What you need to know about cancer of the pancreas. National Cancer Institute. <http://www.cancer.gov/cancertopics/wyntk/pancreas/allpages>. Accessed June 17, 2011.
- [3] Brugge, W.R. Management and outcomes of pancreatic cystic lesions. *Dig Liver Dis.* 40, 854-9. May 27, 2008.
- [4] Yeh, J.J. Prognostic signature for pancreatic cancer: are we close? *Future Oncol.* 5, 313-21. 2009.
- [5] Goicoechea, S.M. et al. Isoform-specific upregulation of palladin in human and murine pancreas tumors. *PLoS* 5, e10347. 2010.
- [6] Trepel, M., Arap, W. & Pasqualini, R. In vivo phage display and vascular heterogeneity: implications for targeted medicine. *Curr Opin Chem Biol.* 6, 399-404. 2002.
- [7] Shangguan D et al. Aptamers evolved from live cells as effective molecular probes for cancer study. *Proc Natl Acad Sci U S A.* 103, 11838-43. Jul 27, 2006.
- [8] Szostak, J., Roberts, R., and Liu, R. Selection of Proteins Using RNA-Protein Fusions. *WO/1998/031700* (1998); *WO/2000/047775* (2000); *U.S. Patent 6,207,446* (2001); *U.S. Patent 6,214,553* (2001); *U.S. Patent 6,258,558* (2001); *U.S. Patent 6,261,804* (2001); *U.S. Patent 6,281,344* (2001). 2000.
- [9] Shen, X., Valencia, C.A., Szostak, J.W., Dong, B. & Liu, R. Scanning the human proteome for calmodulin-binding proteins. *Proc Natl Acad Sci U S A.* 102, 5969-74. Apr 19, 2005.
- [10] Ju, W. et al. Proteome-wide identification of family member-specific natural substrate repertoire of caspases. *Proc Natl Acad Sci U S A.* 104, 14294-9. Aug 29, 2007.
- [11] Shen X et al. Ca (2+)/Calmodulin-binding proteins from the *C. elegans* proteome. *Cell Calcium.* 43, 444-56. Sep 12, 2008.
- [12] Valencia Ca, Cotten Sw, Dong B & Liu R. mRNA-display-based selections for proteins with desired functions: a protease-substrate case study. *Biotechnol Prog.* 24, 561-9. May 10, 2008.
- [13] Liu, R., Kay, B.K., Jiang, S. & Chen, S. Nanoparticle Delivery: Targeting and Nonspecific Binding. *MRS Bulletin* 34, 432-440. 2009.
- [14] Gold L, Polisky B, Uhlenbeck O & Yarus M. Diversity of oligonucleotide functions. *Annu Rev Biochem.* 64, 763-97. 1995.

- [15] Pieken Wa, Olsen Db, Benseler F, Aurup H & Eckstein F. Kinetic characterization of ribonuclease-resistant 2'-modified hammerhead ribozymes. *Science*. 253, 314-7. 1991.
- [16] Ruckman, J. et al. 2'-Fluoropyrimidine RNA-based aptamers to the 165-amino acid form of vascular endothelial growth factor (VEGF<sub>165</sub>). Inhibition of receptor binding and VEGF-induced vascular permeability through interactions requiring the exon 7-encoded domain. *J Biol Chem*. 273, 20556-67. 1998.
- [17] Keefe, A.D. & Cload, S.T. SELEX with modified nucleotides. *Curr Opin Chem Biol*. 12, 448-56. Jul 21, 2008.
- [18] Aurup H, Williams Dm & Eckstein F. 2'-Fluoro- and 2'-amino-2'-deoxynucleoside 5'-triphosphates as substrates for T7 RNA polymerase. *Biochemistry*. 31, 9636-41. 1992.
- [19] Padilla, R. & Sousa, R. Efficient synthesis of nucleic acids heavily modified with non-canonical ribose 2'-groups using a mutant T7 RNA polymerase (RNAP). *Nucleic Acids Res*. 27, 1561-3. 1999.
- [20] Padilla, R. & Sousa, R. A Y639F/H784A T7 RNA polymerase double mutant displays superior properties for synthesizing RNAs with non-canonical NTPs. *Nucleic Acids Res*. 30, e138. 2002.
- [21] Chelliserrykattil, J. & Ellington, A.D. Evolution of a T7 RNA polymerase variant that transcribes 2'-O-methyl RNA. *Nat Biotechnol*. 22, 1155-60. Aug 8, 2004.
- [22] Nimjee, S.M., Rusconi, C.P. & Sullenger, B.A. Aptamers: an emerging class of therapeutics. *Annu Rev Med*. 56, 555-83. 2005.
- [23] Daniels Da, Chen H, Hicke Bj, Swiderek Km & Gold L. A tenascin-C aptamer identified by tumor cell SELEX: systematic evolution of ligands by exponential enrichment. *Proc Natl Acad Sci U S A*. 100, 15416-21. Epub 2003 Dec 15, 2003.
- [24] Cerchia L et al. Neutralizing aptamers from whole-cell SELEX inhibit the RET receptor tyrosine kinase. *PLoS Biol*. 3, e123. Mar 22, 2005.
- [25] Keefe, A.D. and Cload, S.T. SELEX with modified nucleotides. *Curr. Opin. Chem. Biol.*, 12, 448-456. 2008.
- [26] Dua, P., Kang, H., Hong, S-M., Tsao, M-S, Kim, S., and Lee, D. Alkaline Phosphatase ALPPL-2 is a Novel Pancreatic Carcinoma-Associated Protein. *Cancer Res*; 73(6). March 15, 2013.
- [27] Ray, P., Rialon-Guevara, K., Veras, E., Sullenger, B., and White, R. Comparing human pancreatic cell secretomes by in vitro aptamer selection identifies cyclophilin B as a candidate pancreatic cancer biomarker. *The Journal of Clinical Investigation*. Vol 122. Num 4. May 2012.

- [28] Friedman, A., Kim, D., Liu, R. Highly stable aptamers selected from a 2'-fully modified fGmH RNA library for targeting biomaterials. *Biomaterials*. 36:110-23. Jan 2015.
- [29] Broad-Novartis Cancer Cell Line Encyclopedia. *Cancer Cell Line Encyclopedia*. 2013. <http://www.broadinstitute.org/ccle/home>
- [30] Nakanuma Y., Sato Y. Hilar cholangiocarcinoma is pathologically similar to pancreatic duct adenocarcinoma: suggestions of similar background and development. *J Hepatobiliary Pancreat Sci*. 21(7):441-7. July 2014.
- [31] Shibahara H., Tamada S., Goto M., Oda K., Nagino M., Nagasaka T., Batra SK., Hollingsworth MA., Imai K., Nimura Y., and Yonezawa S. Pathologic features of mucin-producing bile duct tumors: two histopathologic categories as counterparts of pancreatic intraductal papillary-mucinous neoplasms. *Am J Surg Pathol*. 28(3):327-38. March 2004.
- [32] Petrelli F., Ghilardi M., Colombo S., Stringhi E., Barbara C., Cabiddu M., Elia S., Corti D., and Barni S. A rare case of metastatic pancreatic hepatoid carcinoma treated with sorafenib. *J Gastrointest Cancer*. 43(1):97-102. March 2012.
- [33] Kim D., Friedman AD., and Liu R. Tetraspecific ligand for tumor-targeted delivery of nanomaterials. *Biomaterials*. 35(23):6026-36. July 2014.
- [34] Xiao, Z., Shangguan, D., Cao, Z., Fang, X. and Tan, W. Cell-specific internalization study of an aptamer from whole cell selection. *Chemistry*, 14, 1769-1775. 2008.
- [35] Banu H., Sethi DK., Edgar A., Sheriff A., Rayees N., Renuka N., Faheem SM., Premkumar K., and Vasanthakumar G. Doxorubicin loaded polymeric gold nanoparticles targeted to human folate receptor upon laser photothermal therapy potentiates chemotherapy in breast cancer cell lines. *J Photochem Photobiol B*. 149:116-128. June 1, 2015.
- [36] Cherukuri P., Glazer ES., and Curley SA. Targeted hyperthermia using metal nanoparticles. *Adv Drug Deliv Rev*. 62, 3. 2010.
- [37] Zhang J., Liu, B., Liu, H, Zhang, X., Tan, W. Aptamer-conjugated gold nanoparticles for bioanalysis. *Nanomedicine*. 8, 6, 983-993. 2013.
- [38] Sharma, J. Chhabra R., Yan H., and Liu Y. A facile *in situ* generation of dithiocarbamate ligands for stable gold nanoparticle-oligonucleotide conjugates. *Chem. Commun*. 2140-2142. 2008.
- [39] Li L., Xiang D., Shigdar S., Yang W., Li Q, Lin J., Liu K., and Duan W.. Epithelial cell adhesion molecule aptamer functionalized PLGA-lecithin-curcumin-PEG nanoparticles for targeted drug delivery to human colorectal adenocarcinoma cells. *International Journal of Nanomedicine*. 9, 1083-1096. 2014.

- [40] Yun H., et. Al. *In vitro* performance of lipid-PLGA hybrid nanoparticles as an antigen delivery system: lipid composition matters. *Nanoscale Letters*. 6, 434. 2014.
- [41] Aravind A, Jeyamohan P, Nair R, Veeranarayanan S, Nagaoka Y, Yoshida Y, Maekawa T, and Kumar DS. AS1411 aptamer tagged PLGA-lecithin-PEG nanoparticles for tumor cell targeting and drug delivery. *Biotechnol Bioeng*. 109(11):2920-31. Nov 2012.
- [42] Wang Y, Kho K, Cheow WS, and Hadinoto K.  
A comparison between spray drying and spray freeze drying for dry powder inhaler formulation of drug-loaded lipid-polymer hybrid nanoparticles. *Int J Pharm*. 15;424(1-2):98-106. Mar 2012.
- [43] Bennet D, Marimuthu M, Kim S, An J. Dual drug-loaded nanoparticles on self-integrated scaffold for controlled delivery. *Int J Nanomedicine*. 7:3399-419. 2012.
- [44] Hu Y., Ehrich M., Fuhrman K., and Zhang C. In vitro performance of lipid-PLGA hybrid nanoparticles as an antigen delivery system: lipid composition matters. *Nanoscale Res Lett*. 9(1): 434. 2014.
- [45] Rose, et. al. Engineering of a novel adjuvant based on lipid-polymer hybrid nanoparticles: A quality by design approach. *Journal of Controlled Release*. 210 (48-57). 2015.
- [46] Zhao, Y. et. al. Discovery and *in Vivo* Evaluation of Novel RGD-Modified Lipid-Polymer Hybrid Nanoparticles for targeted drug delivery. *Int. J. Mol. Sci*. 15, 17565-17567. 2014.
- [47] Su. X, et al. Lipid-Polymer nanoparticles encapsulating doxorubicin and 2'-deoxy-5-azacytidine enhance the sensitivity of cancer cells to chemical therapeutics. *Molecular Pharmaceutics*. 10, 1901-1909. 2013.
- [48] Ramesh M., Ahlawat P., and Srinivas NR. Irinotecan and its active metabolite, SN-38: review of bioanalytical methods and recent update from clinical pharmacology perspectives. *Biomed Chromatogr*. 24(1):104-23. Jan 2010.
- [49] Huang, F. et. al. Self-assembled hybrid nanoparticles for targeted co-delivery of two drugs into cancer cells. *Chem. Communications*. 50, 3103-3105. 2014.
- [50] Ramasamy, T. et. al. Layer-by-layer lipid-polymer hybrid nanoparticles designed for use in anticancer drug delivery. *Carb. Polymers*. 102 (653-66). 2014.
- [51] Diaz, M. et. al. Improved insulin loading in poly(lactic-co-glycolic) acid (PLGA) nanoparticles upon self-assembly with lipids. *International Journal of Pharmaceutics*. 452 (84-91). 2015.
- [52] Zhang L., Chan JM., Gu FX., Rhee JW., Wang AZ., Radovic-Moreno AF., Alexis F., Langer R., Farokhzad OC. Self-assembled lipid-polymer hybrid nanoparticles: a robust drug delivery platform. *ACS Nano*. 2(8):1696-702. Aug 2002.

- [53] Barltrop, J.A. et al. (5-(3-carboxymethoxyphenyl)-2-(4,5-dimethylthiazolyl)-3-(4-sulfophenyl)tetrazolium, inner salt (MTS) and related analogs of 3-(4,5-dimethylthiazolyl)-2,5-diphenyltetrazolium bromide (MTT) reducing to purple water-soluble formazans as cell-viability indicators. *Bioorg. Med. Chem. Lett.* 1, 611–4. 1991
- [54] Colombo, S. Mechanistic profiling of the siRNA delivery dynamics of lipid-polymer hybrid nanoparticles. *Journal of Controlled Release.* 201, 22-31. 2015.
- [55] Zou, P. et. al. PLGA/Liposome Hybrid nanoparticles for short-chain ceramide delivery. *Pharm Res.* 31, 684-693. 2014.
- [56] Yang, Z. et. al. Targeted delivery of 10-hydroxycamptothecin to human breast cancers by cyclic RGD-modified lipid-polymer hybrid nanoparticles. *Biomed. Mater.* 8. 2013.
- [57] Narvekar, M. et. al. A novel hybrid delivery system: Polymer-oil nanostructured carrier for controlled delivery of highly lipophilic drug all-trans-retinoic acid (ATRA). *Intern Journal of Pharmaceutics.* 436. 2012.
- [58] Dhar, S. et. al. Targeted delivery of cisplatin to prostate cancer cells by aptamer functionalized Pt(IV) prodrug-PLGA-PEG nanoparticles. *PNAS.* 105, 45. 2008.
- [59] Huo ZJ, Wang SJ, Wang ZQ, Zuo WS, Liu P, Pang B, and Liu K. Novel nanosystem to enhance the antitumor activity of lapatinib in breast cancer treatment: Therapeutic efficacy evaluation. *Cancer Sci.* Jul 14 2015.
- [60] Zou P, Stern ST, and Sun D. PLGA/liposome hybrid nanoparticles for short-chain ceramide delivery. *Pharm Res.* 31(3):684-93. March 2014.
- [61] Kelly Ka et al. Targeted nanoparticles for imaging incipient pancreatic ductal adenocarcinoma. *PLoS Med.* 5, e85. 2008.
- [62] Cotten, S.W., Zou, J., Valencia, C.A. and Liu, R. Search Proteins with Desired Functions from Natural Proteome Libraries Using mRNA Display. *Nature Protocols.* 6, 1163-1182. 2011.
- [63] Park, K.D., Liu, R. and Kohn, H. Useful tools for biomolecule isolation, detection, and identification: acylhydrazone-based cleavable linkers. *Chem Biol.* 16, 763-72. 2009.
- [64] Park Kd, et. al. *J Med Chem* 1, 1. 2009.
- [65] Frangioni, J.V. In vivo near-infrared fluorescence imaging. *Curr Opin Chem Biol.* 7, 626-34. 2003.
- [66] Hawrysz, D.J. and Sevcik-Muraca, E.M. Developments toward diagnostic breast cancer imaging using near-infrared optical measurements and fluorescent contrast agents. *Neoplasia.* 2, 388-417. 2000.

[67] Sarkaria, J.N. et al. Use of an orthotopic xenograft model for assessing the effect of epidermal growth factor receptor amplification on glioblastoma radiation response. *Clin Cancer Res.* 12, 2264-71. 2006.